THE APPLICATION OF LASER DOPPLER TECHNIQUES TO VIBRATION MEASUREMENT AND POSITION CONTROL

Mark Edward Pleydell

Submitted for the degree of Doctor of Philosophy under the conditions for the award of higher degrees of the Council for National Academic Awards.

Dorset Institute of Higher Education

August 1986.

In collaboration with

Davy McKee (Poole) Ltd., Wallisdown Rd., Poole.

Abstract

The Application of Laser Doppler Techniques to Vibration Measurement and Position Control

M.E. Pleydell

The laser Doppler interferometer reported here was developed to investigate the possibilities of remote vibration and motion measurements. The method is non-contacting and operates with unprepared targets, using the diffusely scattered light to measure the axial component of the motion.

A full description of the motion requires both magnitude and direction of the target motion. The magnitude was found by standard heterodyning techniques, mixing light scattered from the target with a part of the original laser output in a controlled manner. A phase quadrature method was used to identify the direction of the target. This differs from the more usual method of frequency offsetting in requiring only passive optical components and therefore being considerably cheaper. This feature is believed to be novel to the LDI reported here.

Measurements were recorded for target motions over the range 100 mm. to (c.) 1 um. Because unprepared and therefore optically rough targets were used the light received by the detectors was not well behaved. This resulted in instability of the sense of motion signal due to loss of either of the detector signals for displacements above 500 um. However this should not be considered an upper limit to the range of the LDI, as serious loss of the sense signal was rare up to (c.) 25 mm. and measurements were made up to a peak displacement of 200 mm.

Correlations with an accelerometer and an LVDT show that the LDI can reliably measure displacement up to a range of 25 mm. with a maximum target velocity of 32 mm/s limited currently be the signal processing. Theoretical resolution with this device is better than 0.08 um. if full use is made of both detected signals.

ACKNOWLEDGEMENTS

I extend my gratitude firstly to my supervisor Dr. Allan Birchenough, both for his academic support and guidance and for his unfailing moral support when it was much needed. My thanks are also due to Mr. John Brooks and Dr. Mike Lalor for their supervisory roles in the project and whose contributions have been invaluable. Many of the academic members of the Department have listened to my ideas and thoughts with great patience and have offered their comments, in particular Mr. John Reynolds, for his help with the signal processing circuits. I must also recognise here the assistance of the technical, library and administrative staff of the department. In particular Mrs. Margaret Wetenhall for her help in locating many of the papers and articles cited in this text and for drawing my attention to other material of interest. Mr. Ken Okey has earned my admiration for his tolerence of my extended leases of laboratory equipment during the practical evaluation of the LDI. I must thank Mr. Chris Benjamin for constructing and frequently modifying much of the signal processing electronics. Many of the optical component mounts were built in the department workshops and my gratitude is due to Fred, Dave and Morris for their discussions and the high quality of their work. I am indebted to staff at all levels of the department named and unnamed.

Authors Note

All the work in this thesis is the sole and original work of the author except where stated otherwise by acknowledgement or reference.

CONTENTS

Abstract		...	i
Acknowledgements		...	ii
Authors Note		...	iii
Contents		...	iv
List of Figures		...	viii
List of Symbols		...	xi
1.	INTRODUCTION	...	1
1.1	The Laser Doppler Effect	...	1
1.2	The Research Project	...	3
2.	LITERATURE REVIEW	...	6
2.1	The Doppler Effect	...	6
2.1.1	The History of the Doppler Effect	...	6
2.1.2	Existing Laser Doppler Devices	...	7
2.1.3	The History of Solid Target Motion Measurement	...	12
2.2	Physical Principles of L.D. Devices	...	19
2.2.1	Light Scattering by Solid Targets	...	19
2.2.2	Extraction of Doppler Signals	...	22
2.2.3	Sense of Motion Recovery from L.D. Signals	...	23
2.2.4	Signal Detection and Processing	...	27
2.3	Other Non-contacting Measuring Techniques		29
	Figures	...	31

3.	THEORY	...	32
3.1	Laser Doppler Theory	...	32
3.1.1	The Doppler Effect	...	32
3.1.2	Heterodyne Detection	...	36
3.1.3	Coherence Condition	...	42
3.2	Sense Detection	...	44
3.2.1	Frequency Shifting	...	44
3.2.2	Phase Based Sense Detection	...	46
3.2.3	Signal Amplitude Variation	...	50
3.3	Scattering by Solid Targets	...	52
3.3.1	Speckle	...	52
3.3.2	Heterodyning with a Speckle Field	...	58
3.4	Laser Beam Properties	...	60
3.4.1	Coherence Length	...	60
3.4.2	Beam Profile	...	62
	Figures	...	65
4.	EXPERIMENTAL APPARATUS AND METHOD	...	66
4.1	Optical System	...	66
4.1.1	Optical Design	...	66
4.1.2	Optical Hardware	...	71
4.1.3	Optics	...	74
4.1.4	Alignment	...	76
4.1.5	Target	...	78
4.2	Electronic System	...	80
4.2.1	Detectors	...	80
4.2.2	Analogue Electronics	...	81
4.2.3	Digital Electronics	...	85

4.2.4	Control and Drive	...	86
4.2.5	Measurement and Recording	...	88
4.3	Computer Logging and Processing	...	90
	Figures	...	92
5.	DISCUSSION OF RESULTS	...	101
5.1	The Doppler Signal	...	101
5.1.1	The Received Doppler Signal	...	102
5.1.2	Laser Speckle	...	106
5.1.3	Target Finish Effects	...	110
5.1.4	Signal Variation with Target Range	...	113
5.1.5	Count Variation with Range	...	119
5.1.6	Sense of Motion Invariance with Range	...	120
5.1.7	Effect of Target Surface Inclination	...	122
5.2	Variation of Measured Target Displacement with Drive Frequency	...	126
5.3	Correlation Measurements	...	130
5.3.1	Accelerometer Correlations	...	130
5.3.2	LVDT Correlations	...	135
5.3.3	Other Correlation Measurements	...	138
5.4	Sources of Error	...	140
5.4.1	Signal Level Noise	...	140
5.4.2	Count Noise	...	142
5.5	Signal Processing	...	150
	Figures	...	152

6.	CONCLUSIONS	...	192
6.1	Capabilities and Limits of the System	...	192
6.1.1	Displacement	...	192
6.1.2	Velocity	...	195
6.1.3	Sense of Motion	...	197
6.2	Further Work	...	198
Appendix 1	Noise in Heterodyne Detection	...	A.1
Appendix 2	Frequency Shifting	...	A.3
Appendix 3	Mean Phase Across Target Surface	..	A.6
Appendix 4	Error Count Derivation	...	A.8
Appendix 5	Bibliography	...	A.10

List of Figures

2.1	Laser Doppler Anemometer (after Yeh and Cummins) ...	31
3.1	Scattering Geometry for Speckle Formation	65
4.1	Mach Zehnder Based LDI ...	92
4.2	Michelson Based LDI ...	92
4.3	Optical Component Mount ...	93
4.4	Prism and Beamsplitter Mount ...	93
4.5	Detector Assembly ...	94
4.6	Optical Component Base ...	95
4.7	Optical Table ...	95
4.8	Block Diagram of the Electronics ...	96
4.9	Frequency Response of the Analogue Circuits ...	97
4.10	Analogue Signal Processing Circuit ...	98
4.11	Fringe Counting Circuit ...	99
4.12	Counter Control Circuit ...	100
5.1	500 Hz Drive Signal and Detector Signal ..	152
5.2	44.5 Hz Drive Signal and Detector Signal .	152
5.3	0.03 Hz Drive Signal and Detector Signal .	153
5.4	Detected Signals Showing Phase Difference	153
5.5	Detected Signal from an Unfocussed Beam (c.f. figure 5.3) ...	154
5.6	Signal Amplitude Data ...	155
5.7	Signal Amplitude Data ...	156
5.8	Signal Amplitude Data ...	157
5.9	Signal Amplitude Data ...	158

5.10	Speckle Size as a function of Target Range	159
5.11	Mean Phase Difference at the Detector ...	160
5.12	Measured Displacement as a function of Range ...	161
5.13	Sense of Motion Probability ...	162
5.14	Sense of Motion Probability ...	163
5.15	Sense of Motion Probability ...	164
5.16	Mounting for Inclined Target Measurements	165
5.17	Signal Amplitude with Varying Incidence ..	166
5.18	Measured Displacement for Varying Incidence	167
5.19	Signal Amplitude with Varying Incidence ..	168
5.20	Measured Displacement for Varying Incidence	169
5.21	Measured Displacement v. Drive Frequency .	170
5.22	Measured Displacement v. Target Velocity .	171
5.23	Accelerometer v. LDI at 25 Hz. ...	172
5.24	Accelerometer v. LDI at 40 Hz. ...	173
5.25	Accelerometer v. LDI at 50 Hz. ...	174
5.26	Accelerometer v. LDI at 60 Hz. ...	175
5.27	Accelerometer v. LDI at 100 Hz. ...	176
5.28	Accelerometer v. LDI at 250 Hz. ...	177
5.29	Accelerometer v. LDI at 1000 Hz. ...	178
5.30	Accelerometer Response ...	179
5.31	LVDT Correlation Data ...	180
5.32	LVDT Correlation Data ...	181
5.33	LVDT Correlation Data ...	182
5.34	LVDT Correlation Data ...	183
5.35	LVDT Correlation Data ...	184
5.36	LVDT Correlation Data ...	185

5.37	Manual Translation Correlation Data ...	186
5.38	Manual Translation Correlation Data ...	187
5.39	Noise Histogram from Computer Data Logging	188
5.40	Error Data from the LDI ...	189
5.41	Error Data from the LDI ...	190
5.42	Error Data from the LDI ...	191

List of Symbols

a	=	General angle
a_{det}	=	Active area of detector surface
a_i	=	Amplitude scattered by i th point
$A_{1,2}$	=	Time varying amplitudes of beams 1 and 2
$A_{1o,2o}$	=	Peak amplitudes of beams 1 and 2
$A_{1p,s}$	=	Time varying amplitude components of p and s polarisations
$A_{1op,s}$	=	Peak amplitudes of $A_{1p,s}$
A_p	=	Total amplitude at P due to all scattering points
b	=	Arbitrary angle
c_o	=	Velocity of light in vacuo
d	=	Distance between wavefronts
d_m	=	Measurement length
d_o	=	Peak target displacement
d_{p-p}	=	Peak to peak target displacement
d_{sim}	=	Axial structural invariance distance of speckle field
d_t	=	Target displacement
$d(t)$	=	Time varying target displacement
d_{xs}	=	Excess measured displacement
D	=	Path length difference
D_{ff}	=	Far field distance
e	=	Fraction of disrupted measurements also Electron charge
f_b	=	Bandwidth

f_d = Doppler frequency ($f'-f_o$)

f_o = Laser output frequency

f' = Doppler shifted frequency

f_{ref} = Reference beam frequency

f_s = Reference beam frequency shift

f_t = Target drive frequency

F = Lens focal length

$\underline{i}$ = Unit vector in the beam direction

i_{ac} = A.C. compoonent of the detector current

$i_{acp,s}$ = A.C. detector currents resulting from p and s polarisations

i_d = Detector current

$i_{d1,d2}$ = D.C. components of the detector current

i_{d3} = Cross component of the detector current

i_{dd} = Detector dark current

i_j = Johnson noise current

i_o = Peak value of i_{ac}

i_{sh} = Shot noise current

i_{ref} = Detector current due to the reference beam

i_s = Signal current

I_{det} = Intensity seen by the detector

I_{ill} = Illumination intensity

I_{ref} = Reference beam intensity

I_s = Signal beam intensity

k = Detector response at the laser wavelength

k_B = Boltzmann constant

L = Laser cavity length also Mean speckle length

$L_{1,2}$ = Optical path lengths

L_{2-1} = Difference in optical path length

n,m = Integers

p = Phase

p_i = Phase of light at P due to i th scatterer

p_z = Phase due to variation in z

q = Phase shift

r = Incident beam radius also

Detector radius

r_i = Distance from the i th scattering point to P

r_{ill} = Radius of the illuminated region of the target

r_o = Radius of illuminated point on target surface

r_{sp} = Speckle radius

r_w = Beam waist radius

r_z = Beam radius at a distance z from the waist

R = Speckle viewing distance also

Resistance and

Beamsplitter reflectivity

R_d = Beam waist to detector distance

R_{opt} = Optimum beamsplitter reflectivity

S = Discrepancy between focal length and waist

position

t = Time

t_m = Measurement time

T = Beamsplitter transmissivity also

Absolute effective carrier temperature

2u,2v = Rectangular detector dimensions

v	=	Relative velocity between source and observer (Target velocity)
$\underline{v}$	=	Velocity vector
v_b	=	Background velocity
$v_{i,s}$	=	Components of sound wave velocity in the direction of the incident and scattered beams
v_{max}	=	Maximum target velocity
v_t	=	Target velocity
$v(t)$	=	Time varying target velocity
$V(A_p)$	=	Variance in A_p
w	=	Detector width
x_i, y_i, z_i	=	Cartesian coordinates of the i th scattering point
X,Y,Z	=	Cartesian coordinates of viewing point P
z	=	Axial distance from beam waist
λ	=	Optical wavelength
λ'	=	Doppler shifted wavelength
λ_s	=	Sound wavelength
$\lambda_{1,2}$	=	Wavelengths of adjacent laser modes
ρ	=	Target reflectivity

laser in 1960 provided a near monochromatic high intensity light source with a well defined beam which allowed devices based on the optical Doppler shift to be developed. The extraction of the optical Doppler signal is achieved by mixing the detected signal with a part of the original laser output containing no Doppler shift. This results in a constant component corresponding to the levels of illumination due to the two beams being mixed and a time varying term at the Doppler frequency which contains the information about the target motion. The process of optical mixing has the additional advantage of incorporating inherent gain of the signal. The strength of the resulting signal depends on good co-alignment of beam directions and wavefronts of the two signals being mixed, but these parameters have no effect on the detected frequency, making this an ideal method of extracting the Doppler signal.

Laser Doppler (L.D.) devices have found wide application in the field of fluid dynamics, where they provide an ideal non-invasive method of measuring the flow velocity. The two basic requirements are that there are sufficient scattering particles present in the flow to generate signals, and that the fluid is transparent to the laser beam. The field has been covered comprehensively in books by Durst, Melling and Whitelaw (1981) and more generally by Drain (1980), who also makes some comments on solid target motion monitoring. The development of L.D. devices for measurements of solid target motion has been slower than that of the anemometric

devices. This is almost certainly due to the existence of closely related interferometric techniques which rely on co-operative reflection, i.e. the presence of a retroreflector on the target to make very precise measurements of motion. This has restricted the field of L.D. applications to those situations where a well behaved retro-reflecting surface can not be guaranteed. This includes situations where there may be significant lateral and rotational motion of the target, or where the target is contained within a hostile environment where inclusion of a reflector is not possible. L.D. devices have been reported for the measurement of rotating machinery and of sheet and bar formed materials in continuous production lines. Under these conditions there are few suitable alternatives to Doppler techniques.

The current state of laser Doppler research indicates that most of the work is in the anemometric field. However L.D. based solid target monitoring devices are being developed at the Institute of Sound and Vibration Research at Southampton University. Commercially a vibration measuring device is marketed by Dantec, a commercial company which is also involved in research in the field.

1.2 The Research Project

The research project was instigated with the long term aim of applying laser Doppler techniques to positional control loops in robotic systems operating in unco-operative

environments. A primary step towards this is to establish a reliable technique to extract both the magnitude and the direction of motion of an unprepared target using the most economic methods. It was this that the project set out to achieve.

Investigation was directed to a phase based sense detecting technique in preference to the more widely used frequency offset methods because it would require only passive optical components and relatively simple signal processing, rather than the expensive acousto-optic frequency shifting components with their associated electronics and driving circuitry.

Ideally the project should cover measurement over unspecified displacements of the target in three dimensions. In order to measure unconstrained motion it would either be necessary to track a feature of the target, or to fill the working volume with a wave field. Neither of these options were considered to be viable within the available budget. Therefore the research project had to be restricted to the study of motion in a single dimension.

Initially no constraint was applied to the range of target motion to be measured, however in practice limits had to be set to allow optimisation the intensity and speckle size of the scattered light field at the detectors. There were two possible solutions, either increasing the laser intensity and keeping an open ended range, with the associated increase in optical radiation hazard, or using beam manipulating optics to control the size of the beam

delivered to the target over a fixed maximum axial range. The requirement of a single mode laser restricted the available laser power resulting in the choice of a finite range and the use of beam forming optics.

The work presented here is based on the research of others having a bearing on this project and developes the theory of the device, then covers the design, modification, testing and assessment of a polarisation based motion sensing laser Doppler interferometer (LDI) to monitor the paraxial motion of solid targets.

2. LITERATURE REVIEW

2.1 The Doppler Effect

Readers without experience of laser Doppler techniques are advised to read chapter 3 before reading this chapter. This review has been summarised in a paper by Pleydell and Birchenough (1985).

2.1.1 The History of the Doppler Effect

The Doppler effect was first proposed by Christian Johannes Doppler, after whom it is named, in a paper which he presented to the Royal Bohemian society of Learning in 1842. The paper was entitled "On the Coloured Light of Double Stars and other Heavenly Bodies",and whilst it correctly explained the effect, it did not provide the correct explanation for the colours of stars, (White 1982). Until the advent of the laser in 1960, the optical Doppler effect was only observed in astronomical investigations, where the velocity between source and observer are sufficiently large to allow spectroscopic measurement of the shift. It was this astronomic Doppler shift which allowed Hubble to propose his expanding universe theorem, (Open University 1979).

Michelson was relying upon the Doppler shift between light travelling parallel and transversely to the ether in his famous experiment to show its presence. The experiment failed because of the relativistic compensation that occurs, (Born and Wolf 1959, p.301).

2.1.2 Existing Laser Doppler Devices

This section is not intended to be an exhaustive survey as the field of laser Doppler anemometry (LDA) has become large. The references included here are some of the more important in the development of laser Doppler based devices.

The advent of the laser in 1960 provided the first quasimonochromatic light source of sufficient intensity to allow measurement of the optical Doppler effect in light scattered from from relatively slow moving target objects. In most L.D. devices the Doppler shift in light scattered by the target is found by mixing with a beam at a different frequency. The first such device was reported by Yeh and Cummins (1964). Their device (figure 2.1 a) was designed to measure the flow velocity of a transparent fluid. The laser beam is divided into two parts; one is directed into the fluid and illuminates the scattering particles within it. The other passes around the outside of the flow tube and is combined with the light scattered by the particles at the detector, where optical mixing occurs. The addition of small polystyrene spheres ensured sufficient light scattering particles were present in the flow to provide a signal. The most interesting part of this work is the inclusion of a frequency shifting device into the reference arm. This provided a frequency offset, which in this case was used to ensure that the signal at the detector was well removed from d.c., enhancing the post detection processing.

The frequency shifting device was novel, and did not feature in many subsequent laser Doppler experiments. In the light of previous material published by the authors (Cummins and Knable 1963, Cummins et al 1964), it is tempting to suggest that they developed the laser Doppler device as a spin-off from research into diffusion broadening of light by Rayleigh scattering.

Although Gould et al (1964) presented results from optical mixing using light scattered from a rough surface, the scattering target was only driven through an extremely small amplitude. Their interest was in the spatial distribution of phase in the scattered light field, not in the Doppler effect.

Kroeger (1965) reported the first Doppler measurements from a moving optically rough target. Particular details of measurements are sparse, but he indicates the necessary conditions to allow use of light scattered by optically rough targets. The device was based on a Michelson interferometer with focussing optics controlling the size of the illuminated region of the target. Measurements were taken from white paper targets at over 10 m. range, and from semico-operative targets at over 40 m. range, both in a dark environment.

Much of the early work in the field of laser Doppler devices lay in the development of anemometers, possibly because in many situations interferometers could be used to measure solid target displacement, so there was less demand for other techniques.

Foreman et al (1965 and 1966) carried out a wide range of investigations into fluid flow measurements, (figure 2.1 b). In this optical configuration all the laser output was directed into the medium being measured. Doing this ensured that the maximum scattering intensity was achieved, with the unscattered light continuing through the medium, to act as the reference beam on emerging. No frequency shifting was used in this work, reliance being placed on a stable flow giving a constant Doppler shift. Sufficient scattering particles present in the flow gave a continuous signal, allowing the phase locked loop based signal processor to maintain its lock state. A more rigorous analysis of this work is given by Davis (1968), who assesses the effects of specific parameters such as measurement volume dimensions and beam divergence on the accuracy of the results. In 1969 Watson, Lewis and Watson published a general view of the state of LD devices both for anemometric and solid target velocity measurement. This paper also covered some of the requirements of the signal processing for Doppler signals.

Goldstein and Kreid (1967) suggest an alternative geometry for a two beam LDA, in which the laser output is divided, and both parts of the beam are directed into the scattering medium. The unscattered light from one beam is heterodyned with light scattered and therefore Doppler shifted, from the other beam.

The principle of this device is that the unscattered beam

contains no Doppler shift so on combining with light scattered from the second beam into the propagation direction of the first beam and therefore containing a Doppler shift if the scatterers are in motion, the Doppler signal can be recovered. Optically this is the converse of the device described by Foreman above.

A major advance is due to Rudd (1969) who initiated the interference fringe model, (figure 2.1 c). Two beams intersecting in the flow medium generate a virtual fringe pattern at the region of intersection. This virtual fringe pattern is scattered by a transitory particle and is visible at the detector. This technique now forms the basis of most commercially available laser Doppler anemometers, the exceptions being some of the optical fibre based devices. It is also widely used in the measurement of transverse motion of solid targets. An advantage of this method is that as the two beams forming the virtual fringes can be arranged to travel similar path lengths so that it is possible to make flow measurements with white light virtual fringes. The constraints on white light devices are considerably more rigorous than for similar LDAs. White light differential Doppler devices have been reported by Schwar (1971) and Wang (1973). Schwar gave the necessary conditions for beam geometries and employed masks to form and regulate the beams in his device, while Wang employed a diffraction grating in the same role.

By this time the principles of anemometric devices are well established, and the published work since about 1970 shows

an emphasis on applications, particularly in the medical field. Vlachos and Whitelaw (1974) demonstrate a dual beam device for measuring simulated blood-flow velocity. In 1975 Tanaka and Benedek used an optical fibre as a catheter to make in vivo blood flow measurements. This device uses the light reflected from the far end of the optical fibre as a reference beam, which is mixed with light scattered back into the fibre from its environment. Feke and Riva (1978) report a device for measuring the flow of blood in retinal vessels of the eye. Other biological applications included the measurement of vibrations of membranes in the ear (Nokes et al (1978)) using a frequency shifted reference beam device, and by Dragsten et al (1976) who employed a phase compensation device, because the magnitude of the membrane vibrations is less than the displacement required to give optimum fringe variation at the detector.

The introduction of optical fibres also allowed the measurement head to be remote from the rest of the equipment. Perhaps the most comprehensive use of optical fibres in a laser Doppler device is by Knuhtsen et al (1982) who demonstrated a laser Doppler anemometer. This used a polarisation preserving fibre to deliver two orthogonally polarised beams, one of which contained a frequency shift, to a measuring head where the two beams are separated and focussed to cross in the fluid medium. The scattered light was gathered by a multimode fibre and directed to the detector.

Laser Doppler anemometers are currently available from several commercial sources. The majority of these are based on the two beam technique of Rudd (1969).

2.1.3 The History of Solid Target Motion Measurement

The first specific measurements of the motion of a solid target are those of Kroeger (1965), who was mentioned above. Subsequently Foster (1967) investigated four optical methods for measuring the motion of a solid surface. Two of these were based on the Mach Zehnder interferometer, with one using reference beam frequency shifting. The other two methods were based on amplitude modulation of the laser output at microwave frequencies with electronic demodulation to extract a Doppler shift in the modulation frequency. The direct optical carrier Doppler techniques were found to be most suitable.

A Michelson based LDI was developed in 1968 by Botcherby and Bartley-Denniss for length and velocity measurement. Polarisation control was used to increase the optical efficiency and protect the laser cavity from destabilisation. A two beam version with both beams incident at equal and opposite angles to the moving surface allowed compensation for angular misalignment between illumination direction and target direction. It was able to measure speeds from 10 mm/s to 2.5 m/s with an accuracy of 0.1%.

Truax, Demarest and Sommargren (1984) also reported a laser Doppler device for measuring the length of moving surfaces, (figure 2.1 d). It is essentially a dual beam device, and has some interesting features. It incorporates a novel frequency shifting mechanism, based on a periodically driven retroreflector, and employs orthogonal polarisation components to form two superimposed measurement regions from which two sets of signals are derived. Using signal differencing of the two detected signals such as was proposed by Bossel et al (1972), the effects of amplitude fluctuations common to both signals can be reduced. Because dual beam devices normally have a restricted depth of field this device also incorporates cylindrical beam focussing to increase the depth of the measurement region to accommodate out of plane movement of the surface being measured, also increasing the frequency resolution of the device. The frequency shifted beam is also monitored independently to provide accurate demodulation of the detected signal. This device measured velocities up to 40 m/s with an accuracy of 0.4%, with higher accuracy possible for lower velocities.

An interesting derivative of the Doppler principle was used by Barker and Hollenbach (1972) in work on large accelerations. Scattered light was heterodyned with itself after a delay introduced by a variable optical path length. The resulting signal is the average change in velocity over the delay period, that is, the average target acceleration. The device was used for impact studies on armour plate.

In similar measurements in 1983 Kaplan, Maron and Katzir used a scaling technique in measuring rapid accelerations to high velocities. Two scattered beams taken from the target were heterodyned together, the resultant detected frequency being the difference in the two Doppler frequencies seen by the two beams. By adjusting the angles between the two beams derived from the target the detected signal could be scaled according to the target velocity to be measured. Adjustable optical path lengths ensured that synchronous signals were being heterodyned. The device is reported to have measured velocities up to 400 m/s over limited travel.

Eberhardt and Andrews (1970) reported a frequency shifted LDI to measure small vibrations. Since these vibrations are small they modulate the phase rather than the frequency of the scattered light. Examination of the frequency spectrum of the detected signal allows the form of the vibration to be determined. The reference beam phase of this LDI was adjustable to maintain operation at the optimum sensitivity.

Buchhave (1975) described a vibration measuring device which is a reference beam system with frequency shifting to allow sense of motion discrimination. In common with the work of Truax et al (1984) dual detectors are used in this device to reduce common mode noise. The device is designed to measure the axial component of target motion, with polarising optics in the beam illuminating the target to increase the optical efficiency. The coherence length of

the laser used in this device imposed the need for careful positioning to achieve maximum sensitivity.

The introduction of optical fibres allowed a new generation of laser Doppler devices to be developed. The fibre optic catheter of Tanaka and Benedek (1975) has already been mentioned. The earlier devices shared a common feature of relying on the fibre as a means of delivering and collecting light allowing the measurements to be made by a probe at points remote from the main laser Doppler equipment. Cookson and Bandyopadhyay (1978) used a fibre probe to measure the vibration of simulated turbine blades. Ueha et al (1977) went to extremes in linking all the active components in a laser Doppler system with optical fibres.

One of the limiting effects of introducing optical fibres into laser Doppler devices is that the maximum possible working distance between the end of the fibre and the target is reduced. This may be overcome to some extent by focussing the emergent beams (Kyuma et al 1981). One of the more beneficial features of optical fibres is that reflection from the far end of the fibre provides an ideal reference beam. This was found by Tanaka and Benedek (1975) and developed by Dyott (1978) to improve the optical efficiency. Unfortunately this precludes the introduction of a frequency shift into the reference beam for sense detection.

Most of the laser Doppler devices mentioned here use a HeNe gas laser to provide the initial beam at 632.8 nm, with some of the reported systems using an argon ion laser. The semiconductor laser diode offers a good alternative to the gas laser because of its smaller size and lower power requirements . The main difficulty in using this source appears to be its vulnerability to re-entrant light which disturbs the laser stability. Nishihara et al (1984) proposed to overcome this difficulty by using a polarisation preserving fibre to isolate the laser diode from light returning down the probe fibre to a laser diode based Doppler velocimeter. Kersey et al (1983) used a laser diode with a ramped drive current and hence a ramped frequency output injected into an unbalanced interferometer to simulate a heterodyne device. By using an unbalanced interferometer the two beams passing through the device have different propagation times. Consequently when recombined they also have different frequencies. Any change in the optical path length of either arm of the device results in a change in the detected frequency around the null value. The resolution is limited by the duration of the ramp signal and the depth of modulation of the laser output.

Lewin et al (1985) report a vibration monitor which is based on a null detection method. The phase of the signal transmitted through an optical fibre is varied by stretching the fibre using a piezo-electric element, such that the interference state at the detectors resulting from

mixing of the light scattered from the target and the reference remains constant. If it changes then a derived signal from the detectors adjusts the reference phase. In this way the signal driving the reference beam phase mimics the vibration of the scattering surface. There is a maximum amplitude of motion that can be accommodated, depending upon the maximum phase adjustment of the reference path. This method also requires that the variation of the reference phase is linear with the piezo-electric control signal for efficient operation.

The main applications of LD methods for solid target monitoring have been in hostile or difficult conditions where reliable specular reflection cannot be ensured. The devices reported by Bothcherby and Bartley Denniss (1968), and by Truax et al (1984) were both designed to measure the length of hot steel in an industrial environment. The measurement of vibration in rotating machine components is a particularly difficult problem, and more so if transducers cannot be mounted directly onto the rotating component. Markho, Smith and Lalor (1980) have measured slip in the rollers and cage of a roller bearing while Davis and Kulczyk (1969) and Cookson and Bandyapadhyay (1980) examined turbine blade vibration by laser Doppler techniques.

Halliwell, Pickering and Eastwood (1984) report a device for measuring the torsional vibrations of rotating shafts. It is essentially a Michelson based device, using

backscatter from two different points on a circumference of the rotating component. The difference in Doppler frequency between the two signals varies as the velocity between them changes, as would occur in torsional vibration.

2.2 Physical Principles of LD Devices

2.2.1 Light Scattering by Solid Targets

In making laser Doppler measurements from a solid target it is assumed here that the target surface is optically rough. Where this is not the case the situation becomes one of optical interferometry, which has been widely covered (for example Born and Wolf 1959, ch.7).

Some of the work cited below may appear to have a tenuous link with laser Doppler measurements; however, it is implicit in LD work that the target surface cannot be prepared to give ordered scattering, otherwise interferometric techniques could be used with greater signal strengths and reliability. Consequently it is desirable to know as much as possible about the way in which light is scattered by a rough surface, as this dictates the nature of the optical system and the quality of the results.

A rough surface illuminated by a monochromatic beam acts as a collection of small scattering points, each with random phase and amplitude. This gives rise to a complex interference pattern at any observation plane above the target surface. The most important property of this scattered, or speckle, field is the size of the regions across which it can be assumed that the distribution of intensity and phase are approximately constant and therefore may be treated interferometrically. This is the subject of books by Francon (1979) and Dainty (1984), both

of whom deal with the speckle field as a whole. The requirements of laser Doppler devices are more restricted, in that they need knowledge of the size of the invariant regions in the speckle field, and of the variation in speckle size as the viewing and illumination conditions alter with changing target position.

Measurements by Gould et al (1964) showed that the phase of the light scattered by an optically rough surface varied randomly as the target was moved transversely to the illuminating beam. The transverse spatial resolution of the measurements gave some indication of the phase and, by association, the intensity variations in the scattered field. A greater interest was shown in constructing a theoretical model of the scattering process from a surface with specified characteristics. Massey (1965), provides a model for the behaviour of two types of surface, characterised only by the mean size of the scattering points. This model does not include the effects of polarisation, but gives optimum conditions for heterodyne detection with the scattered light in both cases.

In 1967 Beckmann produced a comprehensive analysis of scattering by rough surfaces using a similar approximation to Massey, that the scattering regions have large radii of curvature. His analysis of depolarisation is somewhat tentative, requiring surface normals in the direction of illumination, which makes analysis of depolarisation of normally incident illumination difficult. Gasvik gives an

assessment of depolarisation during scattering by rough surfaces, which is both theoretical and experimental, in two papers submitted simultaneously (1980, 1981). The theory is based on a tangent plane approximation to the slope of the surface at the point of illumination, with an rms slope being one of the characteristics of the surface. It predicts that in some situations the highest intensity scattering will occur in the non specular direction. Results from the experimental work show that the effect only occurs for non normal beam incidence on the surface, and that for normal incidence, the parallel polarisation is most strongly scattered in the specular direction. This is of a direct relevance to this research, where it is required that there is strong scattering of light polarised parallel to the illuminating beam to allow phase based sense of motion detection.

The distribution of intensity across the speckle field, which relates to the probability of obtaining a good signal, has been examined experimentally by Ebeling (1979) and Steeger (1983). Both give results showing the predicted negative exponential distribution of intensities. The measurements due to Ebeling are polarisation independent, whilst those of Steeger show the effect of partial polarisation of the speckle field.

Much of the practical interest in speckle is due to the fact that it derives from a rough surface and therefore may be used to characterise that surface. Younes et al (1984) give results showing the spatial autocorrelation functions

and variation in intensity of the scattered light field derived from a number of machined surfaces, which are considered to be typical of the targets likely to be encountered in many measuring situations. Welford (1977) covers the area of surface roughness measurement by optical techniques in a review article, and Dainty (1984, ch.8) has a chapter on this application of laser speckle. Both of these latter sources give a more general indication of the way in which surface and light fields are related.

2.2.2 Extraction of Doppler Signals

The extraction of the Doppler shift from the optical carrier frequency is most easily achieved by mixing the signal beam with part of the original carrier. This optical mixing process is known alternatively as heterodyning or coherent detection, and is an essential part of most laser Doppler devices. The process is an extension of optical interference and is described in several texts, (see for example Drain (1980), Durst, Melling and Whitelaw (1981) and Yariv (1985)).

The optimum conditions for heterodyne detection with light scattered by an optically rough surface have been described by Massey (1965) for two different types of scattering surface under different viewing conditions. A clear explanation of the requirements for optical mixing of well ordered or predictable beams is due to Siegman (1966), who also covers the case of scattering particles suspended

within a medium, such as occurs in LDA. He states it is essential that the phase difference between the two waves being mixed is less than a given value for all points on the detector surface common to both beams. This has the effect of applying limits either to the curvature or inclination of wavefronts in both beams at the detector surface. This may, in turn, require control of the size of the active area of the detector.

The quality of the signal resulting from heterodyne detection is discussed by Oliver (1961) and Haus and Townes (1962), who show that if the geometric requirements are met then the signal to noise ratio in the detected signal approaches a theoretical limit, with the assumption that the thermal noise contribution from the detector is small. The implicit gain associated with the magnitude of the reference signal is mentioned, but the more practical effect of increased d.c. levels at the detector with a corresponding loss of visibility of the time varying signal receives no comment.

2.2.3 Sense of Motion Recovery from Doppler Signals

In many situations where measurements are made by a laser Doppler device both the magnitude and the sign of the Doppler shift and hence the sense, or direction, of the target velocity are required. There are various ways in which the sense of motion can be recovered from the detected signal. Of these, the majority are based on the

introduction of a deliberate frequency shift into one beam of the system. There are various ways in which this frequency shift can be introduced. The laser Doppler anemometer of Yeh and Cummins (1964) used an acousto-optic or Bragg cell (reported separately by Cummins and Knable (1963)), in the reference beam to provide the frequency offset needed to allow discrimination between increases and decreases in the signal frequency. This technique has the advantage of providing an electronic drive signal at the induced offset frequency, by which the detected signal can be demodulated. Early cells used water as the acousto-optic medium with the acoustic wave being generated by a piezo-electric transducer. The main problem with these is that the transducers can only be driven efficiently at their fundamental frequency, or harmonics of it. With further work (Alphonse 1975) this was partly overcome. The Bragg cell is widely used and is a common feature of commercially available laser Doppler systems. The theory of Bragg cell operation is given in Yariv (1975) and Levi (1980) amongst others. Electro-optic frequency shifting cells based on the Pockels effect have been used in a similar role by Foord et al (1974), Dubnistchev (1977) and Steele (1981), but have not found wide acceptance in general laser Doppler work.

Suzuki (1967) demonstrates how a rotating radial diffraction grating can be used to introduce a frequency shift into the non zero orders of a diffracted beam of light. This technique was employed by Oldengarm et al (1973) in a dual beam laser Doppler device. A later paper

by Oldengarm (1977) shows how by using phase rather than amplitude gratings there is considerable control over the quantity of light diffracted into different orders according to the specific type of laser Doppler device being operated. This same technique has been used by Velzel (1983).

Somewhat more crudely, a deliberate frequency shift was introduced into the reference beam of a Michelson based LD system reported by Halliwell (1979). This relies upon the light backscattered by a rotating optically rough disk from an inclined incident beam. Transmission through a scattering disk has been used in a similar way by Rizzo and Halliwell (1978).

In using both disk and grating based techniques it is preferable that there should be some independent measurement of the frequency shift introduced to allow reliable demodulation of the detected signal.

Laser Doppler devices have also been reported using a discontinuous frequency shift, usually based on a change in the optical path length of the reference beam. A notable example of this is the length measuring device of Truax et al (1984), and it is also part of the demodulation technique for fibre optic sensors reported by Jones et al (1983).

All these techniques require some knowledge of the induced frequency shift for effective demodulation to be possible. However, it is also possible to discriminate between the

two senses of target motion using offset phase components in the detected signal. The offset components can be selected by spatial methods such as was used by Agrawal and McCullough (1981) and Agrawal and Riley (1984). It is more common though, to make use of the polarisation of the reference beam in conjunction with polarisation sensitive optics to separate two components with a phase difference between them, that is to use temporal seperation. This has been widely used in interferometers, where there is no serious distortion of the signal beam, see for example Bouricious and Clifford (1970), or Downes and Raine (1979). Polarisation has been widely used in laser Doppler systems to enhance optical efficiency and for sense detection in anemometric applications where sets of virtual fringe patterns are generated with a phase difference between the sets of fringes, Bossel et al (1972). However phase based sense of motion detection of solid targets has not found wide favour, although it is mentioned in a paper by Drain and Moss (1983).

It is also possible under certain circumstances to obtain the sense of motion directly from the light scattered by the target. Davis and Kulczyk (1969) measured the vibration of a turbine blade using the overall motion of the blade to provide a macroscopic Doppler shift modulated by the Doppler shift resulting from the vibration of the blade. Where extremely fast target motions are expected resulting in a large Doppler shift it is possible to employ spectroscopic techniques to follow the changes in Doppler

frequency. Two such devices have been reported. Belousov et al (1977) use a Fabry Perot interferometer as a dynamic filter, detuned so as to have a near linear response around the Doppler frequency. The magnitude of the Doppler frequency is found from the voltage used to detune the interferometer. A similar principle is used by Smeets and George (1978) with a Pockels cell being driven to maintain an optimum detection condition, with the correction signal providing a measure of the Doppler signal. Boiko et al (1980) use a wedged multiple pass interferometer to measure the Doppler shift in detected radiation as a shift in the lateral position of the fringe system with changing frequency. A triangular mask increases sensitivity to lateral fringe movement. This technique has a lower velocity resolution than optical mixing methods.

2.2.4 Signal Detection and Processing

The photomultiplier was widely used in early laser Doppler work, but the advent of high quality solid state detectors has led to their inclusion preferentially in many situations as they are inexpensive and do not require a high voltage supply to operate. Photomultipliers still find use where light levels are low because of their inherent multiplication and very low noise. The field of photo detectors is covered comprehensively by Yariv (1985).

Post detection processing and extraction of the Doppler signal is based on a relatively small number of techniques.

The signal differencing suggested by Bossel et al (1972), extends either side of the detection process, using the difference of two independently detected out of phase signals to reduce common mode noise.

Once good analogue signals have been obtained there are relatively few techniques used to extract information. One of these is based on the phase locked loop, in which the phase of a locally generated signal is compared with that of the detected signal, and the difference fed via processing to the local oscillator to adjust its frequency to track the detected signal. The control voltage for the local oscillator provides an analogue signal corresponding to the detected frequency and hence the target velocity. The loop may incorporate part of the optical system, Belousov et al (1977), or, more commonly, be purely electronic, see for example Durao and Whitelaw (1974) or Watson, Lewis and Watson (1969). The Doppler signal frequency can also be measured directly from the frequency spectrum of the detected signal, as in the original laser Doppler anemometer of Yeh and Cummins (1964).

If the target displacement is required, particularly in length measuring systems, fringe counting can be used to approximate integration of the detected velocity signal. Resolution is doubled if zero crossing are used as each fringe makes two zero crossings. This method was used by Downs and Raine (1979) in an interferometric device to achieve eighth wave resolution.

2.3 Other Non-contacting Measuring Techniques

There are several other methods of making non-contacting measurements of small amplitude motion or vibration. A fundamental requirement of any non-contacting technique is that it will use some form of modulation of a field effect. Electric and magnetic fields are used in capacitive and inductive transducers respectively. Both of these devices are restricted in their operational range. The inductive transducer response depends upon the material from which the target object is made, only working with conducting target materials in which an eddy current can be excited. Similarly the capacitive transducer operates more effectively with a conducting target but if calibrated can be made to operate on insulating surfaces. In both cases the measurement is made as an average across a region. These devices only operate effectively up to a maximum range of several millimetres.

Geometric and shadow type displacement measuring devices all depend on spatial resolution of the detectors which generally results either in a limited resolution or a limited range. The change in position of a reflected beam with changing target location is used in a commercially available displacement monitor. However, this device is also vulnerable to changes in target surface inclination, and has a resolution directly related to the range of displacement to be measured. The maximum range of motion is +/- 6 mm with a quoted accuracy of 0.1 mm over this range.

Ultrasonic pulse echo and Doppler effect devices are available commercially. These lack the resolution of optical devices and because of the larger divergence of the acoustic beam, are prone to interference from spurious reflections not deriving from the target. An accuracy of 1mm in 2 m is claimed for the pulse echo technique.

A microwave interferometer has been reported, which by using longer wavelength electro-magnetic radiation, overcomes the effect of roughness in many engineering situations, giving specular reflections. This allows a Michelson type arrangement to be used, (Stone 1970).

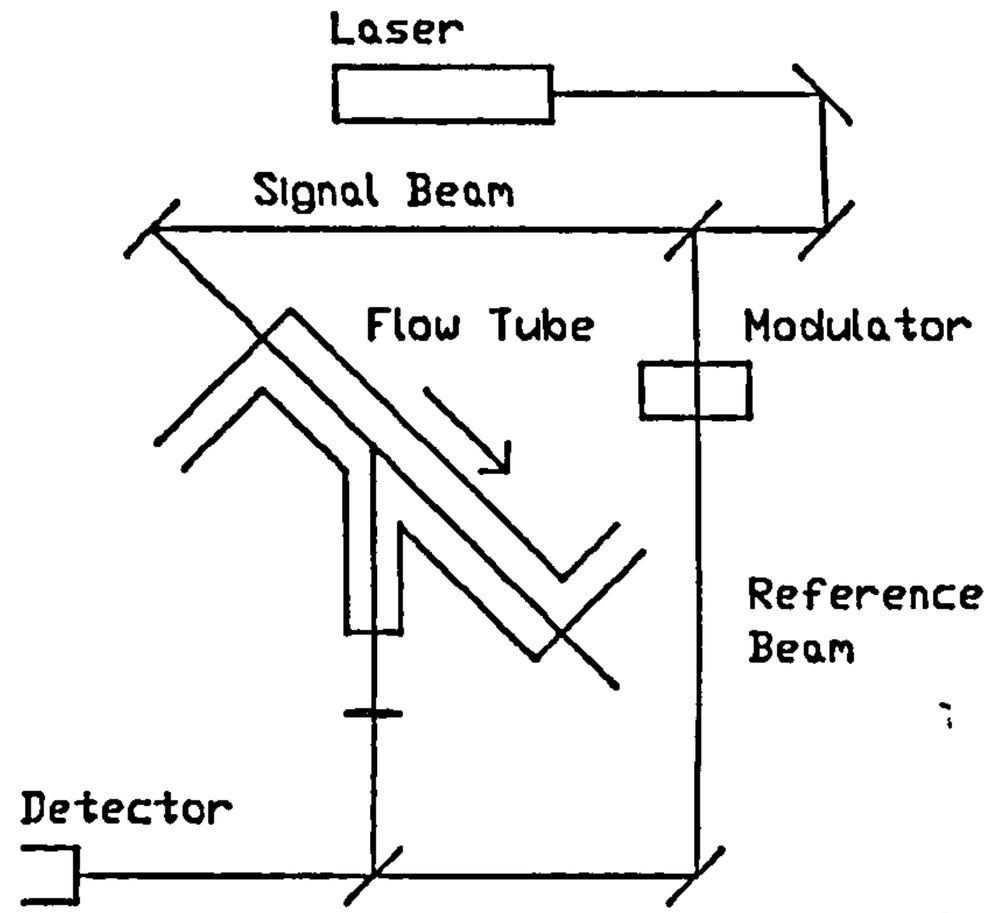

Figure 2.1 a

LDA after Yeh and Cummins (1964)

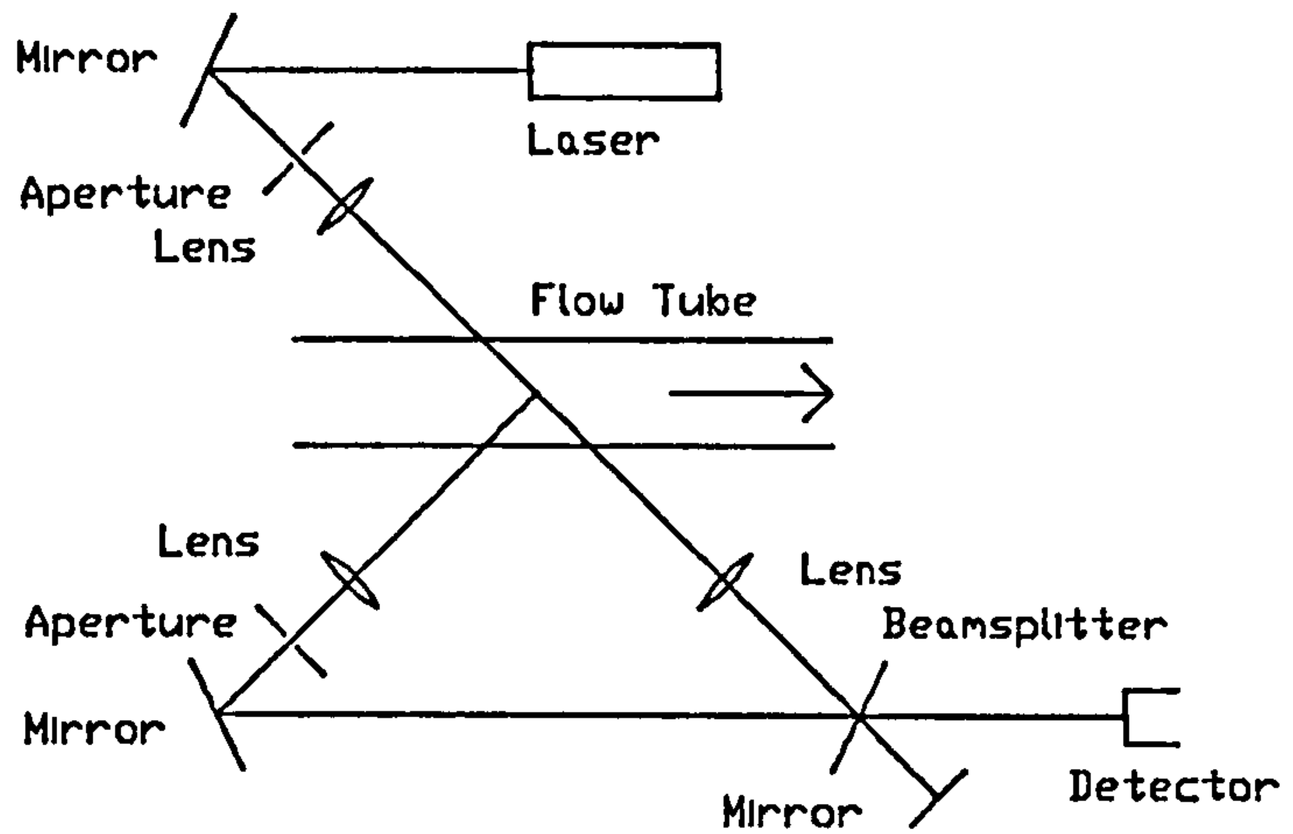

Figure 2.1 b

LDA after Foreman et al (1966)

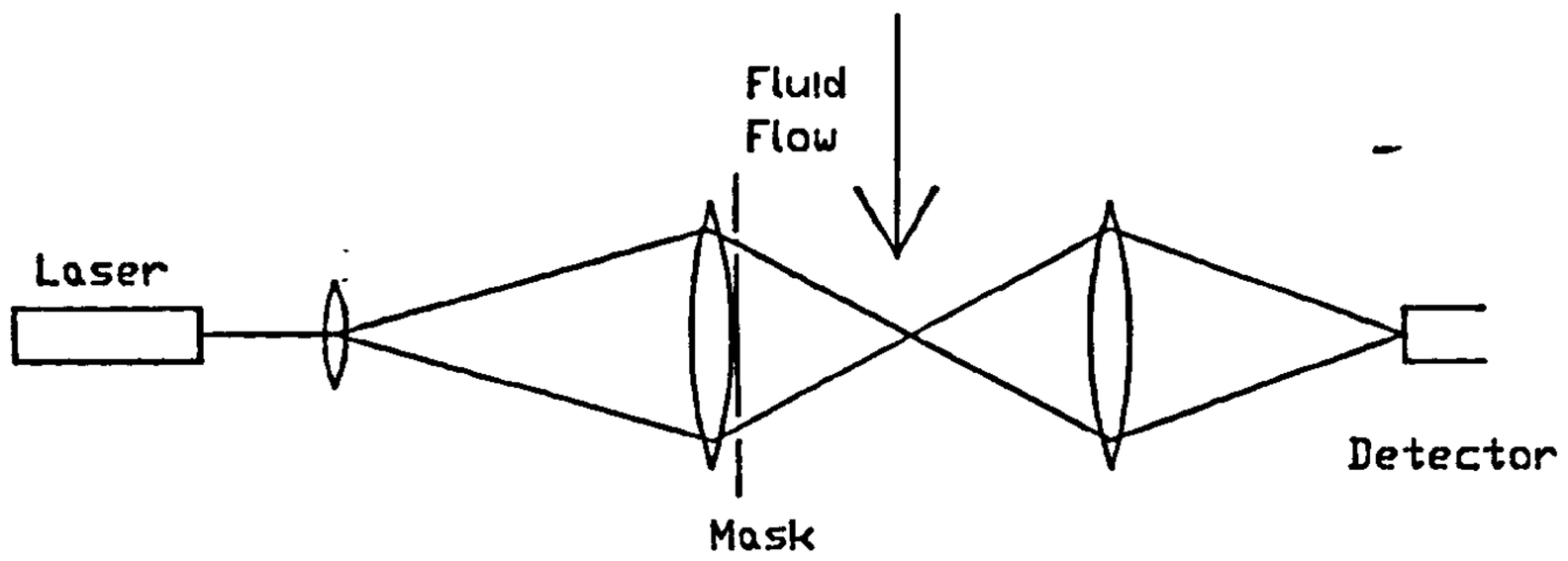

Figure 2.1 c

Dual Beam LDA after Rudd (1969)

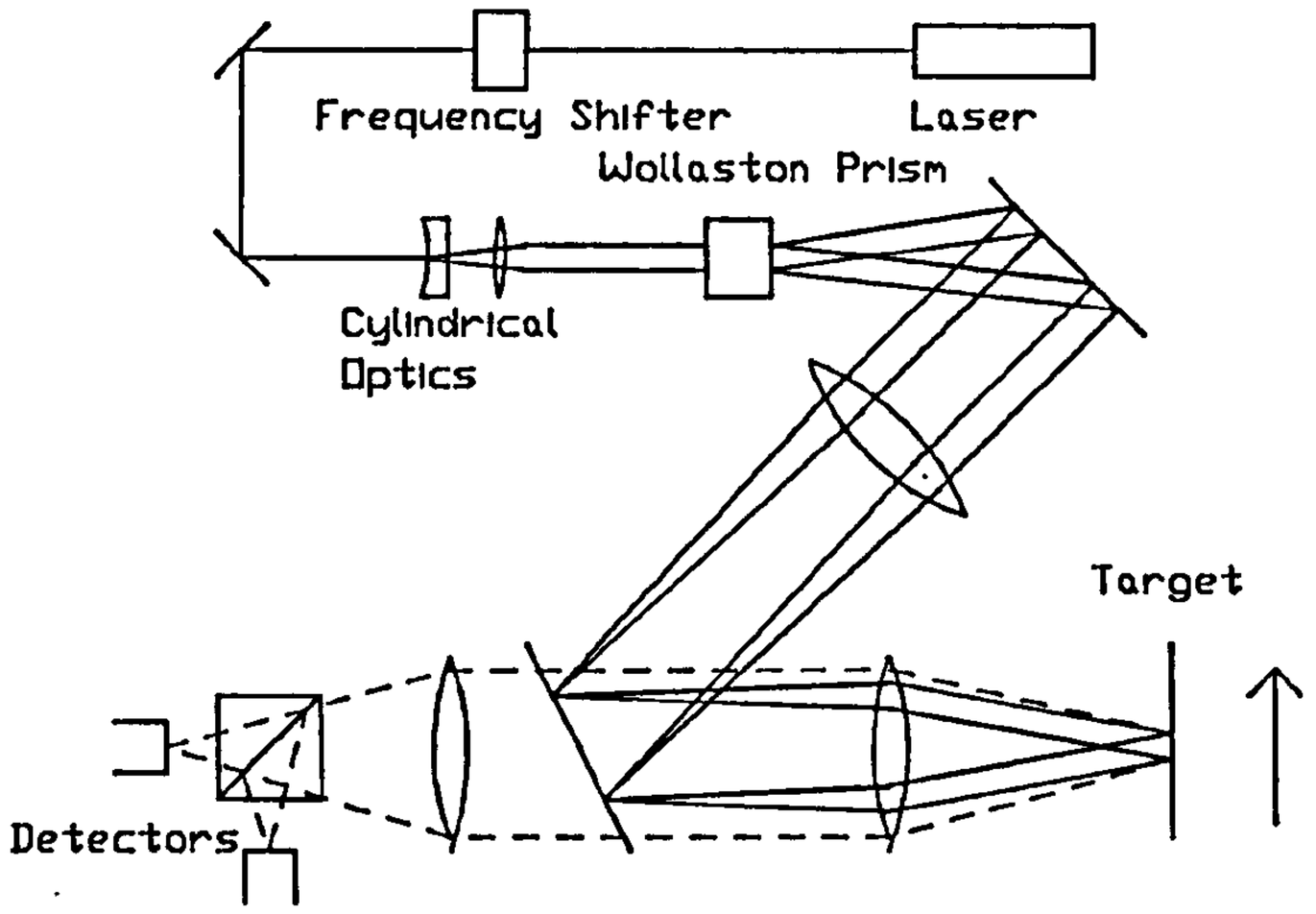

Figure 2.1 d

Velocimeter after Truax et al (1984)

3. THEORY

This chapter presents a theoretical treatment of the physical principles underlying the operation of LD devices, with a particular emphasis on the requirements of the research project. The treatment only extends to the optical part of the LDI. This has been done because it is within the optical part of the system that the signal containing the information about the motion of the target object arises. It is also felt that the operation of the electronic system in extracting the information can more easily be explained in conjunction with descriptions of the equipment which is treated more fully in the next chapter.

3.1 Laser Doppler Theory

This section shows the origins of the Doppler effect, both mathematically and physically, and shows how the Doppler frequency can be detected by mixing the Doppler shifted and original signals.

3.1.1 The Doppler Effect

The Doppler effect is an apparent change in the frequency of a wave field when there is relative motion between the source of the wave and an observer. It was first propounded in 1842 by Christian Johann Doppler, who incorrectly used it to explain the different colours of stars (White 1982), and is derived in many text books, e.g. Levi (1968, p.47).

For a fixed source emitting light at a frequency f_o, with a wave velocity in vacuo of c_o, the wavelength seen by a stationary observer is :-

$$\lambda = c_o/f_o \quad . \qquad (3.01)$$

If the observer approaches the source with a velocity v, the effective velocity of the wave field seen by the observer becomes $c_o + v$. Since the wavelength of the wave is unchanged, the observer sees a frequency f' where :-

$$\begin{aligned} f' &= (c_o + v)/\lambda \quad , \\ &= f_o.(c_o + v)/c_o \quad , \\ &= f_o.(1 + v/c_o) \quad . \qquad (3.02) \end{aligned}$$

When the source approaches the observer the situation is different. The wavelength of the emitted light is shortened. For a source velocity v, the wavelength λ', seen by the observer is :-

$$\lambda' = (c_o - v)/f_o \quad .$$

As the observer sees the wave field at a velocity c_o, which gives a frequency at the observer :-

$$\begin{aligned} f' &= c_o/\lambda' \quad , \\ &= f_o.c_o/(c_o - v) \quad , \\ &= f_o./(1 - v/c_o) \quad . \qquad (3.03) \end{aligned}$$

In physical terms the difference between these two situations is that the waves from a stationary source have a finite distance between them: if the observer moves with

a finite velocity it will take a finite time to move from one wave to the next, which means that a finite frequency is seen. If the source moves, then as its velocity approaches the wave velocity, successive wave fronts are closer together. When the source moves at the wave velocity, all the wave fronts coincide with the position of the source, and there is no distance between them. That is the frequency has become infinite.

The relativistic treatment of the Doppler effect in electromagnetic waves is given in a paper by Temes (1957). The time dilation effect with a magnitude:-

$$1/(1 - (v/c_o)^2)^{1/2} \qquad (3.04)$$

causes a moving source to oscillate more slowly when seen by a stationary observer, reducing the Doppler shift by the time dilation factor above. When the observer is in motion, the clock with which the received waves are timed will run slower by the time dilation factor. When this is introduced into the equations above it gives identical Doppler shifts for both moving source and moving observer cases.

It should be noted that where the source or observer velocities are very much smaller than the wave velocity the difference between the two classical results is minimal. This is of relevance in the operation of the LDI as the Doppler effect occurs twice. The illumination of a moving target by a fixed laser introduces a Doppler shift in the frequency seen by the target. The target then scatters the

light, and in doing so acts as a moving source, with the scattered light being seen by a fixed detector. The resultant frequency seen by the detector for a target with a velocity v, is :-

$$f' = f_o.(1 + v/c_o)/(1 - v/c_o) \quad . \qquad (3.05)$$

As the ratio v/c_o is very small the detected frequency can be approximated as :-

$$f' = f_o.(1 + 2.v/c_o) \quad . \qquad (3.06)$$

In all the above equations, v represents the velocity parallel to the line joining the source and detector. If the target motion is at an angle a to the direction of illumination, the component of velocity parallel to the illuminating beam is v.cos(a), giving a Doppler frequency of :-

$$f' = f_o.(1 + 2.v.\cos(a)/c_o) \quad , \qquad (3.07)$$

or in vector form :-

$$f' = f_o.(1 + 2.\underline{v}.\underline{i}/c_o) \quad , \qquad (3.08)$$

where $\underline{i}$ is a unit vector in the direction of the illuminating beam and $\underline{v}$ the velocity vector.

In practical terms, the change in frequency (or Doppler shift), f_d, of a HeNe beam as a result of scattering from a

target moving parallel to the illuminating beam is :-

$$f_d = f' - f_o$$
$$= 2.f_o.v/c_o \quad . \qquad (3.09)$$

Substituting the output frequency 4.7×10^{14} Hz., and the velocity of light (in vacuo) 3×10^8 m/s gives a Doppler shift in the frequency of 3.16 MHz. for a target velocity of 1 m/s. The corresponding displacement may be found by integration of the velocity signal. This is most easily realised by counting zero crossings of the Doppler signal. Since there are two such crossings for each cycle 6.32×10^6 crossings will occur for 1 m. of target motion. If quadrature based sense detection is employed it is possible to further double this resolution.

The methods used in this project to extract the magnitude and sense of the target motion from the Doppler signal are dealt with in sections 3.1.2 and 3.2.2 respectively.

3.1.2 Heterodyne Detection

The analysis of the heterodyne detection process given below assumes that the laser output is monochromatic. In fact the beam has a definite structure. The effect of the real output of the laser on the detection process is discussed seperately (section 3.4.1).

The main difficulty in detecting Doppler shift in light is that except in the case of extremely large velocities, the magnitude of the frequency shift is small. No existing

photo detectors are capable of measuring optical frequencies directly. Even if they were, the problem of detecting a change of one part in 10^8 is not an easy one. Spectroscopic techniques are not usually viable as they lack sufficient resolution. The most widely used method of extracting the Doppler frequency is optical heterodyning. When two waves at different frequencies are mixed, the resultant contains both sum and difference frequency terms, so by mixing the Doppler shifted light with some of the original beam, a resultant is obtained with a component at the Doppler frequency, which lies well inside the frequency range of current photo detectors, and may be measured.

If the laser output is represented as :

$$A_1 = A_{1o}.\cos(2.\pi.f_o.t) \quad , \qquad (3.10\ a)$$

and the Doppler shifted beam as :-

$$A_2 = A_{2o}.\cos(2.\pi.f'.t) \quad , \qquad (3.10\ b)$$

the result of heterodyning and detection can be found. Here all the A s are signal amplitudes. The mechanism of the detection process must also be incorporated. This process measures the energy delivered to the detector, which is proportional to the square of the signal amplitude, so the output from the detector during heterodyne detection is :-

$$i_d = k.(A_1 + A_2)^2 \quad , \qquad (3.11)$$

where k is the detector response at the laser wavelength.

Substituting for A_1 and A_2 gives :-

$$i_d = k.((A_{1o}.\cos(2.\pi.f_o.t))^2 + (A_{2o}.\cos(2.\pi.f'.t))^2 + 2.A_{1o}.A_{2o}.\cos(2.\pi.f_o.t).\cos(2.\pi.f'.t)) \quad (3.12)$$

The first and second terms on the right hand side of equation 3.12 both behave similarly. The current at the detector due to the first term is :-

$$i_{d1} = k.A_{1o}^2.\langle \cos^2(2.\pi.f_o.t) \rangle \quad . \quad (3.13)$$

The angular bracket represents the time average due to a signal frequency exceeding the maximum response frequency. The value of the time average of the term in the bracket is 1/2, so the intensity is :-

$$i_{d1} = k.A_{1o}^2/2 \quad . \quad (3.14)$$

The second term of equation 3.12 gives a similar expression:-

$$i_{d2} = k.A_{2o}^2/2 \quad . \quad (3.15)$$

Neither of these contain any information about the Doppler shift. The third term of equation 3.12 gives a time varying current at the detector of :-

$$i_{d3} = k.A_{1o}.A_{2o}.(\cos(2.\pi.(f_o + f').t) + \cos(2.\pi.(f_o - f').t)) \quad . \quad (3.16)$$

The first term in this equation is also at a frequency

greater than the detector range, and averages to zero, but the second term, which contains the Doppler shift, f_d, lies within the detector response. This gives the a.c. output of the detector as :-

$$i_{ac} = k.A_{1o}.A_{2o}.\cos(2.\pi.f_d.t) \quad ,$$
$$= i_o.\cos(2.\pi.f_d.t) \quad , \qquad (3.17)$$

where i_o is the peak a.c. current.

The main implication of this result is that the detected signal does not depend only on the scattered light intensity, but also on the reference beam intensity. In this way heterodyne detection can be thought of as an amplifying process. As with any signal processing system, the quality of the input signal determines to a large extent the quality of the output. Consequently, considering the heterodyne process as the first stage of the signal processing, the signal to noise ratio in the detector output is of importance. An analysis is given in appendix 1, with the result that the signal quality improves with increasing reference beam intensity. However as the reference beam intensity is increased the d.c. contribution to the detector output is also increased, which causes a decrease in the visibility of the Doppler signal, and also drives the detector closer to saturation. Consequently there is an optimum reference beam intensity, which depends on the detector characteristics.

It has been assumed in the above derivation that the two beams being mixed have parallel polarisations. For

heterodyning between two linearly polarised beams with an angle b between their directions of polarisation the time varying signal at the detector output falls by a factor cos(b). This assumes a polarisation independent detector, and uses one polarisation direction as a reference. The other beam makes an angle b to the reference, so has a component of amplitude A.cos(b) in the polarisation direction of the reference. Since each amplitude occurs linearly in the expression for the a.c. output of the detector, equation 3.17 above, the output signal will vary as cos b. The conditions for interaction of beams with different polarisations are the Fresnel Arago conditions, see for example Born and Wolf (1959).

It is also possible to treat the situation where light scattered from a moving target is mixed with light from a reference beam as a two beam interference problem. This examines the difference in optical path lengths between the two beams, and derives the intensity at the detector from the phase difference that results from this path difference. If the beam amplitudes are A_{1o} and A_{2o} for reference and signal beams respectively, then, if the optical path lengths are L_1 and L_2, the signal level seen at the detector is :-

$$i_d = k.(A_{1o}.\cos(2.\pi.L_1/\lambda) + A_{2o}.\cos(2.\pi.L_2/\lambda))^2 \quad .$$

$$= \text{d.c. terms} +$$

$$2.k.A_{1o}.A_{2o}.\cos(2.\pi.L_1/\lambda).\cos(2.\pi.L_2/\lambda) \quad . \qquad (3.18)$$

Resolving the cosine terms gives :-

$$i_{ac} = i_o.\cos(2.\pi.L_{2-1}/\lambda) \quad . \qquad (3.19)$$

L_{2-1} is the difference between optical path lengths. Taking equation 3.09 and substituting $1/\lambda$ for f_o/c_o ,

$$f_d = 2.v/\lambda \quad . \qquad (3.20)$$

On substitution into 3.17 this gives :-

$$\begin{aligned} i_{ac} &= i_o.\cos(2.\pi.t.2.v/\lambda) \quad , \\ &= i_o.\cos(4.\pi.v.t/\lambda) \quad . \qquad (3.21) \end{aligned}$$

Since light travels both to and from the target, a target velocity v changes the optical path length at twice this rate, i.e. :-

$$dL_{2-1}/dt = 2.v \quad . \qquad (3.22)$$

Substituting for v in equation 3.21 ,-

$$i_{ac} = i_o.\cos(2.\pi.t.(dL_{2-1}/dt)/\lambda) \quad . \qquad (3.23)$$

Comparing this with equation 3.19 shows the main difference is that the Doppler treatment of target motion is a rate dependant equivalent of the interferometric treatment. The Doppler treatment has been used in this analysis, as the original intentions were velocity measurement; however in the interests of assessing the LDI when constructed, fringe counting was used. This is effectively an integration of the Doppler frequency to give the displacement of the target object. Reasons for this are given in chapter 4.

3.1.3 The Coherence Condition

To achieve efficient heterodyne detection, it is not sufficient to arrange that the two beams to be mixed are incident on the detector surface. Heterodyne detection requires geometric coherence between the two beams. That is, that wavefronts of the two beams are exactly superimposed across the detector surface. This is necessary because the detector output is the average of the intensity across its surface.

For the case of two plane wavefronts, one parallel to, and the other at an angle, a, to a detector surface of width w, the path difference between the wavefronts across the detector is :-

$$d = w.\sin(a) \quad . \qquad (3.24)$$

This corresponds to a phase difference of :-

$$p = 2.\pi.d/\lambda \quad . \qquad (3.25)$$

Consequently, if the path difference is only half a wavelength, the signals will be in phase at one edge of the detector, and out of phase at the other. In the case of Doppler detection, where the two beams are of different frequencies, the intensity changes across the entire detector surface periodically, but if the misalignment is present then at all times the phase difference of half a wavelength will be present across the detector surface. That is, there will be no net change of intensity across

the detector face, so the detector output will remain constant with the signal being lost. The same effect will occur if the wavefronts are of different curvatures, or have radii of curvature sufficiently small to cause significant path length differences across the detector. The exact conditions for coherence were first proposed by Siegman (1966); however it is necessary to minimise path difference effects between the two wavefronts at all points across the detector to achieve optimum signal strength.

Within the LDI the coherence condition is of particular importance, as the signal is contained within the speckles, (see section 3.3.1), in the scattered light from the target. There is no correlation of phase between adjacent speckles, so the presence of more than one speckle on the active region of the detector must be avoided, as this will degrade the quality of the detected signal. This was achieved in the LDI reported here by focussing the reference beam to a small spot on the detector surface in a way similar to that used by Read and Fried (1963). Heterodyne detection can only occur when two beams mix, so by focussing the reference beam, the effective area of the detector is reduced to be similar to the speckle size. This increases the tolerance to misalignment or wavefront curvature in the signal beam. The wavefronts at the waist of the focussed reference beam are planar, which means that the radius of curvature of the wavefronts in each speckle must become small before a significant phase difference can occur to upset the coherence condition.

3.2 Sense Detection

In many situations it is desirable not only to find the magnitude of the motion of the target, but to be able to identify the direction of motion. Information about the direction is carried in the Doppler shifted beam, with a receding target giving a decrease in frequency from the stationary situation, and an approaching target giving an increase in frequency. This information is lost when the signal is heterodyned with the original beam as it is the difference in frequency that modulates the intensity at the detectors. Methods of overcoming the problem are discussed below.

3.2.1 Frequency Shifting

The most widely used method of extracting the sense of motion from a Doppler signal is based on the deliberate introduction of a known frequency shift into the reference beam with which the signal beam is mixed. This technique was used in what is widely regarded as the first reported laser Doppler work, that of Yeh and Cummins (1964) and subsequently in many other devices. Referring to the result in equation 3.17 of section 3.1.3, above, it can be seen that the modulation frequency at the detector is the difference in frequencies between the two beams. Representing the deliberate frequency shift in the

reference beam as f_s, the reference beam frequency can be written as:-

$$f_{ref} = f_o + f_s \quad , \qquad (3.26)$$

and the signal beam frequency may be written explicitly as:-

$$f' = f_o + f_d \quad . \qquad (3.27)$$

The difference of these terms, which would appear at the detector output, is:-

$$\begin{aligned} f_{ref} - f' &= (f_o + f_s) - (f_o + f_d) \quad . \\ &= f_s - f_d \quad . \qquad (3.28) \end{aligned}$$

The signal at the detector output for a stationary target will be at the shifted frequency of the reference beam, and will vary below that for an approaching target, and rise above it for a receding target. The reference beam frequency shift acts as an intermediate frequency, bringing the detected signal within the frequency range of electronic signal processing, which may then be used to extract both magnitude and sense of the target motion. Ambiguity may arise if the reference frequency shift is less than the Doppler shift, but in most situations reference frequency shifts may be made sufficiently high to eliminate this problem.

The advantages of this technique lie in the narrower bandwidth required for the signal processing, and in avoiding low frequencies, where noise effects tend to be

more severe. Against that, it requires a method of introducing the reference frequency shift, an electro- or acousto-optic device with the associated drive circuitry. These devices tend to be expensive. Alternatively, the reference beam frequency shift may be introduced by a direct Doppler method, using a continuously, or discontinuously moving object. Oldengarm (1977), Halliwell (1979), and Truax et al (1984), used a rotating diffraction grating, a rotating diffuse scatterer, and a periodically translated reflector respectively, in different devices. Frequency shifting techniques either require extremely stable control of the mechanism introducing the frequency shift, or monitoring of the frequency shifted beam to allow effective demodulation of the detected signals. A more detailed analysis of frequency shifting is contained in appendix 2.

3.2.2 Phase Based Sense Detection

A practical alternative to frequency shifting is the use of two orthogonal components of the reference beam with a phase difference between them. This technique has been used in interferometric applications, for example Downs and Raine (1979), but is not believed to have been applied to a Doppler based device operating with scattered light from a solid target.

The most general treatment requires that the reference beam is elliptically polarised. This beam can be considered to

be two paraxial waves of the same frequency and arbitrary amplitude, with polarisations at right angles to each other, and an arbitrary phase shift between them. The components may be represented as:-

$$A_{1p} = A_{1op}.\cos(2.\pi.f_o.t) \quad , \qquad (3.29\ a)$$

and

$$A_{1s} = A_{1os}.\cos(2.\pi.f_o.t + q) \quad , \qquad (3.29\ b)$$

where p is taken as the inplane component and s as the perpendicular component, with q representing the phase shift.

Heterodyning the first component with the scattered light gives a signal identical to that of equation 3.17 above. When the reference with the phase shift is heterodyned with the signal, the output of the detector is :-

$$i_d = \text{d.c. terms} + 2.k.A_{1os}.A_{2o}.\cos(2.\pi.f_o.t + q).\cos(2.\pi.f'.t)) \ . \qquad (3.30)$$

Using the same mathematical identity for cos(a).cos(b) the expression containing the a.c. signal becomes :-

$$i_{acs} = k.A_{1os}.A_{2o}.(\cos(2.\pi.(f_o + f').t + q) + \cos(2.\pi.(f_o - f').t + q)) \ . \qquad (3.31)$$

If the arguments of the cosine terms are tidied up, the first term is at a frequency in excess of the detector

response, and averages to zero. The second term gives :-

$$i_{ac} = k.A_{1os}.A_{2o}.\cos(2.\pi.f_d.t + q) \quad ,$$
$$= i_o.\cos(2.\pi.f_d.t + q) \quad . \qquad (3.32)$$

This result differs from that obtained for the other component of polarisation, only in the presence of the phase shift.

If the target motion changes direction, the sign of the Doppler frequency also changes. Rewriting equations 3.17, and 3.32 with a negative Doppler frequency gives :-

$$i_{acp} = k.A_{1op}.A_{2o}.\cos(2.\pi.-f_d.t) \quad , \qquad (3.33\ a)$$
$$i_{acs} = k.A_{1os}.A_{2o}.\cos(2.\pi.-f_d.t + q) \quad , \qquad (3.33\ b)$$

and applying the mathematical identity $\cos(x) = \cos(-x)$ gives :-

$$i_{acp} = k.A_{1op}.A_{2o}.\cos(2.\pi.f_d.t) \quad , \qquad (3.34\ a)$$
$$i_{acs} = k.A_{1os}.A_{2o}.\cos(2.\pi.f_d.t - q) \quad . \qquad (3.34\ b)$$

Comparing the results of equations 3.17, and 3.32 with 3.34 a and b, shows that the sign of the phase shift has changed. By measuring the phase of one polarisation component relative to the other, changes in the sign of the Doppler frequency can be found. The optimum value for q is $\pi/2$, that is that the two signals have a quadrature relationship. This is the method that has been developed and used in this project.

The technique has the advantage that it only requires passive optical components to condition the reference beam,

and to separate the orthogonal components of the reference and signal beams for detection.

It suffers in requiring signal processing electronics that extend down to d.c., increasing the susceptibility to noise. The technique used in the LDI to extract the phase relationship between the two detected signals was designed to minimise the effects of noise or changes in signal level on the sense detection process.

The phase quadrature technique requires that there is some component in the scattered light parallel to each of the pass directions of the polarising beam splitter. This condition can be forced by inserting a linear polariser into the scattered light, with its pass direction equally inclined to the two pass directions of the beam splitter. The direction of polarisation of the illuminating beam must be parallel to the pass direction of the linear polariser to reach the target with maximum efficiency. This polariser is only essential if exact quadrature is required at the detectors, as is the case for eighth wave resolution.

Practically the quadrature condition can be realised in a Mach Zehnder device with a quarter wave plate in the reference path. In a Michelson layout an eighth wave plate is needed as the beam traverses the reference path twice. It is possible to operate the phase based sense detection with any degree of retardance other than integral multiples of half a wave between orthogonal components, which gives

an identical phase relationship between the detector outputs for both senses of target motion.

The availability of two signals in quadrature offers a second potential benefit. If the two signals are considered together, zero crossings occur uniformly and twice as frequently as for a single channel signal. Where digital detection techniques are used resolution may be doubled. If analogue fringe tracking is being used to measure displacement, the two signals in quadrature give a rapidly varying signal at all points of the target motion, eliminating the dead points that would occur at the peaks and troughs of a single channel device and allowing the possibility of greater resolution. If the phase relationship is not perfect quadrature then the distribution of the zero crossings is no longer uniform within the Doppler signal and a combination of both signals does not offer this improvement in resolution. Use of the quadrature signals to increase resolution should be applied cautiously because the stability of the polarisation relationship in a working LDI is uncertain.

3.2.3 Signal Amplitude Variation

The two methods that have been outlined above in 3.2.1 and 3.2.2 modulate the frequency and phase of the reference. A third alternative is based on signal amplitude variation. An edge filter arranged so that the carrier frequency of the signal is centered at the middle of the roll-off will

allow discrimination between signals Doppler shifted up or down in frequency. The ratio of signal level to reference level before and after transmission of both signals through the filter will give a lower signal to reference ratio for a Doppler shift towards the blocking end of the filter, and a higher ratio for a Doppler shift towards the pass end of the filter. This is the basis of the device reported by Boiko et al (1980). Although this method may allow the sense of motion to be discerned, if it is used to assess the magnitude of the Doppler shift the sensitivity of measurement will be limited considerably by the transmission properties of the optics.

3.3 Scattering by Solid Targets

Unlike most conventional interferometers, which use optically flat reflecting surfaces to define the position of the target object, the LDI which is the subject of this study uses light from an optically rough target. The roughness introduces several major changes in the properties of the light returning from the target, which have to be accommodated in the LDI. The most significant of these is the spatial distribution in the intensity of the scattered light. This is the speckle effect and is the subject of books by Dainty (1984) and Francon (1979). It is also covered comprehensively in a paper by Beckmann (1967).

3.3.1 Speckle

When a monochromatic beam of light illuminates an optically rough surface in the x,y plane, the scattered light field is no longer well ordered. This disordering exhibits itself as speckle, a local variation in the intensity at the viewing plane, at some value of $z > 0$. Speckle derives directly from the effect of the surface roughness of the illuminated object. It will be assumed that the surface roughness is a random function of position on the surface, and has a mean value greater than the wavelength of the illuminating beam. Scattering point i on the surface has

co-ordinates x_i,y_i,z_i, where :-

$$z_i = f(x_i,y_i) \quad , \tag{3.35}$$

$$\overline{z}_i > \lambda \quad . \tag{3.36}$$

If the scattered light is viewed at a point P, with co-ordinates (X,Y,Z), figure 3.1, then r_i, the distance from each scattering point to P is :-

$$r_i = ((X-x_i)^2 + (Y-y_i)^2 + (Z-z_i)^2)^{1/2} \quad . \tag{3.37}$$

p_i is the phase resulting from the difference in path lengths from different scattering points :-

$$p_i = 2.\pi.r_i/\lambda \quad . \tag{3.38}$$

Let the amplitude scattered by each point be a_i. The amplitude seen at P due to all the scattering points is the algebraic sum of the amplitude scattered by each point :-

$$A_p = \sum_N a_i.\cos(p_i) \quad . \tag{3.39}$$

If the size of the illuminated region is taken to be small compared with the viewing distance, as is usual in most operating situations, then the changes in the phase due to changes in x_i and y_i will be small, and will be absorbed into the random distribution of phase due to the variations in z_i. That is, the variations in phase at P are effectively only due to the surface roughness. As this is

greater than the wavelength of the illuminating beam, it introduces random phase evenly distributed over the range $-\pi$ to π .

The mean amplitude at P from summing over all the N scattering points is given by :-

$$\begin{aligned} \bar{A}_p &= N.\overline{a_i.\cos(p_z)} \quad , \\ &= N.\bar{a}_i.\overline{\cos(p_z)} \quad , \\ &= 0 \quad . \end{aligned} \tag{3.40}$$

Where p_z is the phase variation due to changes in z. The variance in the amplitude is given by :-

$$V(A_p) = N.\overline{(u_i - \bar{A}_p)^2} \quad , \tag{3.41}$$

where $u_i = a_i.\cos(p_i)$. Making this substitution ,

$$\begin{aligned} V(A_p) &= N.\overline{(a_i.\cos(p_i) - 0)^2} \quad , \\ &= N.\bar{a}_i^{\,2}.\overline{\cos(p_i)^2} \quad , \\ &= N.\bar{a}_i^{\,2}/2 \quad . \end{aligned} \tag{3.42}$$

This analysis follows that of Levi (1980 ch.19). The result states that the mean amplitude at the viewing plane is zero, with a variance of the total amplitude scattered in the direction of P. There is no explicit dependence on the nature of the surface roughness, which implies that the variation in intensity is constant for all surfaces defined as optically rough.

The characteristic size of the speckle can be found by a spatial autocorrelation of the speckle pattern with itself.

The first minimum of the autocorrelation function occurrs at a distance corresponding to the radius of the speckle. This is a lengthy process, and is fully documented in Levi (1980), and Dainty (1984). It gives a mean speckle radius r_{sp}, similar to the radius of the Airy disk resulting from diffraction through an aperture of the same size as the illuminated region and viewed at the same distance, R :-

$$r_{sp} = \lambda.R/r_o \quad . \qquad (3.43)$$

This equation in conjunction with the equations governing the behavior of a Gaussian beam (section 3.4.2) allow the expected speckle size at the detector to be predicted under a given set of conditions.

In physical terms the results of equations 3.42 and 3.43 indicate that monochromatic light scattered from a rough surface lead to a variation in the intensity seen at a viewing plane, with the phase of the light remaining approximately constant over a region dependant on the illuminating and viewing conditions. This arises due to multiple interference of many waves at the same frequency, but with a random phase.

The important point for the operation of the LDI is that each speckle may be treated as having constant phase, and may therefore be mixed with the reference beam to extract the Doppler shift. It should be noted that the speckling effect does not result from, or affect, the temporal behaviour of the scattered light, so does not affect the Doppler signal.

When light is scattered by a rough surface some depolarisation may occur. This has more serious implications for the operation of the LDI, which requires linearly polarised light, able to contribute equally to the two polarisation directions of the detectors. The problem is complex because of the dependency of depolarisation on the nature of the scattering surface and material. Gasvik (1981) has shown that, for rough steel targets, the scattering of a copolarised component occurs most strongly in the specular direction for angles close to normal incidence. Consequently it is assumed in the absence of more information, that the strongest scattered signal of the desired polarisation will occur when the illuminating beam is of the same polarisation. This is the alignment that is employed in the LDI.

Optical detection with a speckle field has difficulties in excess of those for ordinary heterodyning. These arise from the direct dependence of a given speckle pattern on the particular part of the surface from which the light is scattered. Should the illuminated region of the surface change in any way, whether by translation or in size, due to axial motion of the target, the speckle pattern at the viewing plane can be expected to change.

Francon (1979) shows that the speckle pattern is invariant in all but scale for changes in viewing distances greater than the far field distance. The far field distance D_{ff} for

a given illuminated spot radius, r_o, is given by :-

$$D_{ff} = r_o^2/\lambda \quad , \qquad (3.44)$$

see for example Born and Wolf (1959). For a spot radius at the target of 0.3 mm this gives a far field distance of 14 cm at the HeNe laser wavelength. Consequently, if the speckle pattern is viewed in the far field, the variation in intensity with changing range will vary with $1/R^2$ in the expected way. Within the near field, (Fresnel diffraction region), the speckle pattern is shown by Francon to be similar except in scale for axial changes in the viewing distance which are related to the viewing distance by :-

$$d_{sim} << 2.\lambda.(R/r_o)^2 \quad . \qquad (3.45)$$

Here d_{sim} is the change in viewing distance, R, for which the speckle pattern is effectively similar. From this it can be seen that as the viewing distance increases to the far field limit the allowable change in viewing distance becomes larger, until at the onset of the far field the speckle pattern is invariant except in scale for any effective change in viewing distance. Within these allowable changes in viewing distances the speckle pattern will also change its intensity in the normal manner. Clearly this variation in the speckle pattern within the near field will place a restriction on the length over which continuous measurements of the target displacement can be made within the near field.

3.3.2 Heterodyning with a Speckle Field

Heterodyning the speckle field derived from a moving target with a well behaved reference beam requires consideration of the way in which the parameters of the speckle field seen by the detector alter as the target moves.

Assuming a stationary speckle field, with each speckle being of constant phase and of a given size, the wavefront radius of curvature should match the reference beam wavefront curvature to better than a quarter of a wavelength across their overlap region on the detector surface as for the coherence condition of section 3.1.3.

If the scattering surface is in motion, the size of the illuminated region and the viewing distance of the speckle pattern change. Both of these parameters occur in equation 3.43 which gives the speckle size, and it can be seen that if they vary linearly with each other, the effect on the speckle size is not significant. As the viewing range changes the radius of curvature at the speckle seen by the detector changes. This can be taken to be planar at the target ranges involved, consequently the optimum reference beam curvature should be similar, and it is most convenient to arrange for it to be planar.

The more difficult problem is that of accommodating the transition from one speckle to another. This may be due to lateral movement of the speckle pattern, caused either by tilting or transverse movement of the target, or due to axial movement within the near field, or may result from a

change in the size of the illuminated area of the target. It is optically inefficient to use less than the full area of the speckle seen at the detector. However if the overlap area is increased to cover more than one speckle, there will be some contribution from neighbouring speckles, with a different, and arbitrary phase. The signal from this additional contribution will vary at the Doppler frequency but out of phase with the main signal, causing a reduction in the detected signal amplitude. During any speckle transition process there will be a point where there is an equal contribution from both speckles, this will in general be the point at which the detected signal is least visible. As this is unavoidable, it implies that the best detection conditions for heterodyning with a changing speckle pattern are identical with those for a static speckle pattern. This has assumed that the speckle size is constant during the target motion. This is not the case, but by careful control of the incident beam conditions it can be realised closely over a wide range of target ranges.

3.4 Laser Beam Properties

The derivations of the effects relevant to LDI operation have generally assumed that the laser is a source of monochromatic light. In reality this is not the case. The way in which the real properties of the laser output affect LDI behaviour are described below.

3.4.1 Coherence Length

The discussions of the effects on which the LDI is based have so far assumed that the ouput of the laser is a monochromatic beam. In fact the output may comprise several narrowly divided frequencies, each a resonance state of the laser cavity. Interaction of these frequencies restricts the possible continuous range over which the heterodyne process can occur.

If the laser cavity is of length L, and two adjacent modes have wavelengths λ_1 and λ_2, their resonance conditions can be written as :-

$$2.L = n.\lambda_1 = (n + 1).\lambda_2 \quad . \qquad (3.46)$$

For a given path length difference, D in a heterodyne or interference experiment, the phase relationship between the mixed waves at each wavelength will not necessarily be the same. There will be a particular value of D at which they are in fact out of phase. this can be expressed as :

$$D = m.\lambda_1 = (m + 1/2).\lambda_2 \quad , \qquad (3.47)$$

where m is an integer. By direct comparison with equation 3.46, this can be seen to occur when D = L . Any change in the path length about this point which brings the signal at λ_2 into phase, will also put the signal due to λ_1 out of phase. At a detector this results in a negligible change in the detected intensity. As D increases to 2.D the two signals move back into phase with each other. This will occur for all even multiples of D. At all odd multiples of D the two wavelengths will be out of phase. This restricts the free path length over which a target can move and still give continuous Doppler signals to somewhat less than 2.L. A paper by Foreman (1967) gives the visibility of an interference signal as a function of optical path difference for a laser output with two symmetric and asymmetric modes and for three and more symmetric modes. It shows that visibility of the interference process only drops to zero where the modes are symmetrically spaced under the gain curve of the laser. The coherence length problem may be overcome by removing all except one of the resonance modes of the laser, either by carefully controlled operation of the lasing condition, or by transmission through a second resonant cavity, usually a Fabry Perot etalon, which has a resonance coinciding with only one of the laser resonances.

A single laser mode will also suffer this coherence length restriction due to the finite width of the resonance. A frequency difference between the two sides of the resonance leads to a very much larger coherence length, to the extent

that loss of intensity causes loss of signal before coherence restrictions become significant. Lasers are commercially available having only one resonance mode, and one was used in this work. The finite linewidth of the laser output also introduces a corresponding small broadening of the Doppler signal as shown by Rudd (1969). Differentiating equation 3.09 above with respect to the optical frequency gives:-

$$df_d = df_o.v/c_o \quad . \qquad (3.48)$$

Dividing through by equation 3.09 :-

$$df_d/f_d = df_o/f_o \quad . \qquad (3.49)$$

This spread in the Doppler frequency is extremely small. It is shown by Adrian and Goldstein (1971) that effect of the finite size of the detector aperture will result in a greater loss in resolution due to variation in viewing angle of the target velocity vector. This in turn is still a negligible factor in most cases.

3.4.2 Beam Profile

A typical laser beam can be assumed to have a Gaussian intensity profile, with circular symmetry about its axis. This Gaussian shape is a result of the configuration of the laser resonator.

The behaviour of Gaussian beams is well documented (see for example Drain 1980, Levi 1980). This is of considerable

benefit in controlling the shape, divergence and wavefront curvature of the beam to take specific values at a given point along the beam axis. Controlling the beam is necessary both to obtain the desired reference beam spot size at the detector and to control the divergence of the beam illuminating the target surface, as this dictates the size of the speckles seen by the detector.

For a beam of radius r incident on a thin lens of focal length F, the radius of the beam waist, r_w, (measured to the point at which the intensity falls to $1/e^2$ of its axial value), is given according to Drain (1980) by :-

$$r_w = \lambda.F/(\pi.r) \quad . \qquad (3.50)$$

The radius of the beam at a distance z from the position of the beam waist is :-

$$r_z^2 = (\lambda.z/\pi.r_w)^2 + r_w^2 \quad . \qquad (3.51)$$

There is also a discrepancy between the expected axial position of the beam waist after focussing, and the actual position. This discrepancy, S, becomes smaller as the focal length of the focussing lens increases:-

$$S = F/(1 + (\pi.r_w/\lambda.F)^2) \quad . \qquad (3.52)$$

This term only becomes significant when long focal length lenses are being used.

These equations can be used to obtain a waist in the reference beam at a known position, and of a known radius

based on knowledge of the original laser beam output characteristics. This point has been pursued further in chapter 5, where it has been modified to restrict the illuminating beam radius below a given value for a fixed range of motion, enforcing a minimum size on the expected speckle pattern for this range.

Many of these equations were used in conjunction with those relating to speckle formation in a series of computer programs. By doing this, the effects on the detected speckle size of altering different parameters within a given optical layout could be examined quickly.

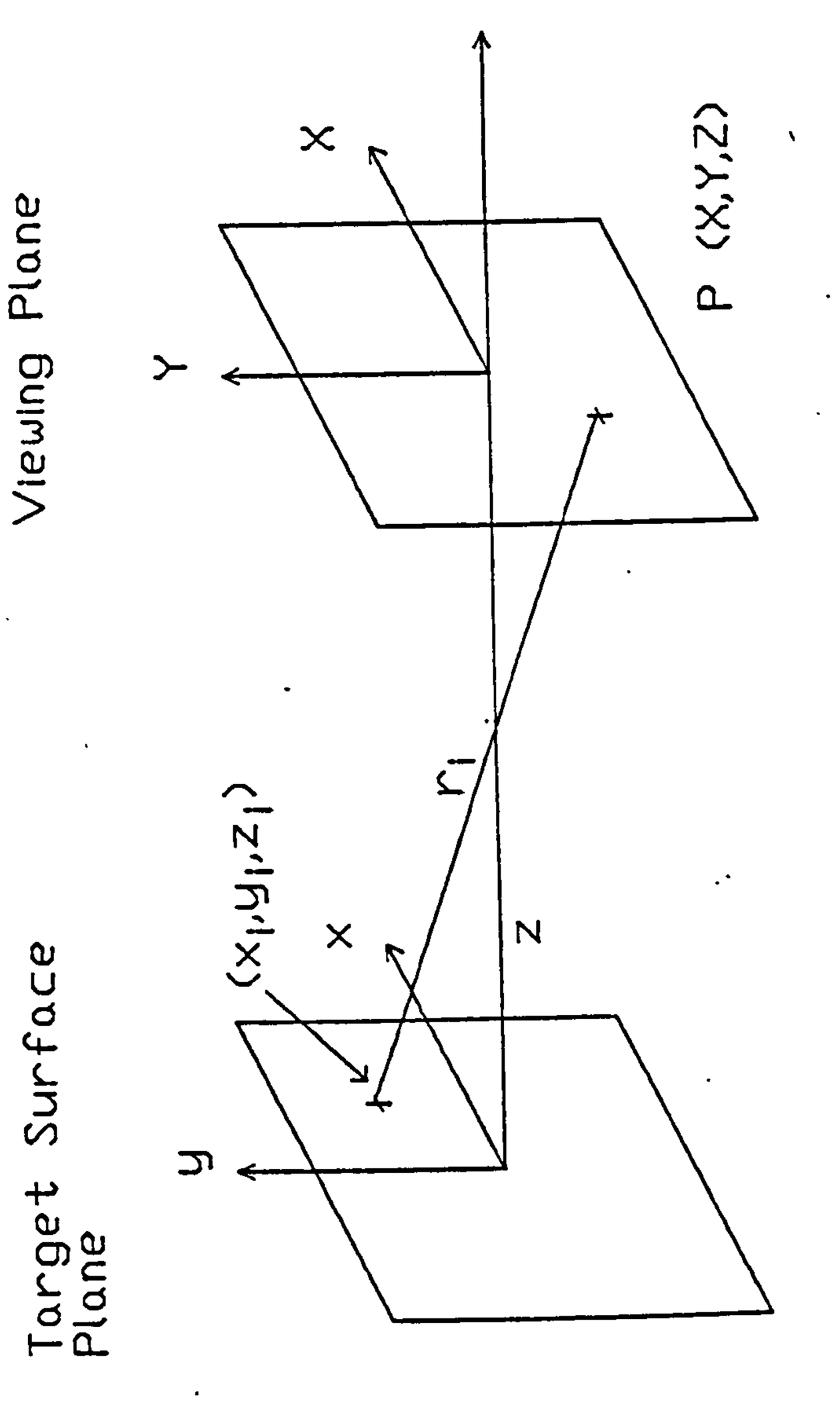

Figure 3.1

Scattering Geometry for Speckle Formation

4. EXPERIMENTAL APPARATUS AND METHOD

4.1 Optical System

This section encompasses the parts of the LDI in which light is the signal carrying medium, and the factors which dictated the choice of optical configurations and components to be used.

4.1.1 Optical Design

A considerable amount of time was devoted to investigating the different functions required from an axially measuring LDI. The initial difficulty was in recognising the relevant factors involved. These included the need for an accessible reference beam path to allow for conditioning of the reference signal, the possibility of modifying the behaviour of the illuminating beam, and the apparently simple process of ensuring that the device would only measure the axial component of the target motion. More practically, the design had to be optically efficient.
Of these conditions, the need to restrict measurement to the axial component of the target motion was dominant, and led to a choice of layouts based either on Mach Zehnder, or Michelson interferometers. Both of these required the use of an amplitude dividing component to act both as a beam splitter, and as a beam combiner, to mix the reference and signal beams. The beam combiner in particular is inefficient in that a considerable amount of light does not

reach the desired destinations. However, attempts to increase the efficiency by geometric methods result in sacrifice of the purely axial nature of the device. The use of polarisation based techniques was precluded as their requirements conflicted with those for phase based sense detection.

Initial work was on a Mach Zehnder system (figure 4.1). This was based on two separate beam splitters. The first separated off the reference beam, and as this required only a relatively low intensity, the reflection from the front surface of a 45° prism or a 45° inclined optical flat provided sufficient light, and prevented direct reflection of light into the laser cavity. The system also had a single pass reference beam making optical processing, in this case the production of a circularly polarised beam, more amenable.

The beam combiner was a 50/50 cube element, this splitting ratio giving optimum efficiency (see below). It was this element that gave most problems, as it directed a considerable amount of light from the illuminating beam into the reference path in the opposite direction to the reference beam. Although this light passed through the retarder plate and became circularly polarised, a significant quantity still found its way back into the laser, causing destabilisation. It was during modifications to the Mach Zehnder layout, that an operational Michelson design was found (figure 4.2).

This was unexpected, as it required the reference beam to

make a double pass through the quarter wave plate (QWP). The anticipated result of this operation was that the emergent beam would be linearly polarised at some arbitrary inclination to the incident beam, and according to the theory (section 3.2.2 above) non-viable for phase based sense detection. In order to achieve the desired circularly polarised emergent reference beam an eighth wave plate was required, and such a component was not a standard commercially available item. The alternative was to use a variable retardance compensator, but this was not viable due to the cost of the component.

The obvious reason for the Michelson layout providing a workable sense of motion signal is that the retarder was not giving exactly a quarter wave retardance. However the other polarisation sensitive components and the electronics were checked to ensure that this was the case. On its arrival the QWP had been checked in a single pass mode and was found to give what was then considered to be a circularly polarised transmitted beam. As it was originally anticipated that the plate would be used in a single pass mode this was sufficient for it to be incorporated into the system. The advent of the working Michelson layout required that the plate was tested in a double pass mode. It was found that for two rotational positions of the plate the double pass transmitted beam was linearly polarised, as would be expected, with these directions corresponding to the fast and slow axis directions of the plate. Between

these positions the transmitted beam was not linearly polarised, and showed considerable ellipticity. It is this ellipticity that both indicated the failure of the QWP and provided a sufficiently large phase difference to allow operation of the sense detection electronics.

Although the Michelson design was based on what can only be called a faulty component, it was decided to operate the LDI in this layout. Although the phase difference between beams was unknown it was considered to give sufficiently stable sense of motion signals for the device to operate. In its favour the Michelson layout had the advantage of shorter air paths, reducing the effects of environment on the system. More usefully, as the Michelson layout used only one beam splitter it was considerably more optically efficient.

In the M.Z. layout it can easily be shown that the combining beam splitter gives maximum efficiency if the splitting ratio (ignoring absorption) is 50/50. If the splitter reflectivity is R and the transmission T, then for an illuminating beam intensity I_{ill} and a target reflectivity ρ, the intensity seen by the detector can be given by :-

$$I_{det} = \rho.R.T.I_{ill} \quad . \qquad (4.01)$$

Neglecting the effect of absorption in the splitter gives the relationship :-

$$R = 1 - T \quad . \qquad (4.02)$$

Substituting this into equation 4.01 and differentiating gives :-

$$dI_{ill}/dR = \rho.(1 - 2.R).I_{ill} \quad . \qquad (4.03)$$
$$= 0$$

for maximum efficiency, which implies :-

$$R_{opt} = 0.5 \quad . \qquad (4.04)$$

In a Mach Zehnder based device assuming that the reference beam is derived by a front surface reflection from an inclined plate the fraction of the light from the laser reaching the detector(s) neglecting absorption, is $0.24.\rho$, with 4% of the laser output available for the reference beam. In a Michelson based layout the fraction of light reaching the detector(s) is $0.25.\rho$, with 50% of the laser output being directed into the reference beam. If absorption and loss by reflection from component surfaces is included the Michelson based layout looks even more favourable as it contains fewer components and consequently less opportunity for loss.

Good stability of the laser was important for effective operation of the LDI. It was possible to monitor this by introducing a prism into the laser output in a way that did not deviate the beam but reflected a small fraction of it onto a detector. This showed that some degree of destabilisation was present in all optical configurations. However the effect was least serious with a Michelson layout as it contained fewer reflecting surfaces. The

presence of a focussing lens was also beneficial as it could be slightly misaligned, preventing direct retro-reflection, and also defocussing subsequent reflections, decreasing their intensity at the laser. There is no indication in the results that disturbances of the laser cavity had an adverse effect on the measurements made by the LDI.

4.1.2 Optical Hardware

This includes the optical component holders, their mounts, the surface on which the designs were laid out and the laboratory conditions under which the work was done.

The optical components used in the construction of different LDI layouts can be grouped into those that are essentially planar, and mounted vertically, and those that are solid, and can be mounted on a horizontal surface. All the planar components were mounted by compression between two polythene rings against a lip in a circular hole. Compression was achieved using four screws evenly spaced around the circumference of the 50 mm. diameter hole (figure 4.3). Components smaller than 50 mm. diameter were mounted on a 50 mm. diameter plate before being mounted in the holder: no components had diameters greater than 50 mm. Mounting the retarder plate was a little different since it was necessary to rotate this component during alignment. It was found that by loosening the compression screws the component could be rotated in its mount against the

friction of the polythene rings. This gave a reasonably smooth and controllable rotation, with the component being locked in position, when correctly aligned, by tightening the compression screws.

Solid optical components, such as prisms and beam splitter cubes, were mounted on individual horizontal tables, with optional clamping to hold the component in position (figure 4.4). The polarising beam splitter, used to seperate orthogonal components of the light directed at the detectors, was mounted, along with the detectors, in a custom made unit (figure 4.5). This allowed the detector components to be accurately positioned before being locked into place, and used as a unit.

The laser head was mounted with two adjustable set screws close to each end of the head. These allowed the laser head to be adjusted over a sufficiently large range of height and angle for accurate alignment. Once in position the laser was locked by a third set screw at each end.

All these optics holders were manufactured in the Institute workshops and were designed to have an axis 56 mm above the mounting blocks and 81 mm. above the surface of the optical table. This was the minimum height of the aperture of a commercially available Bragg cell, which was considered to be the largest component likely to be used in the LDI. All holders were spray painted matt black to cut down stray reflections which could be both disruptive to the operation of the LDI and possibly a hazard to the eye.

The holders were all bolted onto 100 x 75 x 25 mm. thick steel bases (figure 4.6) using two M6 cap head bolts. These bases were ground as a group to have parallel upper and lower surfaces. A layer of felt was glued to the lower faces to prevent them slipping on the optical table top. Each base was bored with at least six holes, allowing up to three component holders to be mounted on them if required. This made it possible to mount holders to within 35 mm. of each other if necessary.

Using free moving steel blocks allowed flexibility in the layout of LDI designs, but good linearity could be achieved by butting the blocks together if necessary.

The sensitivity of the LDI to any variation in optical path lengths required that the optical part of the device was isolated from environmental vibration. The anti-vibration optical table on which the LDI was built is based on a suggestion by Ford (1984) (figure 4.7). The table surface was a piece of wire re-inforced glass 1.7 m. x 0.9 m., which provided a reasonably inflexible flat surface. It rested directly on two 0.6 x 0.6 m concrete slabs, providing good support across most of the table top. The slabs rested on two partially inflated car tyre inner tubes, which in turn rested on the top of a stout laboratory table.

The arrangement provided a large flat surface which showed high immunity to environmental noise. This was important, as any motion in the table surface would be transmitted to the optical components, causing changes in the optical path

lengths within the LDI, giving unwanted signals at the detectors. The only difficulties with the table were slow deflation of the inner tubes and a tendency to rock about an axis joining the centres of the two concrete slabs when the weight was redistributed on the table top. The rocking motion had a period of about 1 second, and died away in about 10 seconds. This indicated underdamping probably due to over inflation of the inner tubes, but exact variation of the pressures was difficult and the table was considered acceptable with no modification.

The risk of a blow out in either of the inner tubes was accommodated by placing wooden blocks under the corners of the concrete slabs, with a clearance of about 10 mm. The table top was thus free but prevented from collapsing.

The laboratory housing the LDI was kept in partial blackout. This increased visibility of the laser beam for easier alignment and protected the equipment from direct sunlight. It also allowed easier operation of the system and greater safety from accidental eye exposure to the laser beam by reducing the pupil size as compared with blackout where the pupil is more open and may receive greater exposure.

4.1.3 Optics

All optical components were purchased from commercial suppliers. Where possible, relatively large apertures were used to minimise diffraction effects and to accommodate the

possibility of multiple passage of a beam through the element. Exceptions were the clean up polariser and the polarising beam splitter. This was in part due to the expense of polarising optics, and partly due to the roles of these components within the LDI system.

Right-angle prisms were used where beams had to be turned, as they did not require adjustment in the vertical plane. An added benefit from using prisms was that retro-reflections from the faces perpendicular to the incident beam aided alignment of the system.

Many of the optical elements were broadband antireflection coated to minimise the amount of stray light within the system, as this could have a destabilising effect on the laser. As stated above (4.1.1) the small amount of destabilisation that was noted did not appear to disturb the operation of the LDI.

Two lasers were used during the project: the first was a Hughes Corporation 5 mW. HeNe laser; the second a frequency stabilised 1 mW. Spectra Physics model 117 HeNe laser. Both of these had a linearly polarised output. The frequency stabilised laser was bought to overcome the coherence length restrictions that could occur with an unstabilised device. This was not a condition that caused any problems in the work covered here, but is of relevance for possible future investigations which may examine the possibilities of measurement of larger ranges of motion by various optical techniques. It is common practice to protect the

laser in a system from the effects of stray reflections to prevent destabilising the resonant cavity, which cause erratic changes in the laser output. The conventional method of protection, using a linear polariser and quarter wave plate, was not considered to be ideal in this case. Whilst it would provide the required circularly polarised reference beam, it would also illuminate the target with a circularly polarised beam, the effects of which were unknown, but likely to complicate the quadrature detection process.

4.1.4 Alignment

The alignment of the optical system in any given configuration can be divided into two parts. The first is concerned with the spatial position of the beams, the second with the state of polarisation at all points within the system.

Physical alignment of the LDI was accomplished by working outwards from the laser, using a target at the desired beam height to align each component as it was inserted. The laser was located near the centre of the table and the set screws supporting it were then adjusted until the beam was parallel to the surface of the table at the desired height. It was convenient to support the laser head close to the exit aperture and at another point along its body. This was because the exit aperture could be adjusted to the correct height and the direction of the beam changed by altering

the height at the other support point. The laser could then be placed more symmetrically on its supports for finer adjustment. Correct beam height and direction were achieved when the laser accurately illuminated a target at the desired height at two widely spaced positions.

Once locked in position, the laser output acted as a reference by which all the other components of the system could be aligned. Each component was inserted sequentially and adjusted until the beam height at a target beyond the component was the same as it was prior to insertion. With focussing optics this required the target to be moved to two points along the beam, ensuring that it was still parallel to the table surface. In this way the entire alignment could be achieved relatively easily.

The direction of polarisation of the laser output was given in the device specifications, which also stated that the laser tube was coaxially mounted within its housing. This allowed the direction of polarisation to be altered by a simple rotation of the laser head in its mount. The direction of polarisation was confirmed by setting a vertical glass plate at Brewster's angle to the laser beam and rotating the laser head until the reflected light was extinguished. Checking was by means of a light chopper and one of the detectors, the output being displayed on an oscilloscope. When the extinction position was established the plate was replaced by a polaroid in a graduated mount. This was rotated to give extinction and then adjusted to 45° from the extinction position. The laser was then

rotated until extinction again occurred. The direction of polarisation of the laser output was now at 45° to vertical. Since many target surfaces do not completely depolarise the scattered light, alignment of the incident polarisation at 45° should give the maximum scattering at the same polarisation. This should then give equal components from the polarising beam splitter in the detection section of the LDI. No particular direction of polarisation was required by the reference beam as the necessary elliptical polarisation state could be introduced by rotation of the retarder plate.

The clean up polariser was then placed in the path of the laser beam and rotated to give maximum transmission. Both detectors and the polarising beam splitter were used, allowing comparison of the two outputs. The optimum position of the clean up polariser was taken when the two signals were of equal size. Although this may not be exactly at the direction for maximum transmission, it is sufficiently close not to cause any significant loss in detected signal while providing the best condition for the operation of the sense detection electronics.

4.1.5 Target

Several different types of target were prepared in an attempt to try and accommodate the variations that may occur in a real measuring situation. The types are described below but were all based on short lengths of

dural bar, the end face being prepared in different ways. A series of targets were finished with different grades of emery. This gave surfaces which were characterised by many fine parallel scratches. The targets thus had a one dimensional periodicity which was expected to be a common feature of many machine finished targets.

Targets were also prepared with both matt black and white finishes, and no intended directional character. Attempts to use fresh magnesium oxide as a high reflectivity matt white surface failed. The oxide was deposited directly from the combustion of magnesium ribbon and the resulting layer was not sufficiently rugged. Liquid paper painted onto the face of a dural bar provided a more stable, and probably more realistic matt white alternative. The black targets were made by spraying target surfaces with a matt black heatsink paint. Both finishes dried to a rough texture and did not show any indication of the characteristics of the surface on which they were deposited. In some cases targets had half the face covered, and half bare metal, to allow rapid comparison under the same conditions. A small number of measurements were made from a matt silver target and from reflective perspex. This latter reflected light specularly and caused serious destabilisation of the laser.

4.2 Electronic System

The electronic system covers both the electronic signal processing of the LDI and the other instrumentation that was used to drive the target and to measure the behaviour of the LDI independantly.

A block diagram of the electronic system is given in figure 4.8. This shows both analogue and digital parts of the system, and their relationship with the rest of the LDI.

4.2.1 Detectors

The detectors used in the LDI were silicon p-i-n photodiodes. These were chosen for both practical and financial reasons as they were more rugged and smaller than photomultipliers. Further, they did not require a separate power supply, were also considerably cheaper, and more readily available. The particular photodiodes used were type BPX 65, with a cited quantum efficiency of over 70 % at 632.8 nm, with no operating conditions mentioned. They have an active area of 1mm x 1mm which is sufficiently large to accommodate most anticipated speckle sizes.

Problems were encountered in finding a suitable amplifier circuit to allow the photodiodes to operate with a reverse bias applied to them, this mode giving optimum efficiency. However, since the diodes were designed for fast operation the loss of speed due to absence of biassing was not a problem, particularly as the analogue electronics had a far lower cut off frequency.

4.2.2 Analogue Electronics

The analogue electronics caused some difficulties in constructing the LDI. Ideally a high speed analogue system was needed, capable of operating down to d.c., as this would allow a wide range of Doppler signals to be examined, corresponding to a wide range of allowable target velocities. Attempts based on the 5539 high speed op amp, known to be successful elsewhere, were unstable. Consequently a lower frequency cut off was accepted and the LF 351 formed the heart of all the analogue electronics.

Two identical channels were constructed, one for each detector. The detector output was first converted by a current to voltage converter. The current to voltage converters were mounted in a seperate metal enclosure close to the detectors in an attempt to minimise the effects of interference. The laser and detector mounts and the wire re-inforcing in the optical table were also earthed to reduce external interference. The signal from the converter was a.c. coupled into a voltage amplifier, (gain 22), giving an output suitably large (c. 0.1V) to give a convenient display and for data logging. Coupling was necessary to remove the effects of the large d.c. light levels at the detectors, but was thought to be responsible for some loss of signal at very low signal frequencies; however, this was not observed when the LDI was used. The frequency response of the voltage amplifiers is shown in figure 4.9. which clearly shows the roll off in response

above 100 kHz. As the signal passed through three op amps before digitising, the rapid fall in response shown by the LDI for frequencies above 100 kHz can easily be understood. The digitising electronics are also included in this section because a significant part of their operation is analogue. The reasons for the decision to digitise the signals have been outlined in section 4.2.3, but the essential point is that the amplitude of the detected signal contains no information about the motion of the target so in digitising nothing is being lost.

The main difficulty of the digitising process was to ensure that the squaring process occurred unambiguously at a similar level on both detected signals repeatably. It was assumed that noise was present in the analogue signal. This precluded the use of zero crossing detection as spurious triggering of the Schmitt triggers could occur. The introduction of absolute hysteresis levels, while solving this problem, introduced a difficulty of its own. The hysteresis levels of the two channels would have to be set to identical values. If the two signals were of different amplitudes, then the larger signal would reach its hysteresis level ahead of the lower signal, thus eroding the phase difference between them. In order to preserve the phase difference the hysteresis levels had to be related to the detected signal amplitudes. This was achieved with the circuit shown in figure 4.10, with the envelope of the signal providing a reference from which the hysteresis levels are derived.

The signal from the amplifier is full wave rectified, and passed through a low pass filter which also has a small gain. The output of this filter is a close approximation to the envelope of the original signal. Inversion provided both positive and negative envelope signals from which the hysteresis levels of the crossing detector could be derived by simple manually set voltage dividers. As the signal level changes so the envelope and hence the hysteresis levels alter so that switching always occurs at the same fraction of the signal height.

The main problem with this circuit was loss of digital output when the analogue signal decreased rapidly in amplitude, temporarily leaving the hysteresis levels behind. This was caused by the response time of the low pass filter being too slow. However, decreasing the response time resulted in the output of the low pass filter effectively following the signal at low frequencies, reducing the device to a zero crossing detector, making it vulnerable to noise. The problem could be compensated for by using a smaller fraction of the envelope as the hysteresis level, but this also potentially increases the sensitivity of the device to noise, particularly at low signal levels. A compromise was reached between reducing the fraction of the envelope used and reducing the filter response time, resulting in satisfactory operation when the LDI was used. When the analogue signal level increased rapidly, it effectively left the envelope signal behind,

resulting in hysteresis levels that were lower than would occur with a stable signal level. This did not adversely affect the LDI operation.

The fraction of the envelope signal to be used as the hysteresis level was set manually. A sine wave from a signal generator was input simultaneously into both channels of the envelope detector. This was also displayed on an oscilloscope with the digitised output from one channel. Adjustment of the hysteresis levels caused the rising and falling edges of the output to move relative to the input wave. Once the switching level of the first channel had been set, slightly below half the amplitude of the input wave, both outputs were superimposed on the oscilloscope. An expanded oscilloscope trace allowed very precise superposition of the two output signals to be achieved by adjusting the hysteresis levels of the second channel to match the first. Setting the levels in this way prevented any differences in the gains of the low pass filters and precision rectifiers from being passed on to the output signals. Several factors influenced the fraction of the signal amplitude at which the hysteresis levels were set. If the fraction was made small, the immunity to noise would decrease, but as the levels would be on the steeper parts of the signal, the time during which ambiguous switching could occur would be reduced. The final setting was slightly below half the envelope level, which was found to operate satisfactorily. The value of adaptive hysteresis levels was ascertained during the setting up procedure by

reducing both levels to zero. When this was done spurious additional pulses were seen at the Schmitt trigger outputs, implying that adaptive levels did improve the detection of the Doppler signal.

4.2.3 Digital Electronics

The decision to operate the LDI as a fringe counting device in the first instance led to the need to use digital electronics for counting and sense of motion. The alternative to fringe counting was signal frequency measurement. However this would lead to some intrinsic loss of response due to the finite time needed by a frequency to voltage converter to aquire a sufficient quantity of signal to assess its frequency accurately. In a fringe counting mode the device measured displacement, which allowed easier comparison with other techniques. All the digital circuits used in the construction, with the exception of the decade counters, were C-MOS 4000B series.

The use of digital signals for fringe counting allowed an extremely effective sense of motion detector to be used. This was based on a D type flip flop. The two digital signals were connected to the clock and data inputs. At each positive clock pulse, the signal level at the data input was transferred to the output. If the clock signal was ahead of the data signal, then as the clock signal went high, the data signal, which lagged it, would be low; the output would therefore be low. If the clock signal lagged

the data signal, then as the clock pulse went high, the data signal would already be high, so a high signal level would be transferred to the output. This method of deriving the sense of motion signal had the advantage of being very simple and updating the sense of motion signal every cycle. The fringe counter was based on a commercially available 7217 C-MOS four digit up/down decade counter. Two of these counters were linked in series to form an eight digit counter. The circuit diagram is given in figure 4.11 which also shows the manual start/stop and reset controls; these were rendered inactive if external control was used. All the inputs were buffered to protect the counter with a +5 V. supply from the 15 V. digital signals. These chips also have multiplexed BCD outputs, which could allow future growth of the counters for interfacing for positional control or similar operations.

4.2.4 Control and Drive

Much of the assessment of the LDI was based on measuring periodic motions. In order to measure the distance travelled by the target during each cycle, it was necessary to link the target drive unit signal to the counter. A control unit was built which could reset the counter, and begin the count, stopping it after it had logged a specific number of cycles. The circuit of this device is shown in figure 4.12. It is based on a 12 bit C-MOS 4040B counter. When the reset/start button is pressed and released the

data level at the rising edge detector is pulled low for a short period. This disables the signal line. It also causes a short pulse to be generated by the reset line latch. This pulse resets its own source latch, resets the hold latch, allowing the count to continue and resets the 12 bit counter. It also arms the latch responsible for sending a reset signal to the main counter. However, since it is only desirable to begin the counting operation when the drive signal is at a known value, (i.e. on an edge, corresponding to a transition through the zero volt level), this latch does not trigger until a positive going edge arrives at the clock. The signal line is disabled so that a positive going edge which may occur during the reset process does not cause an ambiguous start to the count.

The hold signal goes high when the selected output of the 12 bit counter goes high, that is after 2^n positive going edges. During this interval there are $2^n - 1$ cycles of target motion. A six way switch was used to select 1,3,15,63,511 and 2047 cycles of drive motion, depending on the drive frequency being used, to give a reasonable measuring time. The monostable multivibrator in the signal line responds to negative going edges by producing a very narrow pulse. This was included to prevent the width of the signal pulse causing a delay in the start time of the count process which would cause a loss of counted fringe signals. Drive to the target was from a signal generator (Feedback PFG605), which had an output of 0 - 100 V p-p on sine,

square, triangular and trapezoidal waveforms up to a maximum frequency of 1 kHz. This source was used both with the target drive unit, (a Goodmans electromechanical vibrator with a maximum stroke length of about 3 mm.), and with the X/Y plotter used to carry the target for longer throw measurements. The electromechanical drive unit was capable of operating up to the 1 kHz. limit of the signal generator and down to d.c., but with a non-linear frequency response. The X/Y plotter had a linear response but had a top frequency limit which depended on the amplitude of motion being used.

4.2.5 Measurement and Recording

The signals from the LDI were monitored and examined on two oscilloscopes, the first a Gould 20 MHz digital storage device, type OS 1420, the other an ordinary 12MHz type OS 253. The 12 MHz oscilloscope was used mainly to display the Lissajous figure from the two amplified analogue signals, while the digital oscilloscope was more useful in freezing parts of different waveforms to examine particular behaviour, and enable polaroid photographs to be obtained. All analogue a.c. signals in the LDI were measured with a phillips model 2454 millivoltmeter which had a frequency range from 2 Hz to 2 MHz. This was used to measure LD signal levels, LVDT output at higher frequencies and the accelerometer output. On occasions where a second voltmeter was needed, and for operation of the LVDT at low

frequencies, a Keighley model 168 digital multimeter was used.

The accelerometer was a Bruel and Kjaer, model 4371, which has a calibration certificate dated 7th Dec. 1981, on which the capacitance of the accelerometer and its dedicated cable are 1197 pF, with a voltage sensitivity of 0.850 mV/(ms^{-2}). This calibration was checked and found not to have drifted within the accuracy of the recalibration.

The linear variable differential transformer (LVDT) was a Penny and Giles model HLP/90/SA1/25/1K with a 25 mm. stroke length. It was a d.c. to d.c. device, and was energised to 5.000 +/- 0.001 V. with a stabilised laboratory power supply for all these measurements, the voltage being checked at the start and end of each set of gathered data. The transducer shaft was screwed into a tapped hole in the center of the rear face of the target ensuring reliable coupling of the target motion.

Much of the data recording for assessing the LDI was based on setting up a particular set of operating conditions, and either making comparative measurements between two devices as one variable was altered, or more simply in recording the LDI output as one variable was altered. Instrument readings and accumulated fringe counts were recorded manually. The exception to this was when an attempt was made to assess the spread of analogue signal levels under various conditions. For this a data logging program was written, as discussed below.

4.3 Computer Logging and Processing

Computers were widely used throughout this research in various roles. Much of the routine data processing was carried out by loading the raw data into data files and using them as required. Programs were written as they were needed for specific operations. The two main programs used in this project are for data logging and for displaying results graphically; of these only the first is of relevance to this section.

The data logging program was written to allow a large quantity of signal level data to be collected and processed into histogram form. From the histogram, the distribution of signal levels was considered to give a different view of the operation of the LDI. The program collected 10,000 data points directly from the LDI electronics. The collecting process used an onboard 8 bit analogue to digital converter. This operated over a +/- 2.5 V input, giving a resolution of slightly less than 20 mV. per bit. The data was then collated into a 256 interval histogram, making maximum use of the available resolution. This histogram could be printed out along with the corresponding data, which could also be stored on disk.

The value of this data lies in the relationship of the variables, as it shows the amount of time spent by the signal at any particular signal level. It was particularly useful in obtaining mean and deviation data for the signal level, and in highlighting situations where signals

maintained a particular level for long periods. It was used specifically in this latter role to compare the effects of different response times in the envelope filtering circuits using real LDI signals; with larger response time, the histogram showed that the signal spent less time near the zero level. It also allowed the quantity and distribution of noise to be examined when no signal was present, although in this role it lacked resolution. The program suffered from being slow, but this was necessary to collect and process sufficient data to compile a useful histogram. Many small simulation programs were written in the earlier stages of considering possible designs and techniques for the LDI. A large number of these became redundant as ideas were superceded, but gave a useful insight into LDI operation. One of the more useful programs modelled the radius of a Gaussian beam propagating through a given optical arrangement. Different situations could be modelled by altering parameters within the program . For example it was particularly useful in locating the beam waist position of the focussed reference beam, and achieving the desired size and divergence. An associated program could be used to predict the size of speckles resulting from different illuminating beam parameters. This allowed the maximum speckle size to be realised over the anticipated operational range.

processing of the collected data also became computer dominated, with raw data being held on disk and processed and displayed as required.

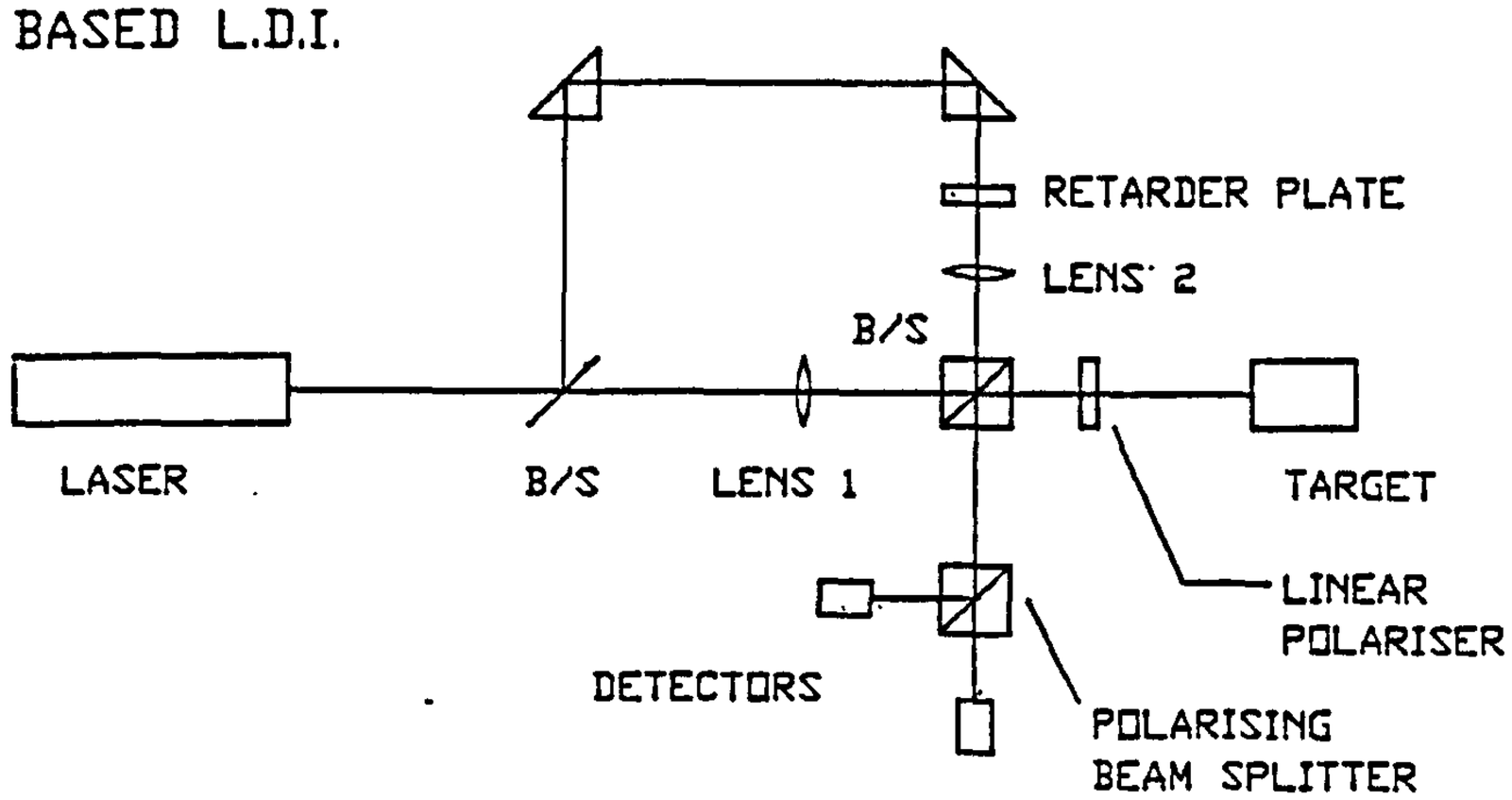

Figure 4.1

Mach Zehnder Based LDI

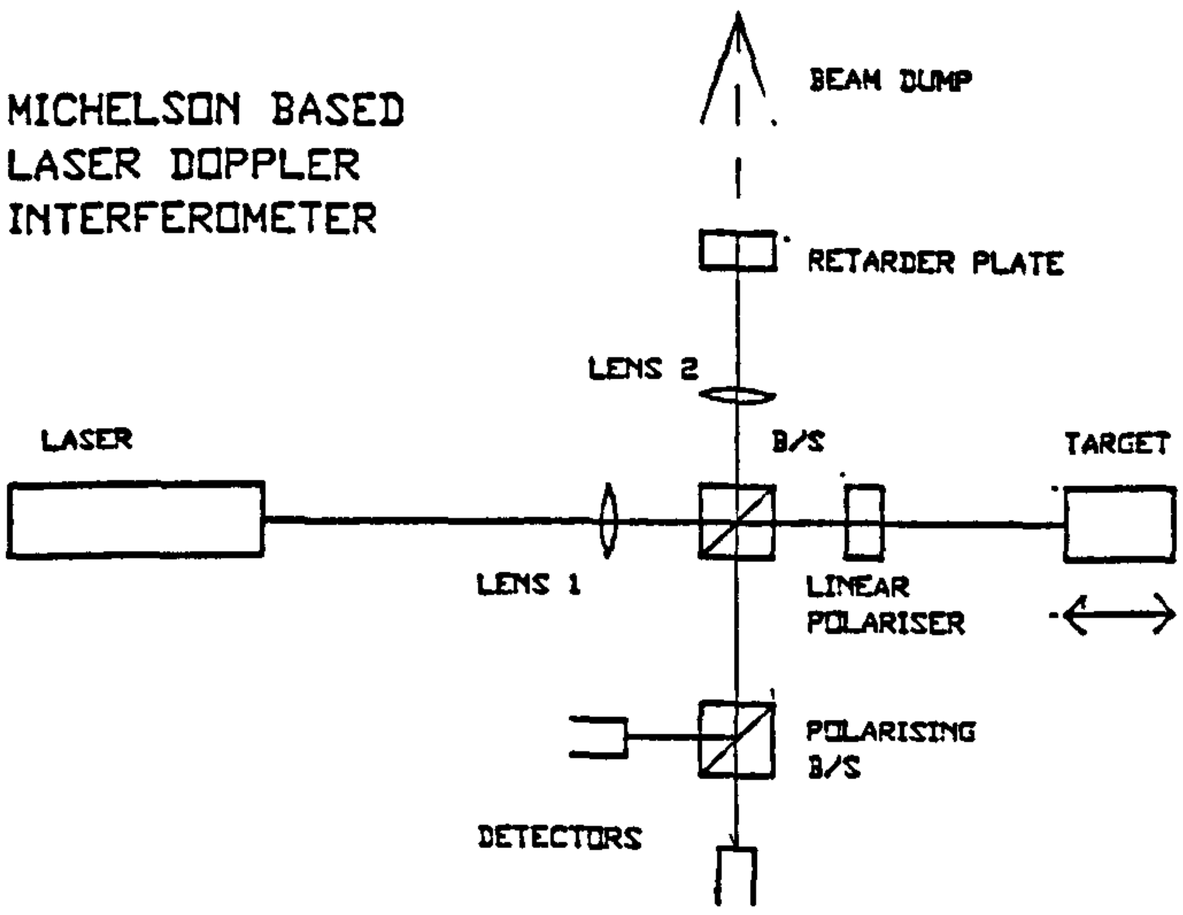

Figure 4.2

Michelson Based LDI

CIRCULAR COMPONENT MOUNT

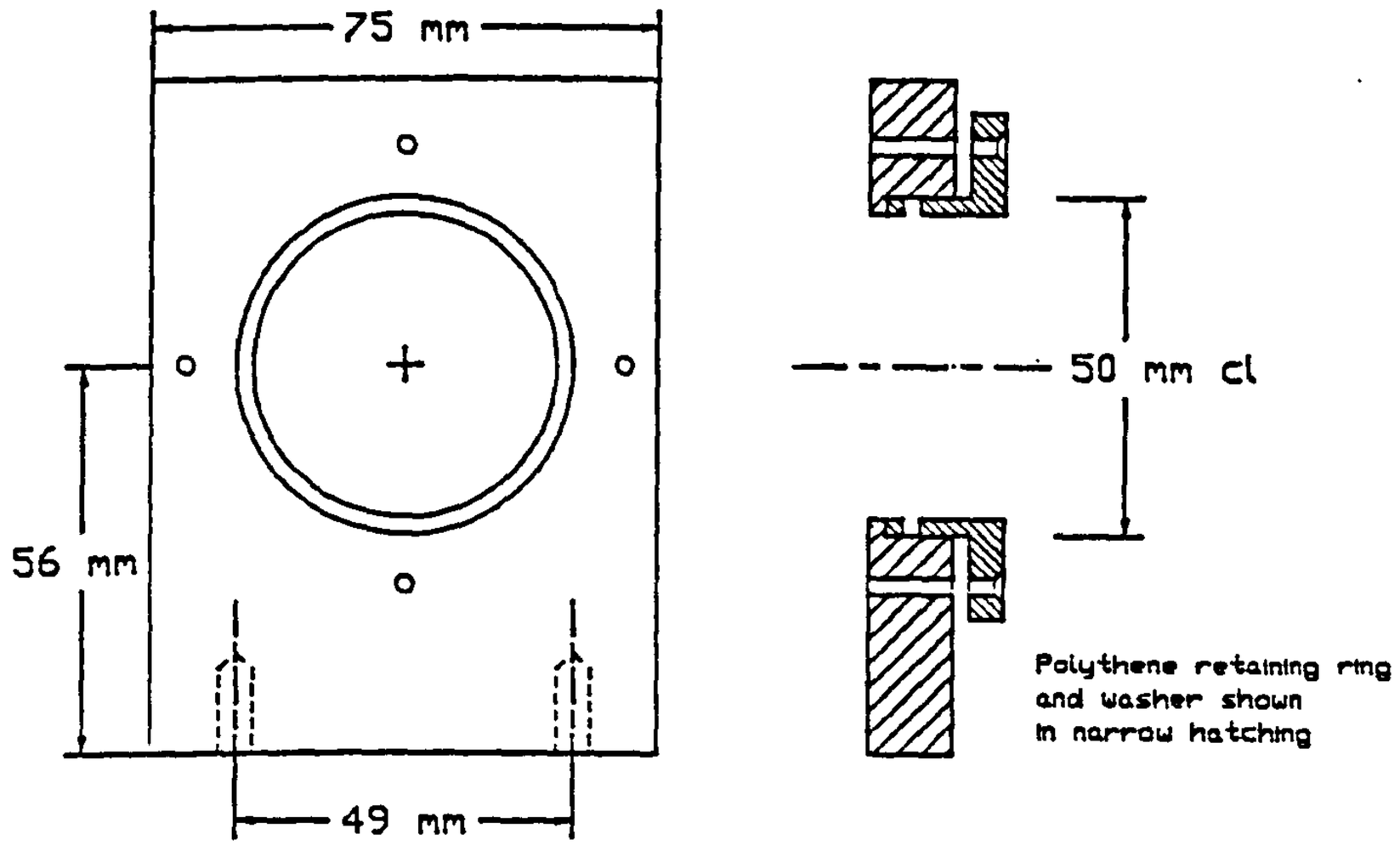

Figure 4.3

Optical Component Mount

PRISM. AND BEAM SPLITTER MOUNT

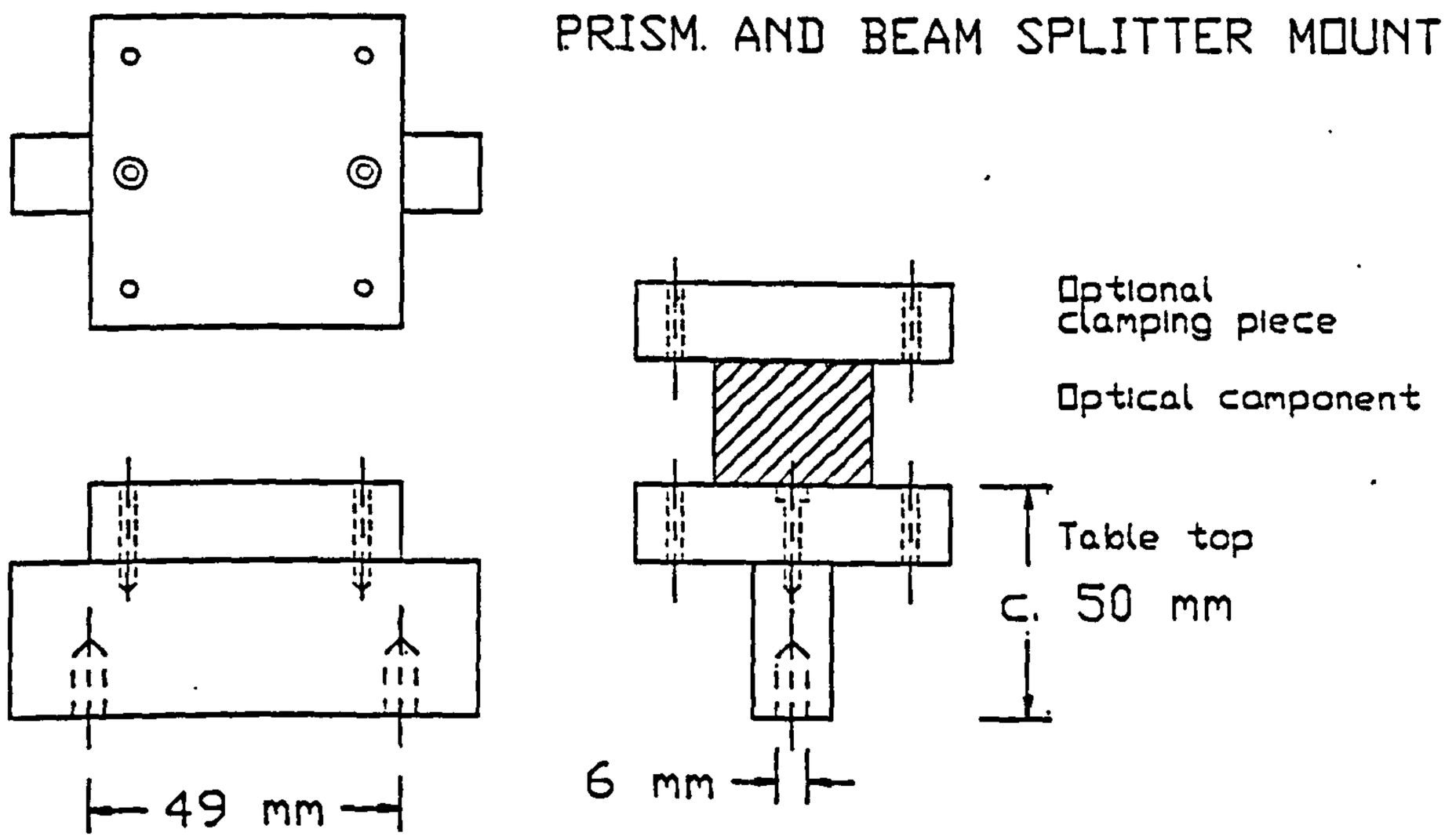

Figure 4.4

Prism and Beamsplitter Mount

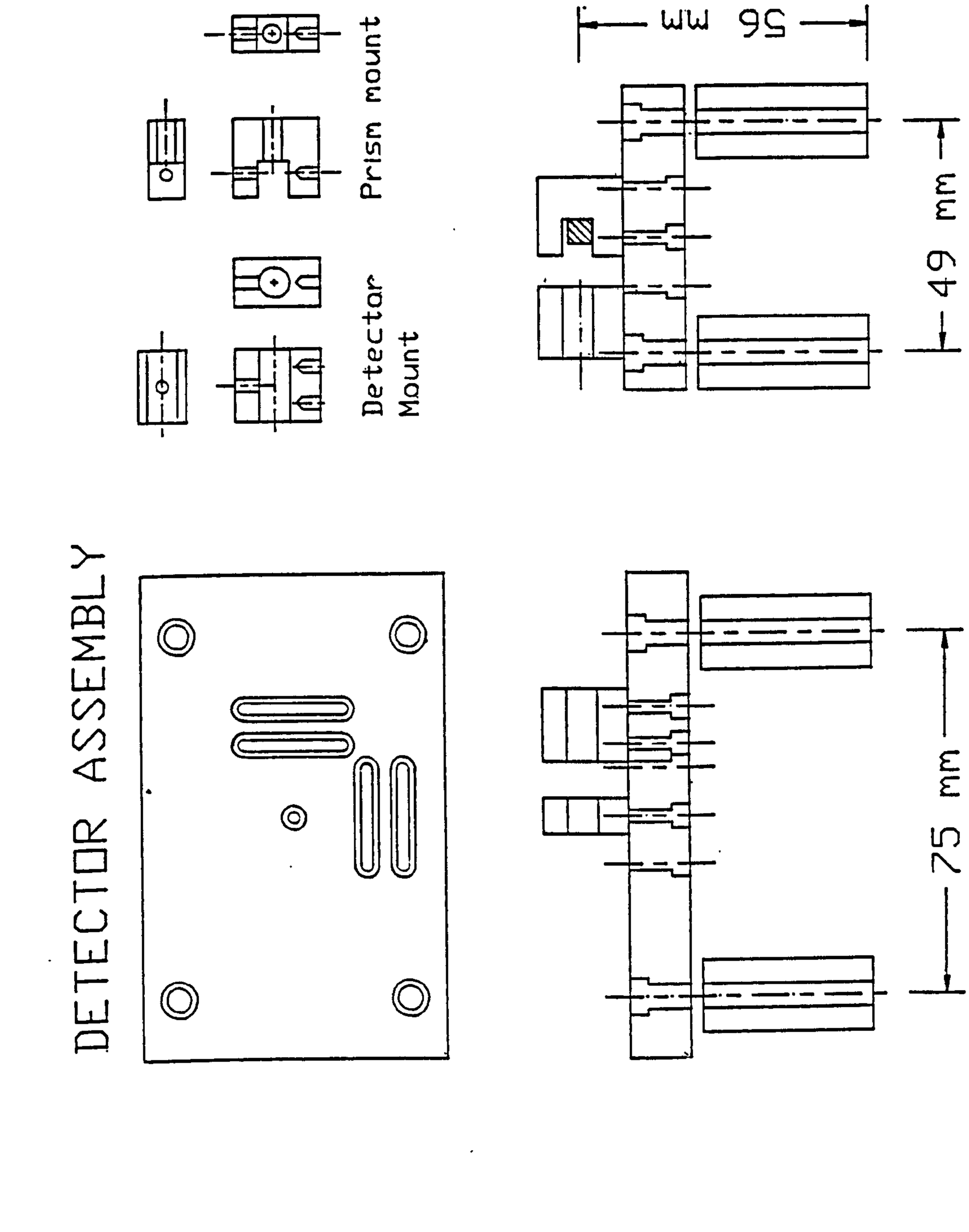

Figure 4.5

Detector Assembly

BASE FOR OPTICAL COMPONENT MOUNTS

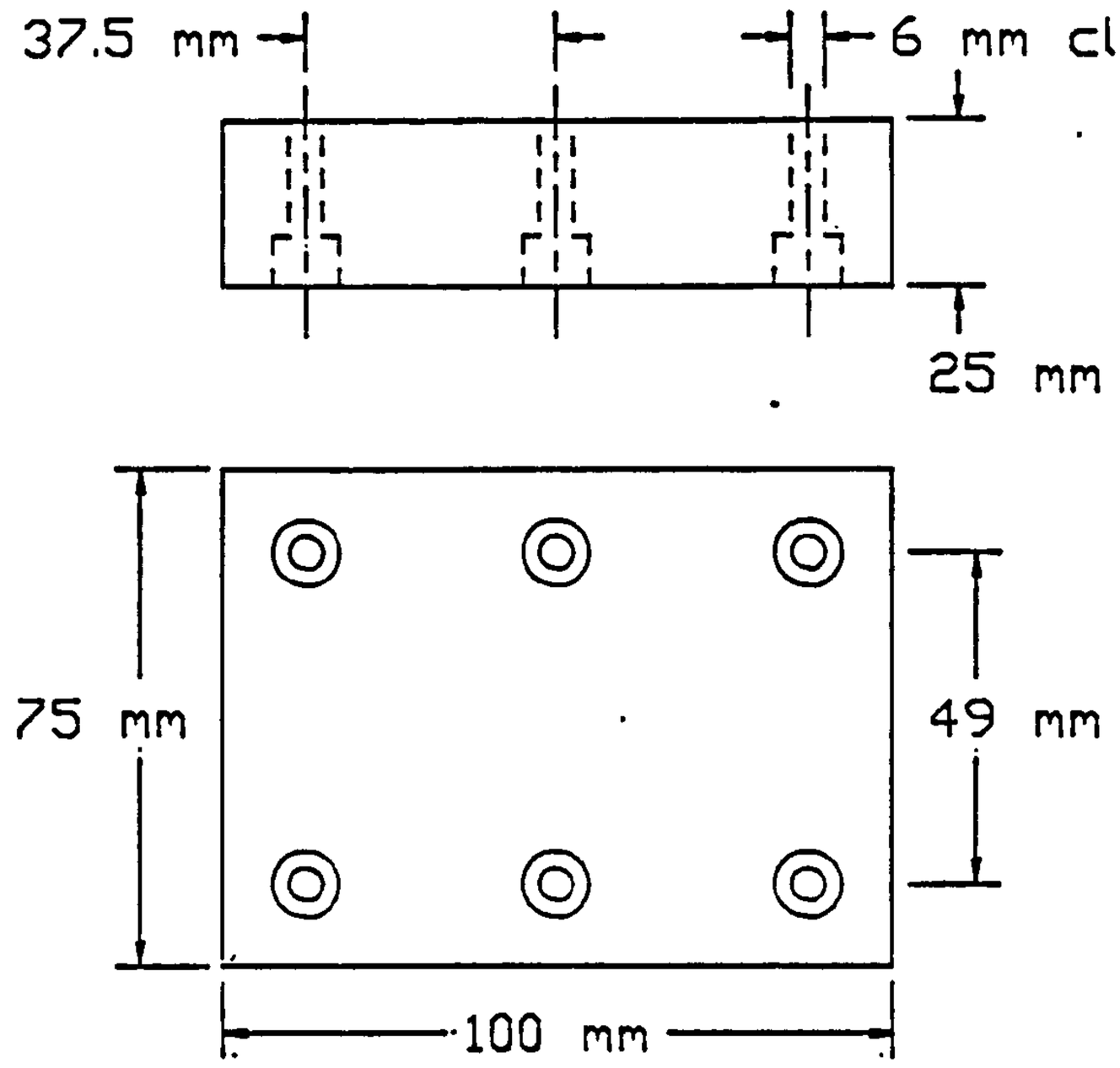

Figure 4.6

Optical Component Base

OPTICAL TABLE

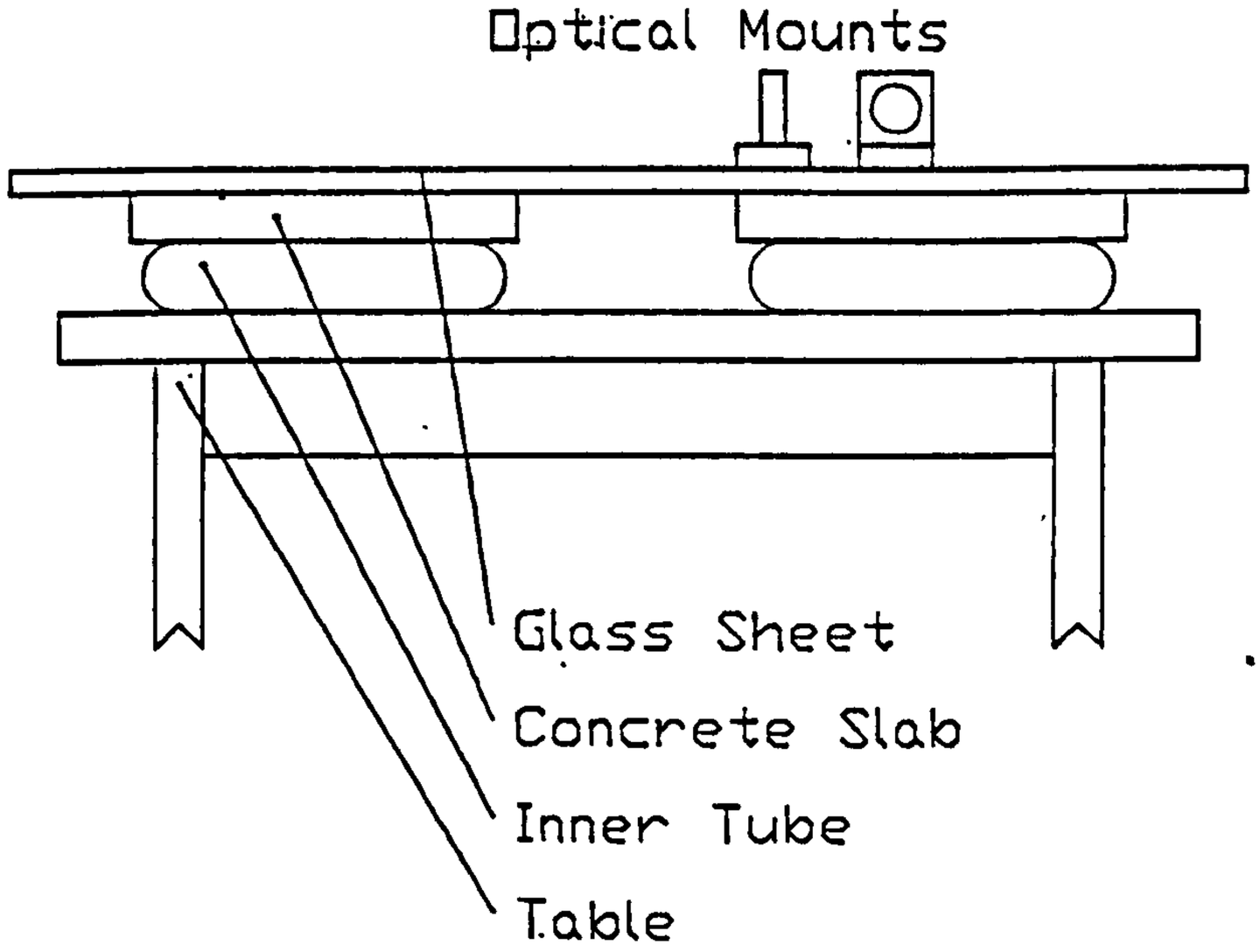

Figure 4.7

Optical Table

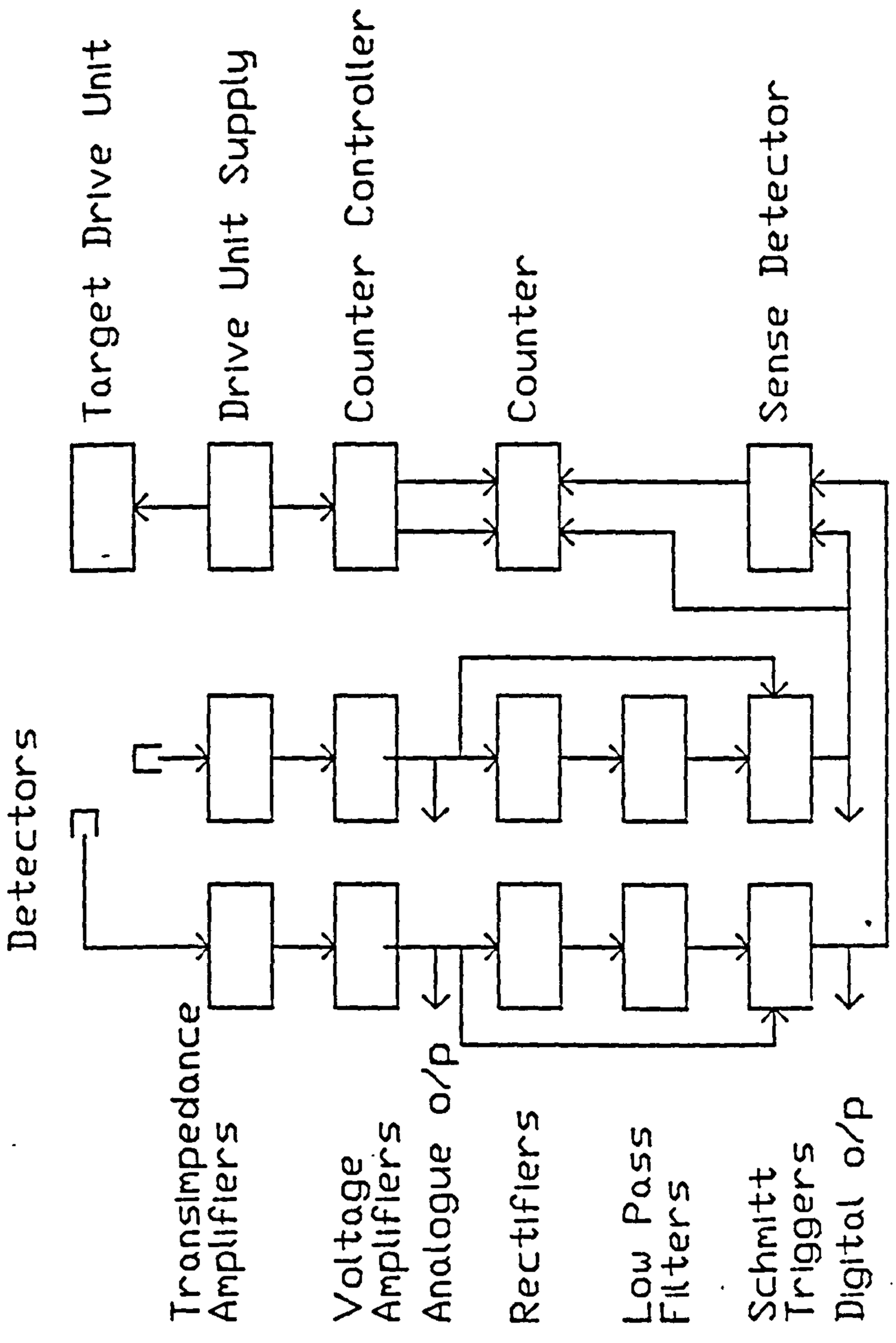

Figure 4.8

Block Diagram of the Electronics

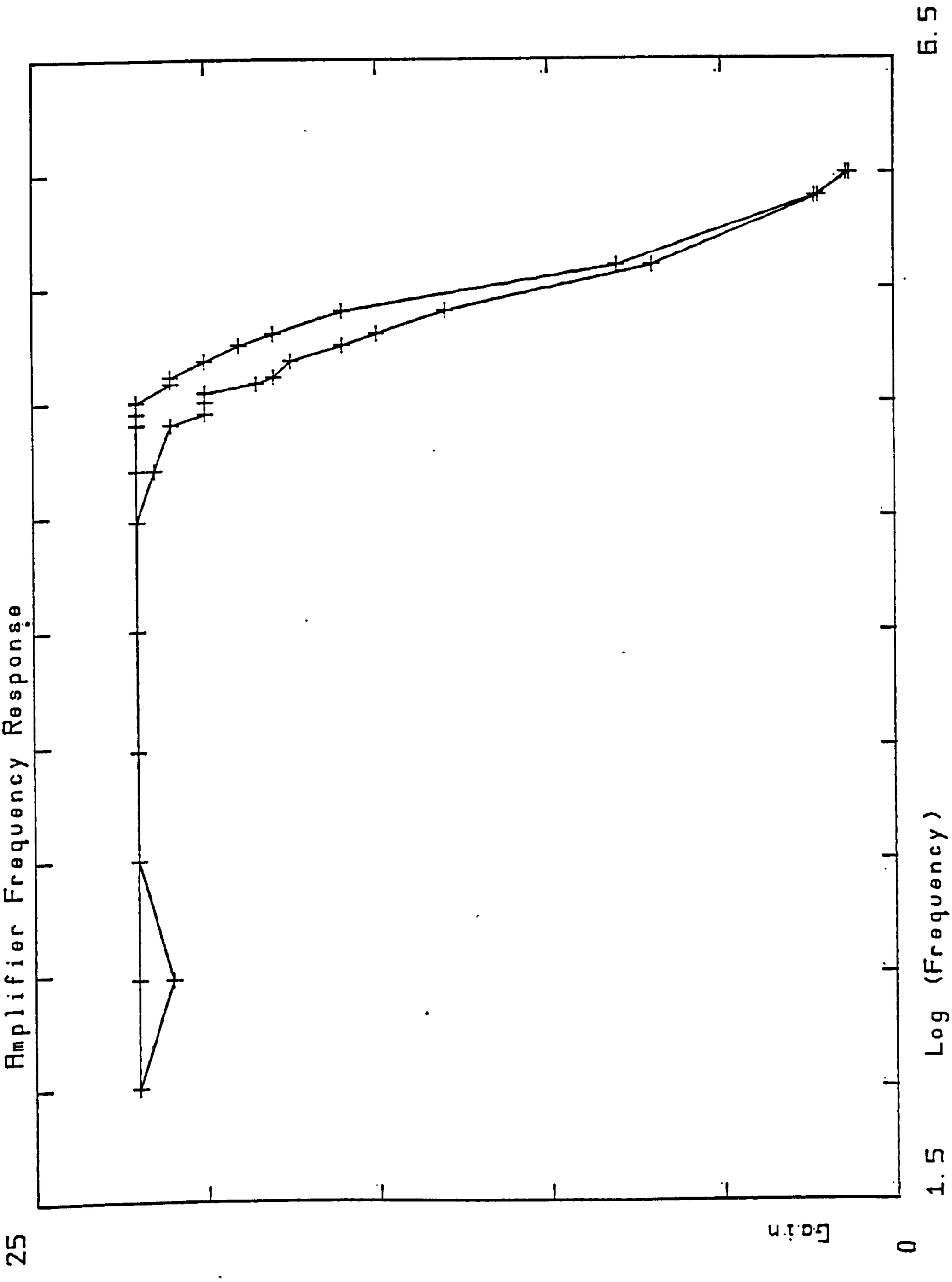

Figure 4.9 Frequency Response of the Analogue Circuits

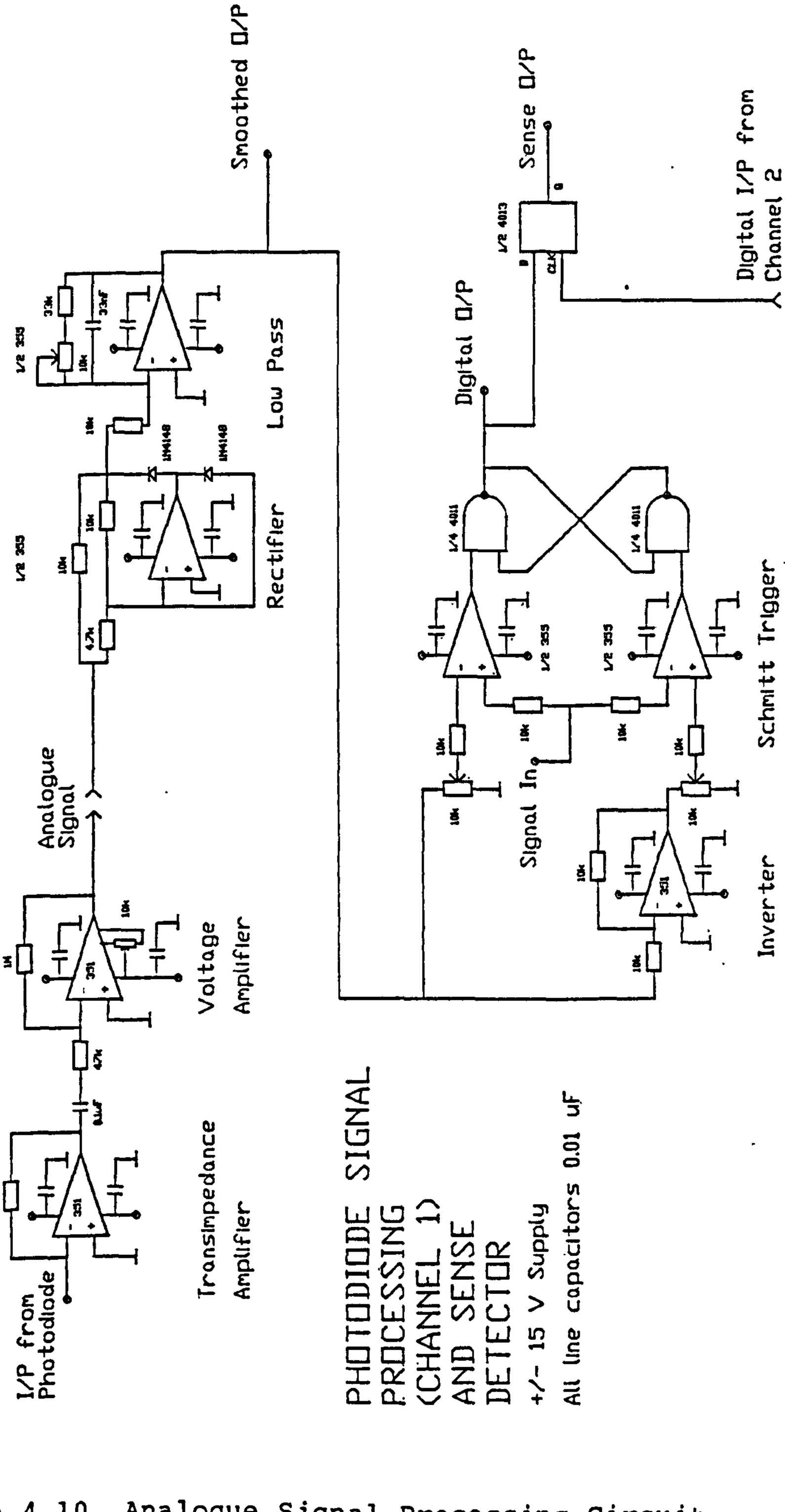

Figure 4.10 Analogue Signal Processing Circuit

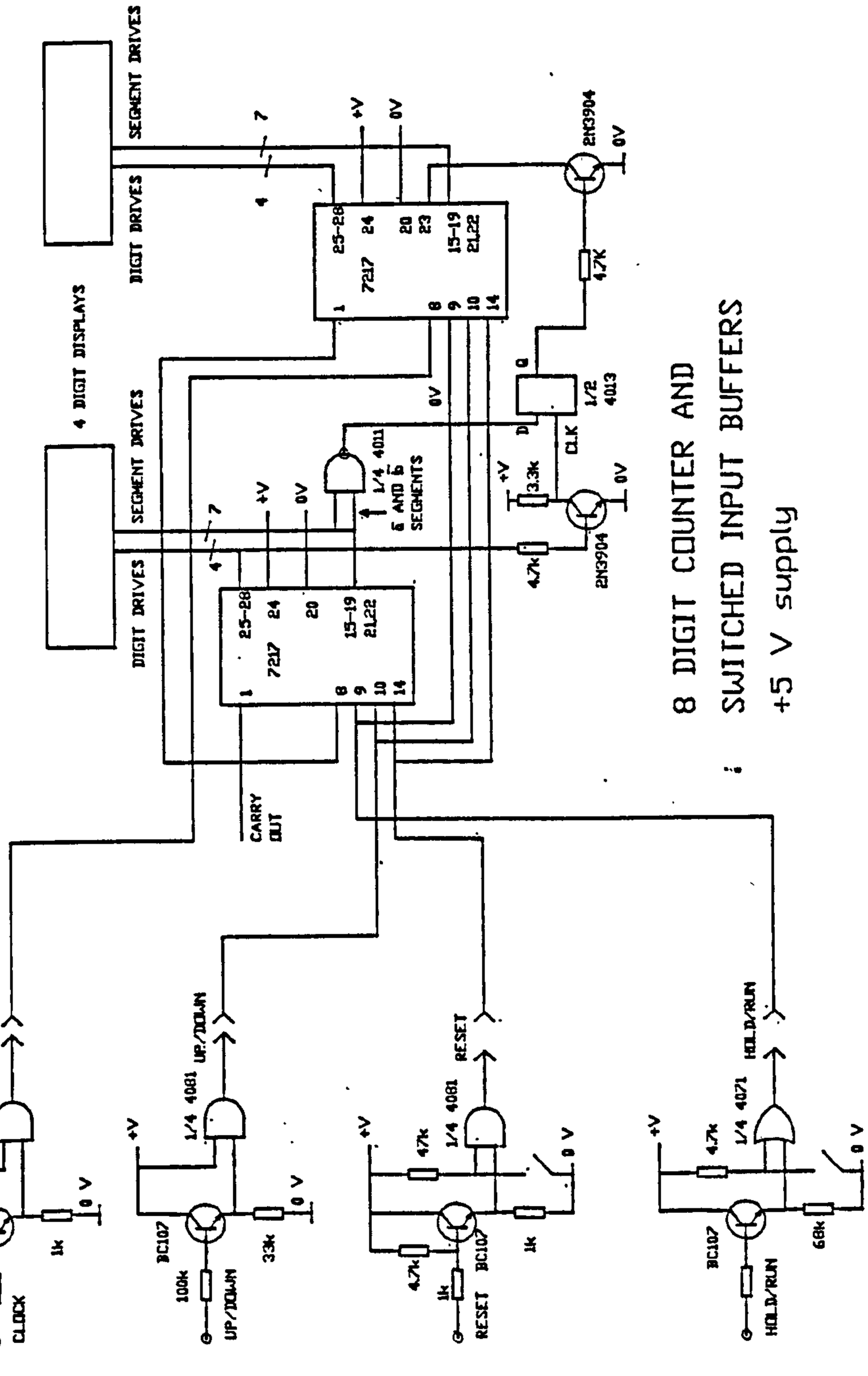

Figure 4.11 Fringe Counting Circuit

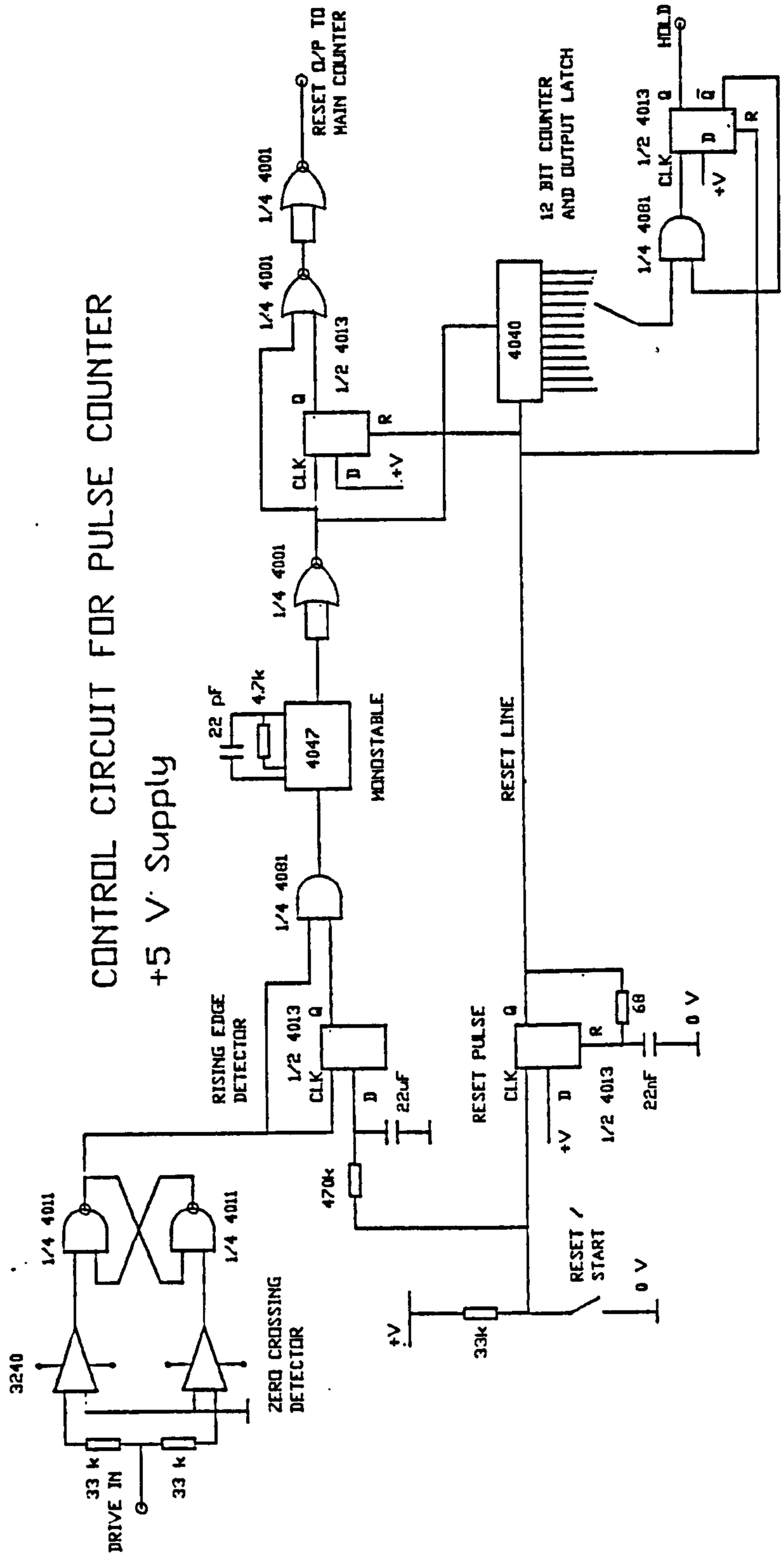

Figure 4.12 Counter Control Circuit

5. DISCUSSION OF RESULTS

In the previous chapters the relevant theory of LD devices has been covered and the experimental apparatus and method discussed. This chapter presents the results of measurements made with the LDI to assess its performance. The LDI may be considered both as a measuring device, and more generally as a signal processing device. This leads to a formal division of the results into those relating to the comparison of the LDI with other displacement measuring devices, such as the LVDT or accelerometer, and those assessing the intrinsic behaviour of the LDI. The first group is self contained, being concerned with the quality of the correlation between the LDI and other techniques, and assessing the errors that arise. The second group is less clearly defined, as these results are dependant on the interaction of the LDI with the target object, and other factors not directly linked to the LDI. It is these results that will be dealt with first, as they lead to an insight of the capabilities of the LDI and consequently a better understanding of the comparative measurements with other techniques.

5.1 The Doppler Signal

The passage of the signal through the LDI can be divided into three parts; (a) the generation by the target of a scattered light field containing a Doppler shift, which is dependant on the nature of the moving target and the

BOURNEMOUTH UNIVERSITY LIBRARY 74

illuminating beam; (b) the optical processing of this signal, selection of a single speckle, heterodyning and polarisation separation; and (c) electronic processing of the detected signal to extract the required information. In most signal processing systems the quality of the original signal dominates the quality of the final result, this is true of the LDI and has lead to an emphasis on the quality of the detected signal in the results presented here. It should be noted that the signal is available for measurement only after it has reached the amplification stages of the electronic signal processing so will incorporate the effects of the electronics.

5.1.1 The Received Doppler Signal

Typical Doppler signals are shown in figures 5.1-5.3. This signal is the output from a single detector, monitoring one polarisation component of the detected light heterodyned with the reference beam. It has passed through two stages of amplification with a combined gain of 22. The op-amp integrated circuits used in these amplifiers have a flat frequency response up to 100 kHz. Figure 5.1 shows a signal (lower trace) from a target being driven at 500 Hz (upper trace) with a peak to peak amplitude of 2.2 um. This corresponds to a maximum velocity of 3.5 mm/s , which gives a Doppler frequency of 11 kHz , well below the maximum frequency of the amplifiers. The small amplitude of the

vibration ensures that the detectors are only seeing a single speckle from the scattered light field, which results in a stable signal amplitude. Signals of this quality were easily obtained for a wide range of operational conditions of the LDI.

Figure 5.2 shows the signal from a target being driven at 44.5 Hz (upper trace), 0.36 mm p-p (from an LVDT measurement). The lower trace shows the Doppler signal, which exhibits strong peaks near the stationary points of the target motion, (the maximum points of the drive waveform). The offset between the two traces is due to the delayed response of the electro-mechanical target drive unit to the drive signal. The maximum velocity of this target is 100 mm/s corresponding to a Doppler frequency of 316 kHz. The Doppler frequency varies sinusoidally from 0 to the maximum value for a sinusoidal drive to the target, which means that in this particular case the frequency limit of the amplifiers is exceeded for a considerable fraction of the drive cycle, resulting in a decay in the signal amplitude towards the centre of the drive cycle. This effect also occurs in the correlation measurements between the LDI and a calibrated accelerometer in section 5.3.1.

There is also a signal level loss occurring during the low speed section of the target motion, which appears on the lower trace. This is possibly of greater concern in that it is possible to restrict the LDI to target velocities below

the limits imposed by the electronics, but it would considerably restrict the usefulness of the device if a lower velocity limit were also set. This attenuation is thought to be due to a d.c. blocking capacitor in the amplifier circuits acting as a high pass filter. The capacitor is necessary to block the d.c. detected light signal associated with the heterodyne process, and background light, which would otherwise drive the amplifiers into saturation. This problem is discussed further in section 5.5. Figure 5.3 shows the effect of laser speckle as the other main source of Doppler signal degradation. This figure shows a drive signal at 0.03 Hz 30 cm p-p (upper trace), and the Doppler signal level (lower trace 1V/division). The large amplitude of the target motion is allowing speckle effects to become predominant. As the target moves from maximum range at the left of the figure, to its nearest point there is an increase in the detected light level, shown by the upward trend of the signal level. This trend is broken by a series of peaks which correspond to the presence of a single speckle at the detector surface, with the troughs corresponding to the transition from one speckle to another. For a small amplitude motion, or a larger amplitude motion wholly within the strong signal level range, close to the LDI, the drop in signal level caused by speckle transition is not a severe problem. However if the motion being investigated does cause a change in the speckle pattern at the detector surface then loss of information may occur and the

measurements rendered invalid. Measurements of the effect of speckle are discussed in section 5.1.2.

Two detected signals are required for the sense of motion of the target to be found, and it is important that these signals are of a similar level, since the loss of either signal into the background noise makes the other signal redundant. It has been shown (Gasvik 1981) that for normally incident illumination, peaks in the parallel component of polarisation are scattered most strongly in the reverse (specular) direction, while the orthogonal component may be scattered most strongly in an off specular direction. Since it is the parallel component that is of principle concern here, this result implies similar signal levels may be expected for the two components derived (at + and - 45°) from the scattered light. This was verified during many of the measurements from the LDI by displaying the two analogue signals on a separate oscilloscope as a Lissajous figure, allowing their amplitudes and phase to be monitored. Although they were rarely in perfect quadrature and of equal amplitude, strong deviation from this ideal only occurred during speckle transition, or at large target ranges. An enlarged section of the two signals is shown in figure 5.4 which shows good quadrature, but different amplitudes.

5.1.2 Laser Speckle

The formation of laser speckle has been discussed in section 3.3.1. It is included here because the presence of speckle in the scattered light field affects the measurements that may be made from that field. When a target is in axial motion the speckle pattern at the detector surface will change, causing a variation in the signal level. This can lead to a loss of both the measured displacement and the sense of motion. Results of measurements of displacement show a good immunity to loss of signal due to this effect, but the effect on the sense of motion signal is more severe. Two methods of assessing this have been pursued.

The first is based on direct measurements of the duration of uninterrupted sense of motion signals derived from a target being driven at large amplitudes with a sawtooth wave, giving a constant target velocity. The target was mounted on the crosshead of an X/Y plotter to give the length of motion required.

Two sets of data were recorded, the first from a target driven at 0.025 Hz with an amplitude of 113 mm p-p. Nine readings gave a mean clear range of 35.3 mm with a standard deviation of 14.8 mm. The second set used a 200 mm p-p motion at 0.025 Hz. Nineteen readings gave a mean clear range of 46.7 mm with a standard deviation of 20.4 mm. The mean range of the target for this data was 40 cm in both cases.

The second method of measuring the speckle length was based on a simple statistical model. This predicts the mean speckle length from a group of displacement measurements made under identical conditions from different points on the target surface. Since each different illuminated point generates a different speckle field, a fraction of these measurements will be disrupted by speckle transition causing signal loss. If the mean speckle length is L, and the measured target displacement is d_m, then the probabilty of a randomly positioned measurement crossing between speckles is:

$$P(\text{Speckle transition}) = d_m/L \ . \qquad (5.01)$$

The fraction of disrupted readings e is equal to this probability for a large enough total number of readings. If e is known the mean speckle length can be found as,

$$L = d_m/e \ . \qquad (5.02)$$

Data was recorded from a target driven at 50 Hz with an amplitude of 42.9 um p-p, with a standard deviation of 0.05 um. This amplitude was measured from 15 sets of data taken at 5 locations across the target face, each measurement being over 15 cycles of target vibration.

Measurements of the sense signal quality were taken by logging the number of fringes during 15 cycles of the target vibration, using the sense of motion signal to control the direction of the accumulated fringe count.

A total of 126 readings were recorded and these were distributed equally either side of zero. In the ideal case the count logged in this manner should be zero on all occasions. Allowing for the possible ambiguity in the digitising process a difference of one count between the approaching and receding halves of each cycle would be acceptable, leading to a logged count in this case of 15 fringes. Depending upon the acceptable error different criteria may be used to define an erroneous count logged by this process. Two cases of 1% and 5% of the displacement signal were taken as error levels. The 1% level made 78 of the total 124 counts erroneous, which, using equation 5.02 above, gives an expected clear run length of :-

$$42.9 \times 124/78 = 68.1 \text{ um.}$$

The 5% error case gave 52 erroneous readings, implying a clear run length of :

$$42.9 \times 124/52 = 102.2 \text{ um.}$$

Three readings exceeded 95% of the measured target displacement, of which two were very close to the actual displacement, indicating total failure of the sense signal. There is a large discrepancy between these two approaches to the measurement of the length over which well defined sense detection can be realised.

This discrepancy is due to the characteristic length of

each measurement. The first method only recorded clear sections of the sense of motion signal with a length greater than 10 mm, while the second recorded all those clear sections with a length of greater than 42.9 um. Since this latter case includes all those sections of the signal that fit the former case, and many smaller clear lengths, it must give a mean clear signal length which is smaller than the method using a 10 mm size limit. The first set of data was also selective, taking no account of those periods of the signal not containing a clear length greater than 10 mm. The second set of data looked randomly at the signal, giving a probability of a clear length occurring, a factor not included in the first method, which is consequently ambiguously large.

The main conclusion of this analysis is that the longer the desired measurement range, the lower the probability of it being uninterrupted by a breakup of the sense of motion signal. This in turn will increase the time required to locate a measurement condition that allows the desired measurement to be made.

A possible method of overcoming this problem, and more generally of reducing the statistical effects of the scattered light, is the use of more than one set of detectors, possibly in conjunction with some degree of self referencing signal level measurement, to predict the onset of signal loss, and allow secondary verification of the sense of motion signal. If secondary verification were introduced, it should only be used to confirm the sense of

motion of the target, and not its magnitude, as it would necessarily measure a different part of the speckle field and therefore have to be placed off axis, and consequently see a component of the axial velocity. This could be kept to extremely low levels, but would not be a constant error, and would lead to the undesired introduction of sensitivity to transverse components of the velocity being measured.

5.1.3 Target Finish Effects

Although the speckle size in the scattered field is only weakly dependent on the surface roughness of the illuminated object, the intensity distribution does have a strong dependence. This arises as a result of the directional nature of many of the target surfaces that were used. These were the end faces of short lengths of 1" diameter dural bar, which had been finished with emery paper of different grades in the range 320 to 500. These targets scattered light with a high intensity band in the scattered field, with the plane of the band perpendicular to the direction of the scratches. There are two possible mechanisms for this effect, either that the parallel scratches act as a reflection diffraction grating, with a range of line spacings, which smear the orders of diffraction to form the higher intensity band, or that the surface is acting as a collection of orientated reflecting regions. These regions are the sloping sides of the approximately prismatic scratches with their axes parallel

to the scratch direction, and formed by the abrasive grit particles. These will preferentially reflect light into a plane perpendicular to the axes. The effect may be a combination of both explanations. A considerable quantity of literature on scattering from optically rough surfaces exists containing comments on this type of behaviour, this has been discussed in section 3.3. The high intensity band contains the detection direction for an illuminating beam normally incident on the surface. This means that many results from targets with a directional finish may have larger than expected signal levels. However since many anticipated targets will have machined finishes with a directional nature it is reasonable to include this data.

Although the majority of measurements were taken from dural targets, data recorded from matt black, white and silver surface gave measureable signals, with those from the white and silver targets allowing measurement over similar ranges to the dural targets. None of these targets had any directional nature in the surface finish, and the scattered light showed no preferred scattering direction.

The reflectivities of various target materials are tabulated by Levi (1968). Taking the case of the matt white surface with a reflectivity, ρ, of 70 %, which can be assumed to conform closely to Lambert's law it is possible to calculate the quantity of light received by the detectors on scattering. Taking a typical target to detector distance, R, of 40 cm and a detector surface area,

a_{det}, 1mm x 1mm and allowing for the transmission of the beam splitter, T, gives a ratio for normally incident to normally detected intensities of :-

$$I_{det}/I_{ill} = T^2.\rho.a_{det}/(2.\pi.R^2) \quad . \tag{5.03}$$

Substituting the values suggested above gives an intensity ratio of about 2×10^{-7}. Although this seems a small figure it still provides sufficient detected intensity from a 1 mW laser to ensure effective heterodyne detection.

5.1.4 Signal Variation with Target Range

One of the original aims of this project was to investigate the possibility of making measurements of large displacements to a reasonable degree of accuracy. To achieve this there must be a detectable signal from the target at all points along the measurement range.

Several sets of data assessing the variation of signal level with changes in target range have been collected, covering a range of different measurement conditions. The crudest are derived from a target driven over a single sweep of 30 cm. This was the largest linear displacement that could be brought to the experimental rig for measurement. Figures 5.3 and 5.5 show the signal level (lower trace) and the drive signal for the target (upper trace). At the left of the figure the target is at its maximum distance from the LDI (55 cm), with the datum point for measurement being the beam splitter/combiner element and at the right its closest (25 cm). Figure 5.3 records the signal level, (vertical scale 1V/division), with a lens focussing the illuminating beam. The signal level with a focussing lens in place is higher but decays faster than when no lens is present, as shown in figure 5.5 (vertical scale 0.5V/division). The peaks that interrupt the general intensity trend in the case of the focussed beam are wider, indicating a greater probability of realising large displacement measurements, within the confines of the focal length of the focussing lens. The signal level for the

unfocussed beam is lower but extends beyond the limits of measurement by this technique. This is presumed to be due to the smaller speckles generated by a larger but less rapidly changing spot size from an unfocussed illuminating beam.

The other sets of data that were recorded to investigate the variation in signal strength with changing target range, all consist of a series of discrete measurements from a target driven at different frequencies and amplitudes. They all give a local average of the signal level within the range covered by the amplitude of vibration, with the particular average depending upon the waveform of the drive wave. This will allow measurement of displacement and detection of sense of motion at that range. These results are shown in figures 5.6 to 5.9. Figures 5.8 and 5.9 are taken from emery finished dural targets illuminated by a focussed beam.

Many of the intensity versus range plots show depressed signal levels at very short ranges. This loss in signal level is not generally sufficient to cause the digitising and counting processes to fail, so in practical terms does not affect the operation of the LDI. However it is worth investigating. There are two possible explanations, one based on the speckle size at the detector plane, the other on diffraction by an aperture corresponding to the illuminated region of the target surface.

Consider the case of a focussed beam illuminating a region of diameter r_o on the surface of a target at a range R,

from the detector plane. The radius of the speckle, r_{sp}, at this plane is given by equation 3.43 as:-

$$r_{sp} = \lambda.R/r_o \quad . \qquad (3.43)$$

The illuminating beam converges from the lens to the beam waist, then diverges. The beam radius r_z has been given in equation 3.51 (section 3.4.2) in terms of the distance, z, from the beam waist as :-

$$r_z = ((\lambda.z/\pi.r_w)^2 + r_w^2)^{1/2} \quad , \qquad (3.51)$$

where r_w is the waist diameter. If the detector plane is offset from the waist position by a distance R_d, the viewing distance from the target surface to the detector is:-

$$R = z + R_d \quad . \qquad (5.04)$$

When the target is inserted into the illuminating beam, the beam radius at that point becomes the radius of the illuminated region, i.e.

$$r_{ill} = r_z \quad . \qquad (5.05)$$

Substituting equation 5.04 into 3.51 and the result into 3.43 gives an expression for the speckle size at the detector, with target motion through the focussed beam as:-

$$r_{sp} = \lambda.(z + R_d)/((\lambda.z/\pi.r_w)^2 + r_w^2)^{1/2} \quad . \qquad (5.06)$$

Typical values for these parameters from the LDI give the expected speckle size at the detector plane as shown in figure 5.10.

The speckle size decreases rapidly as the target moves inside the beam waist, towards the LDI. It is this which may account for the depressed short range signal level readings, as when the speckle size is small, more than one speckle may be detected. As the speckles have a random phase relationship with each other, the most likely effect of this interaction is neither totally constructive, nor totally destructive, but will cause a decrease in detected signal level.

The same argument may be applied to an unfocussed illuminating beam. This may be considered as originating from a waist at the center of the laser cavity, and diverging from that point. In this case R_d is the offset between the detector plane, and the position of the beam waist in the laser cavity. It may be seen that if the detector plane is equivalent to the position of the beam waist, and if all measurement is to occur at a distance from the position of the beam waist, as must be the case for an unfocussed illuminating beam, then equation 5.06 may be rewritten as :-

$$r_{sp} = \lambda.z/(\lambda.z/\pi.r_w) \quad ,$$
$$= \pi.r_w \quad . \qquad (5.07)$$

Under these conditions the detector sees a constant speckle size. If the speckle size is sufficiently large then this

is the ideal situation. In the case of the existing laser, it would give a speckle radius of 0.396 mm. To achieve this ideal situation of coincident positioning of the detectors with the beam waist is unwieldy when a practical LDI is considered, as it will require undesirable additional optical components, either to bring the signals to the detector position, or to image the original beam waist at a new position. The former option is less cumbersome, but severely restricts the flexibility of the device. The latter retains control over beam size and divergence, but introduces a waist position that will either be at a considerable distance from the laser with a low divergence, and hence larger speckle size, or will be closer but with a higher divergence giving a smaller speckle size. Neither option contributes to a tidy and practical LDI design. Consequently variation of the speckle size must be accepted as necessary for a more compact design.

The second possible explanation of the signal intensity variation with changing target range is based on meeting the coherence condition at the detector surface. This requires matching the wavefronts of the two beams being mixed at the detector surface. Assuming that the reference beam is focussed to a waist at the detector surface, it has a plane wavefront. For the coherence condition to be met, the difference in path lengths between the centre and the edge of the mixing area should be less than half a wavelength. Considering the scattering surface of the

target to be a point source, at a distance R from the detector plane, which is assumed to be a circular aperture of radius r_{ap}, the difference in path lengths between beams travelling to the center and edge of the aperture is:-

$$d = r_{ap}^2/R \quad . \qquad (5.08)$$

As the target approaches the detector plane the path difference increases. At a range of 40 cm., with a detector radius of 0.5 mm., the path difference is 0.625 um. which is approximately the wavelength of the HeNe laser. A pathlength difference of half this figure will be reached when the target recedes to a range of 80 cm. In the experimental equipment, the detector has a 1mm. x 1mm. active surface, so signal loss due to significant deviation from the coherence condition could be expected. However, if the focussed reference beam waist is smaller than this, the effective active area of the detector surface is reduced and the coherence condition will be met for shorter ranges. Alternatively, if the reference beam is not being focussed to a waist at the detector surface but has curvature of the same sense, if not of the same degree as the scattered light from the target, the coherence condition will be more nearly met. A comparison of the mean phase difference across a circular and a square active surface has been made. For a given range, R, the mean phase difference

across a circular surface of radius r, is :-

$$\overline{p} = r^2/(\lambda.R) \quad . \qquad (5.09)$$

For a rectangular aperture of dimensions 2u x 2v it is:-

$$\overline{p} = 2.\pi.(u^2 + v^2)/(3.\lambda.R) \quad . \qquad (5.10)$$

The variation of the mean phase difference for a square aperture 1mm x 1mm is shown in figure 5.11, and derivations of these equations are given in appendix 3. This assumes a point source and a plane reference wave at the detector surface. It also indicates the range below which serious loss of signal might be expected to occur by this mechanism.

The short range loss of signal may be due to operation of both coherence condition and speckle size effects. However it is thought that the longer range fall off may only be attributed to speckle effects and normal fall off in intensity with increasing distance.

5.1.5 Count Variation with Range

The variation of the measured displacement with increasing target range is shown in figure 5.12 which shows that the measured displacement is constant up to a maximum range, beyond which there is a breakdown of measurement, and count loss occurs. The exact range of the onset of signal loss depends on the target reflectivity and beam focussing, typical ranges being 50-60 cm. It is significant that this

loss of the count corresponds to the loss of signal, as this indicates that the background amplitude noise of the LDI is not likely to cause spurious counting in the absence of an optical signal.

The measured target motion in the flat part of each figure does contain small variations. These are most probably due to slight misalignments of the target motion direction to the illuminating beam, causing the measured component of the motion to change.

These measurements show there is no drop in count corresponding to the drop in signal level at short ranges of measurement that was apparent in section 5.1.4 above.

5.1.6 Sense of Motion Invariance with Range

It was important to establish the stability of the sense of motion signal derived from orthogonal phase components of the optical signal, as this dictates the usefulness of the LDI in making measurements of non-cyclic motion. This was done by driving a target over a reasonably large amplitude, and recording the correspondence of the sense of motion signal with the direction of the drive signal to the target. A large amplitude was used as the data was thought to be useful in ascertaining the possible length of motion that could be measured before a speckle transition, or other disruptive effect, destroyed the continuity of the measurement. Data was gathered from a number of different points on the target surface. The reliability of the sense

signal was measured by the percentage of logged data for each of the possibilities, motion in either direction, or an indeterminate signal. Three different optical configurations were used. This gave a variation in the results, figures 5.13 - 5.15, which is attributed to the strength of the signal and to the speckle size. As was stated above, (section 3.2.2), the sense of motion signal requires good signals to be detected by both channels of the LDI. Although both detectors are ideally viewing the same section of the scattered light field, depolarisation by the target may lead to different light levels at each detector. Depolarisation becomes the main factor in determining the loss of the sense of motion signal. With targets that depolarise more strongly it can be expected that the sense of motion signal will fail at shorter ranges than for targets that do not depolarise the scattered light. The reduction in range will depend on the degree of depolarisation.

If a clean up polariser is used in the path of the scattered light, it ensures that both detectors receive equal intensities, but these will be equal to the lowest intensity that would have been received by either of the detectors without a polariser present. This results in a loss of signal occurring at a similar point with or without a clean up polariser present.

Figure 5.13 shows the stability of the sense of motion signal for a focussed illuminating beam with a clean up polariser in the beam. Near the illuminating beam waist, at

about 40 cm. from the LDI datum, the stability is high. This is attributed to the small illuminated region generating large speckles at the detector plane, resulting in good signal stability and consequently good sense of motion signal stability. The rapid decrease in signal either side of the beam waist is probably due to relatively rapid beam divergence leading to smaller speckles and loss of signal quality. This is supported by figure 5.14, which shows similar results from an unfocussed illuminating beam. Although the reliability of the signal is lower the fall off is less rapid than for the focussed beam above. When the clean up polariser is removed (figure 5.15) there is no significant change in the trend of the results over that derived from an unfocussed beam with the polariser present. It could be suggested from the negative sense probability plot of figure 5.15 that at short ranges the sense signal was of a poorer quality. This would be expected, as the beam diverges from the LDI, generating smaller speckles at the detectors for closer targets.

5.1.7 Effect of Target Surface Inclination

It may not always be possible to illuminate the target at a point where the surface is normal to the direction of illumination. The effects of changing angle of incidence of illumination on signal level and measured displacement were investigated for two cases, shown in figure 5.16.
The first used a target driven with the motion

perpendicular to the illuminating beam at normal incidence on the target face, the other with motion parallel to the beam at normal incidence. The measured signal levels and displacements for these two cases are shown in figures 5.17, 5.18, and 5.19, 5.20 respectively. The spread in signal levels results from the transverse motion of the target scanning the speckle pattern across the detectors, and the arbitrary angles on the figures are a result of not knowing prior to the measurements where minima or maxima would occur. The target was mounted on a spectroscope table to provide accurate rotation, and the signal level data logged by computer collection of 10,000 values, allowing the distribution to be assessed.

The measured displacements behave as would be expected, with the values related to the cosine of the angle between the illuminating beam and the motion of the target. The main implication of this, which may not have been so obvious elsewhere, is that the LDI is sensitive to any motion which has a component in the axial direction. In turn this requires that the measurement direction is selected carefully when making a particular measurement.

A problem was encountered during these measurements with the preferential scattering direction from the dural target face, (section 5.1.3), which could cause excessively high signal levels as it traversed the detectors. The target was mounted so that the long axis of the preferential scatter region crossed the plane of incidence to minimise this

effect, but no specific orientation was used. This may be responsible for a significant feature of these plots, which is a discrepancy between the measured position of maximum or minimum count and the maximum signal levels. It is possible that this relates to the results obtained by Gasvik (1981) for scattering from inclined optically rough surfaces. Where the drive motion was axial the signal level and maximum count coincided, but for transverse motion this did not occur. A repeat of the measurements for the transverse case gave less conclusive results.

Comparison of the signal levels for the two cases show that the axial motion gave larger signal levels by a factor of 2-3 times. This may arise from the relative stability of the speckle pattern for axial motion, which is lost when the target is in transverse motion. It is possible that where a large signal would be expected due to normal incidence, and strong backscattering, the blurring caused by speckle motion reduces the level, and as the target rotates so that the component of transverse motion decreases, the blurring effect is reduced, giving larger signal levels. This should occur symmetrically about the normal incidence position, but from the results that were obtained, this does not seem to be the case. It is also possible that the direction of the scratches on the target face may provide a mechanism to explain the effect. The scratches may be considered to be approximately parallel and roughly V shaped. When the target is aligned so that an illuminating beam is incident normally to the sides of the

scratches it will be specularly reflected in the same direction. This will cause peaks in the scattered light at angles either side of the normal to the surface, where the angle is the same as the mean slope of the scratch sides. This mechanism should result in two peaks in the scattered light either side of the normal incidence position, and will only occur when the scratches are aligned perpendicularly to the plane of incidence, otherwise the scattering will be out of plane, and not detected.

While neither of these explanations gives a full account of the effect, it shold be noted from the figures that the measurement of the target is not adversely affected by it, so it does not detract from the operation of the LDI as a measuring instrument. Also implicit in these results is the ability of the LDI to measure the axial motion of a target which does not have a face perpendicular to the direction of motion. Additionally, a qualitative assessment of a matt white target showed that the scattered light level varied far more slowly with changing angle of incidence than for a dural target. This would be expected as the scattering will be more closely Lambertian (Levi 1968).

5.2 Variation of Measured Target Displacement with Drive Frequency

In this section the discussion centres on the measured displacement under a given set of conditions. By analogy with discussion above, if the displacement is measurable by the LDI, then it is implied that the signal level is sufficiently large, and that it will be possible to extract a sense of motion signal within the constraints mentioned in section 5.1.2 on laser speckle.

The results from measurement of target displacement with changing target drive frequency, and hence, target velocity, are shown in figures 5.21 to 5.22. Figure 5.22 contains normalised data from three data sets, one of which is shown in figure 5.21. These results are all derived from a triangular wave driven target of relatively large amplitude. This is because the electro-mechanical drive unit that was used at high frequencies and small amplitudes did not have flat frequency response so variation of the drive frequency caused a change in the amplitude of the vibration. The accelerometer correlation measurements, (section 5.3.1), were made at higher frequencies, and implicit in these is a measure of the stability of the LDI with changing drive frequency.

The results given here all show similar behaviour, which may be divided into three regions. The first region, at the lowest frequencies, contains some erratic measurements, but the general trend is of increasing measured target

displacement with decreasing target frequency. Because the measurement process was governed by recording the number of fringe counts during a fixed number of target drive cycles, the measurement time increased with decreasing drive frequency. This implies that the excess measurement in the displacement is directly proportional to the measuring time. The source of the excess measurement is probably additional motion occurring between the LDI and the target, specifically in this case, by vibration of the X/Y plotter on which the target was mounted to realise larger amplitude motion. This was due to a cooling fan in the plotter. (The conditions under which background motion can introduce excess counting are outlined in section 5.3.2, on LVDT correlation measurements, which also used relatively low frequencies.)

At the high frequency end of these plots, the measured displacement drops off extremely rapidly. This is caused by the 100 kHz. maximum operational frequency of the analogue signal processing being exceeded by the frequency of the signal at the detectors. For these measurements the target was driven by a triangular wave, which should cause total loss of signal abruptly as the detected signal reaches the 100 kHz limit. However, as the target is not massless there is a small lag in accelerating to this velocity at the beginning of each drive cycle, and a short period of deceleration at the end, during which the signal frequency at the detectors falls below 100 kHz. allowing a

displacement signal to be recorded. The position of the 100 kHz signal frequency onset was found from the equation for the Doppler frequency of the scattered light from equation 3.09, section 3.1.1 as:-

$$f_d = 2.f_o.v/c_o \quad , \qquad (3.09)$$

and the target velocity for drive by a triangular wave as:-

$$v_t = 2.d_t.f_t \quad . \qquad (5.11)$$

d_t is the peak to peak target motion, taken from the measurements of the pen traces, and f_t is the target drive frequency.

These can be rearranged and substituted to give the target drive frequency that corresponds to the maximum signal frequency, f_d, of 100 kHz.

$$f_t = f_d.c_o/(4.f_o.d_t) \quad . \qquad (5.12)$$

The position of the onset of signal frequencies exceeding 100 kHz is shown on the figures by vertical lines.

Between these two regions, in the centre of each plot, it could reasonably be expected that the measured displacement should agree well with the actual displacement of the target. The plateau regions of the figures have a small negative slope, which may be due to the running together of the low frequency noise and the high frequency roll off. More seriously the value of the displacement measured by the LDI is depressed from the expected value. This may partly be accommodated in the method used to check the

length of the displacement. Since the target was mounted on an X/Y plotter, the plotter pen was used to draw a series of parallel lines, one for each different drive frequency. Subsequent manual measurement of these gave an approximate value for the length of target motion. Since the LDI measurements were recorded over several cycles of motion, the pen lines became saturated in ink, causing them to spread, so measurements taken from these lines may be higher than the real length of motion. Examination of the pen traces under a travelling microscope gave similar lengths for the pen lines as were obtained by manual measurement, and showed no indication of the precise length of the actual target motion. The measured pen trace lengths are shown on the figures as a horizontal line.

Other possible mechanisms that have been found to cause a depression of the fringe count are either partial or total loss of signal due to loss of optical power, or through exceeding the maximum frequency of the analogue electronics, neither of which apply to the results above.

5.3 Correlation Measurements

A series of correlation measurements were made to assess the performance of the LDI over a range of different operating conditions, which were broadly defined by the limits of operation of the devices with which the correlations have been made. This is indicative of the capability of the LDI, in that no easily available device could cover the same anticipated range of operation. The range of correlations covers accelerometer, LVDT, and manual methods, and these are the divisions that have been used below. In all cases the least squares line fitting of the LDI data to the correlation device has been within the 5 % significance level, and much of it lies within 0.2 % levels.

5.3.1 Accelerometer Correlations

Accelerometer correlations were carried out for target drive frequencies in the range, 1000 to 25 Hz. The upper frequency limit was imposed by the signal generator, the lower limit by the fall off in the accelerometer response, and the maximum achievable amplitude was defined by the limits of the drive unit with the exact values dependant on the drive frequency.

Some of the results of the correlation measurements are shown in figures 5.23 to 5.29. The non-linear sections of all the plots with drive frequencies below 75 Hz, are due to the detected signal frequency exceeding the maximum

frequency response of the analogue electronics, as has been discussed above in section 5.2. Measuring the position of the turn over point from those plots that exhibit the effect allows the maximum signal frequency of the electronics to be found independently of direct measurement. The target was driven by a sinusoidal motion for these correlation measurements, and the target displacement can be represented as :-

$$d(t) = d_o.\cos(2.\pi.f_t.t) \quad . \qquad (5.13)$$

From this the target velocity can be found by differentiating to give :-

$$v(t) = 2.\pi.f_t.d_o.\sin(2.\pi.f_t.t) \quad . \qquad (5.14)$$

This has a maximum value of $v_{max} = 2.\pi.d_o.f_t$. The displacement measured by the LDI is the peak to peak displacement d_{p-p}, which is twice d_o, so the maximum velocity of the target in terms of measured parameters is:-

$$v_{max} = \pi.d_{p-p}.f_t \quad . \qquad (5.15)$$

This converts directly to signal frequency by multiplication by a scaling factor, (= 3.16 MHz/(m/s)), as derived in section 3.1.1. The values of target drive frequency, measured displacement, target velocity and signal frequency at the turn over point are tabulated below.

Table 5.1 Cut Off Points in Accelerometer Data

Target Drive Frequency Hz	Target Displacement Measured (p-p) mm	Target Velocity mm/s	Signal Frequency kHz
60	0.170	32.044	101.26
50	0.220	34.588	109.30
40	0.270	33.929	107.22
25	0.320	25.133	79.42

These results are in good agreement with the expected fall off in the response of the analogue signal processing.

The data from the 25 Hz correlation measurement is in question, as it does not conform with the other data sets, either above in measuring the turn over point, or below in correlation of the changing slopes of the linear sections of the main accelerometer correlation results, due to the fall off in accelerometer response.

The linear portions of the plots show an increasing gradient with decreasing target frequency. This is due to decreased accelerometer response as the drive frequency of the target decreases. The accelerometer was connected directly into a millivoltmeter, (Phillips model PM2454) with an input impedance of 1 M Ohm, 33 pF. This combination acted as a high pass filter with a roll off frequency of 130 Hz. Knowledge of the impedance of the accelerometer and the millivoltmeter allows the expected accelerometer response to be predicted from simple a.c. circuit theory. The expected accelerometer response is plotted against the

slope of the linear portions of the correlation measurements in figure 5.30. If all the data points are used the correlation the least squares fit is within the 5% significance level. However, by disregarding the indicated points, the correlation between expected and measured accelerometer response is further improved. It should be noted that as the target drive frequency was reduced for successive sets of correlation data, the onset of the maximum frequency became smaller, leading to less points in the linear part of the plot, which in turn makes accurate prediction of the accelerometer response less reliable.

Since the gradients of these correlation plots are sensitive to the operating frequency of the target drive unit, they were not the best method of obtaining information about degree of agreement between the accelerometer and the LDI. The intercept and correlation coefficient data is of more use. As the expected relationship between the LDI and the accelerometer is linear, a least squares line fit is appropriate in assessing the results. The accelerometer data has been taken as true, although it is derived from acceleration information, and makes assumptions about the exact nature of the motion of the target. The fit is of the LDI results to the accelerometer results. Correlation coefficients for the data are shown in table 5.2, and on some of the figures. They are all within the 5 % significance level and all except the 25 Hz. results lie within the 0.2 %

significance level, which indicates an extremely good linearity between the accelerometer and the LDI.

The intercepts of the linear portions of the plots (Table 5.2) tend to deviate further from zero as the target drive frequency decreases. However this trend is not well enough defined to be the sole source of errors in the measurements.

Table 5.2 Accelerometer Results

Drive Frequency Hz	Number of Cycles n	Data Logging Time s.	LDI Intercept um.	Correlation Coefficient
1000	2047	2.047	-0.0021	0.9999
500	2047	4.094	0.0485	0.9993
250	2047	8.188	0.0690	0.9998
100	2047	20.47	0.0499	0.9999
75	2047	27.29	0.7552	0.9927
60	511	8.52	4.406	0.9980
50	2047	40.94	-0.3095	0.9999
40	511	12.78	0.2443	0.9999
25	511	20.44	51.0459	0.9582

Measurements were made in conjunction with the correlation data, to assess the presence of background noise and the stability of the measured data. This is of more general relevance and is discussed in section 5.4.

5.3.2 LVDT Correlations

All displacement amplitudes for these readings were in the mm. ranges, to ensure that the LVDT was able to operate with a reasonable degree of accuracy. Resolution of 1 mV in the LVDT output corresponded to 5 um. displacement.

The correlation of displacement measurements made with the LVDT, figures 5.31 to 5.36, do not show quite the same degree of order as those for the accelerometer. Since the response of the LVDT can be taken to be flat for all the drive frequencies that have been employed here, the slopes of the individual plots should provide information.

Table 5.3 LVDT Results

	Drive Frequency Hz.	Number of Cycles Counted n	Data Logging Time s.	LDI Intercept mm.	Plot Slope	Correl. Coeff.
a	0.1	7	70	0.177	0.962	0.9948
b	0.1	15	150	0.176	0.999	0.9986
c	0.1	1	10	0.142	0.991	0.9937
d	0.1	3	30	0.114	1.114	0.9978
e	0.1	3	30	0.313	0.871	0.9405
f	0.1	3	30	0.261	0.969	0.9978 *
g	0.05	15	300	0.427	0.991	0.9929
h	0.05	3	60	1.513	0.983	0.9969 **
i	0.05	3	60	1.200	1.026	0.9990 **

* As data set e with spurious points removed.

** Trapezium drive wave used rather than sinusoidal drive wave. Data set h incorporates data set i, see below.

For the data taken with the target under sinusoidal drive the maximum amplitude that was used was 2.5 mm., for the trapezium drive the amplitude took values up to 20 mm. This was because of an initial concern about the stability of the signal over longer target displacements, which was subsequently found to be over cautious.

In all the LVDT correlation measurements the target velocity is too low to cause signal loss by exceeding the maximum frequency of the electronics as occurred with the accelerometer.

Data sets d and e are interesting, in that under apparently identical circumstances very different sets of data were obtained. When cleaned up by removing two points, one where the LVDT became misaligned..and gave an extremely low reading, the other where the LDI count apparently failed, data set e gave considerably improved results. These two sets of data d, and e or f were taken from a Mach-Zehnder and a Michelson based design respectively. The M-Z design was later found to have a loosely mounted component, which was introducing additional noise into the detected signal. This may account for the poor quality of this data.

It is difficult to comment on the behaviour of the intercepts that are shown due to the limited number of data points. However it is assumed that the presence of non zero intercepts is an indication of an approximately constant noise in the signal. Consequently the ratio of accumulated noise to measurement time should be constant for any given

set of measuring conditions. Those sets of data recorded at 0.05 Hz do show larger intercept values than those for 0.1 Hz, but in both cases there is not sufficient data to allow further comment.

The intercepts for the data derived from the target driven by a trapezium wave show considerably larger values than those for small amplitude sinusoidal motion. The target velocity during these measurements is too small to push the Doppler frequency above the response limits of the elctronics. There may have been some signal loss at larger displacements due to speckle effects at the detectors. This would show up on the correlation plots as a slight curvature, concave downwards, which would force the intercept value of a straight line fit artificially high. There is some indication that, for motions above about 15 mm. this might be occurring. If measurements of greater than 15 mm amplitude are removed from data set h the slope of the resulting data is 1.085 with an intercept of .811 mm. (Correlation coeff. = 0.99971). This is an improvement on the full data set.

It is also possible that where the drive is of a trapezium nature, there are longer stationary periods than with a sinusoidal drive. During these periods the effects of background motion will dominate the fringe counting process. This is considered to be the main source of noise within the LDI and is discussed in section 5.4.2 below.

The slopes of all the plots are close to unity, with correlation coefficients typically better than 0.99. From

this it can be assumed that the magnitude of the error is not related to the size of the measurement being made. These correlations show that the LDI is capable of making measurements of motions over several mm. Direct comment on the validity of each individual reading is difficult, but the implication is that individual measurements are reliable within the limits discussed in section 5.4.

As with the accelerometer correlation measurements, further data were gathered to assess the type and magnitude of the errors that could occur during measurement. These are discussed below (section 5.4).

5.3.3 Other Correlation Measurements

Additional displacement measurements were made using a non-periodic target motion. The target was mounted on the pillar of a travelling microscope (T.M.), which was driven manually, either via a screw adjustment, or directly. The former method allowed well defined motion, up to the the limit of the drive screw; the latter, although less controlled, was capable of longer displacements, up to a maximum of 150 mm..

All the data collected from the T.M. measurements had the sense of motion signal controlling the direction of count of the fringe counter. This was done for two reasons; firstly to eliminate the effect of unwanted vibration from the displacement being measured, and as a test of the ranges of motion over which a sense of motion signal could

be sustained. The duration of the measurements could not be measured accurately for manual drive, which in turn meant manual starting and stopping of the fringe counter; however, typical recording times were about 5 seconds.

The quality of the results of these measurements, figures 5.37 and 5.38, is comparable with those derived from the accelerometer and LVDT correlation measurements. The main point of interest here is that the results are from a single displacement of the target, rather than the result of an averaging process over a very large number of cycles of motion. This adds credibility to the quality of the measurements made by the LDI.

A specific feature of one of these sets of data, figure 5.37, is that at higher displacements there is a loss in fringe count. This is attributed to the onset of a region of low signal level, probably due to the speckle nature of the scattered light. On moving the target so that a new part of the surface was illuminated, and a new speckle pattern generated, measurement was possible over the much larger ranges as shown in figure 5.38.

Within these data, there are implications for other facets of LDI operation. These mainly centre on the use of direction sensitive fringe counting, and relate to the possible improvements that may be realised by counting the fringes at the detector both with and without sense of motion. From these two pieces of information it may be possible to achieve a more precise displacement for a vibrational target motion. This is discussed further below.

5.4 Sources of Error

Various sources of error in the LDI measurement have been noted above, and some explanations introduced for them. A general discussion of these should enable further understanding of the LDI and its principles of operation. With many of the displacement measurements that were made there were also other data sets, recording the number of signal pulses logged by the LDI during similar periods or to measure the asymmetry of the signals derived from cyclic motions, as well as those measurements made purely to assess various types of noise within the system.

The sources of error may be separated into those due to noise arising from different parts of the system, and those due to restrictions in the operating conditions of the LDI. This division is arbitrary, and some overlap occurs.

5.4.1 Signal Level Noise

Measurements of amplitude noise in the optical signal from the LDI is not directly possible with available facilities. This is due to the separate mounting of the LDI and target, resulting in a small background motion between them giving rise to an unavoidable Doppler signal. Since the signal level is prone to variation due to the speckle effect, it is not even viable to collect a large number of readings from a given configuration and apply a statistical analysis.

The various analogue signal levels that are accessible within the LDI have been recorded. They may be divided into those arising from optical effects, and those from the electronics. The noise levels were measured with a Phillips r.m.s. millivoltmeter, model 2454 B with a frequency range of 10 Hz to 12 MHz. With the detectors blacked out the noise levels at the two analogue signal outputs were 4.0 mV and 15 mV rms, for channels A and B respectively. This difference arises from the transimpedance amplifiers (current to voltage converters). Independant noise figures for the separate units are given for the same frequency range, in table 5.4 below.

Table 5.4 Noise Levels (mV rms)

	Channel A	Channel B
Transimpedance Amp.	0.18	0.40
Voltage Amp.	0.46	0.46

Sets of noise levels were collected with the measurements of signal variation with target range. These recorded the noise after analogue processing, with no target in the illuminating beam, but with a reference beam on the detectors. This gave a value of 36 mV rms with very little variation. This is supported by results from the histogram measurement of signal levels at the voltage amplifier output. These were taken using an 8 bit analogue to digital converter with an input range of +/- 2.5 V, giving a resolution of 19.5 mV per bit. A typical histogram is shown in figure 5.39. It was found that with no optical input to

the detectors, these levels of noise did not give rise to spurious fringe counting, and consequently do not contribute to errors in measurement of displacement.

The noise in the signal level received less attention than the noise in the received fringe count for the same reasons as mentioned when discussing the variation in signal level with changing target parameters - that the device operates in a displacement measuring mode, and it is the frequency of the detected signal not its amplitude that carries this information.

5.4.2 Count Noise

The main source of count noise in the LDI is attributed to motion between the target and the LDI additional to the deliberate motion being measured. Since the correlation measurements of section 5.3 were derived from devices attached to the target, or physically linked to it, they are immune to this background motion. This is one of the features of the LDI, that it does measure the effect of all motion between itself and the target. A secondary source of count error arises from the inherent accuracy of the digitising process. This results in a +/- one count uncertainty.

The effect of background motion was demonstrated in the difference between the correlation measurements made with the LVDT for sinusoidal and trapezium target drive waveforms (section 5.3.2). Most of the measurements were

made with a sinusoidal drive to the target, but two sets of results used a trapezium wave containing long stationary periods. The intercepts of line fits to the trapezium data show large values corresponding to excess LDI fringe counts over the expected driven amplitude of the target. An explanation of this is based on the fraction of the measuring period where the target drive signal is zero.

Given that there is a background motion v_b, which is assumed to be periodic, that is both the LDI and the target have a fixed mean position in space, then the average displacement due to this background is zero. Where continuous motion in one direction is being measured the background motion cyclically modulates the deliberate motion, averaging out over a measurement period considerably larger than the mean background period. If the natural period of the background is longer than the measuring period full cancellation may not occur resulting in the introduction of a count error. Generally background motions can be expected to be of small amplitudes, so the effect on the count will still be relatively small.

Where the target motion is periodic, it is necessary to count the displacement fringes without sense of motion controlling the direction of the count, otherwise no net count would be logged. In this situation, the effect of background motion is more significant. Where the background is slower than the target motion, it still behaves as a frequency modulation of the desired signal frequency

arising from the deliberate target motion, and cancels itself out. However since the target motion is periodic, there is some fraction of the measurement time when it can be expected to be moving at a lower velocity than the background. When this occurs the target motion acts as a modulation on the background motion, which will be logged during this period instead of the signal. This effect will also be minimal if the background velocity is small compared with the target velocity, since relatively few spurious counts can occur before the target signal resumes dominance. In more conventional terms, the degree of error that may be introduced in this fashion depends on the depth of frequency modulation of the target signal frequency by the background signal frequency. An expression for the magnitude of the background effect is given in appendix 4 This may be approximated from the rms velocity of both target and background taken over a sufficiently large time to give good averaging. If these are v_t and v_b respectively, then the fraction of the time during which the background dominates can be expressed as :-

$$f = v_b/v_t \quad . \qquad (5.16)$$

In one cycle of target motion at a frequency f_t, the time during which the background dominates is :-

$$t = v_b/(v_t.f_t) \quad , \qquad (5.17)$$

during which time an excess count d_{xs} is logged, where :-

$$d_{xs} = v_b.t \quad ,$$

$$d_{xs} = v_b^2/(v_t.f_t) \quad . \qquad (5.18)$$

This will be a fixed fraction of the total logged displacement of the target, d_t.

In practical terms, the effect will be more noticeable for a target motion that contains large stationary periods in which background noise intrudes. Results from the error logging by the LDI lend some support to this idea. Those measurements made over a similar period to the data sets but with no drive motion at the target and counting all the detected fringes gave relatively large counts, corresponding to the total distance travelled due to background motion. When the periodic motion of target and background were logged with sense detection controlling the fringe counter, the accumulated count was considerably smaller. With no drive to the target and sense of motion controlling the counter the number of logged signals was yet smaller. That any residual count remains when sense of motion control is applied to the counter may be attributed to incomplete background cycles being logged during the measurement period. This will occur if the background motion frequency and the drive frequency are harmonically related, as in this situation the fringe counter will see similar points on the background motion during each cycle, and if these are not symmetrically distributed about the background wave they will result in an asymmetric

background fringe count. The same effect occurs if the measurement time is not an integral multiple of the background noise frequency or if the background motion shows extreme asymmetry.

Figures 5.40 to 5.42 show the various error measurements that can be made from the LDI. These all derive from the same measurement conditions and are associated with a correlation between the LDI and the LVDT. The target was driven by a trapezium wave with a frequency of 0.05 Hz. and counts were collected over three drive cycles. The figures show the accumulated fringe count with and without drive to the target and with and without sense of motion signal control of the fringe counter. In those plots where there is no drive to the target the horizontal axis has been preserved to allow comparison, but is a false axis.

The most interesting set of error data for the purposes of compensating for the general trend of the LDI, in giving a higher than real result, is that obtained with no drive to the target and no sense of motion signal controlling the counter. This logs the total background motion of the target, which is thought to be responsible for the errors in fringe counts that do occur. As the temporal structure of the background noise in not known it is not possible to reconstruct the background motion. However, a mean background velocity can be derived and may be inserted into the original equations for the effect of noise. Unfortunately this measurement cannot be derived

simultaneously with the signal from the moving target. Ideally the necessary information about the background noise should be derived from a cumulative fringe count recorded simultaneously as the data but with sense of motion eliminating the periodic signal. This in turn assumes that the main signal will cancel exactly when the sense of motion is applied to the counter. Figure 5.40 indicates that this is not the case and that some signal dependence is retained, with larger fringe counts occurring at larger drive amplitudes.

The plot of fringe count logged with no target drive but with sense of motion controlling the counter (figure 5.41) shows very low accumulated fringe counts when compared with the total background count indicating that the background motion is strongly periodic as would be expected.

Other measurements of background count show a distinct correlation between the measurement period and the magnitude of the total background count. This is interesting, in that the effect was not observed in the correlation measurements themselves, where it could have been expected to manifest itself as a trend in the intercepts of the lines fitted to the data points. As mentioned above, a set of data derived when no drive is applied to the target can be subjected to a simple statistical analysis. Table 5.5 shows the mean background count and the measurement time over which it was obtained. In each case there are more than 10 data points being averaged, and the data is derived from results collected

over several days, which allows plenty of scope for different degrees of background noise.

Table 5.5 Background Count v. Measurement Time

Measurement Time s.	Mean Background Count	Count Rate
70	9036.2	129.1
150	23858.0	159.1
300	55421.0	184.7
30	6668.0	222.3
30	5308.7	177.0

Although there is some variation in the mean fringe count rate the figures are of similar magnitudes implying that the effect of background motion is always present to a similar degree in a given measuring environment. Comparison of this result with the intercept data from the correlations with the LVDT does not indicate any conflict. The magnitude of the intercept values from the accelerometer are typically sub single fringe size, and may reasonably be attributed to very small fringe counting errors averaged over the total number of fringes recorded. There is no evidence to indicate that background motion has any adverse effect on measurement of vibration at high frequencies. Consequently the intercept data from the accelerometer can not be included for discussion here. This is not the case for the intercept data from the LVDT results which do show distinct intercept values. However

because of the data reduction used the results show the vibration amplitude not the total fringe count. Consequently as most of the LVDT correlation measurements were carried out at the same frequency the intercept values will correspond to the average number of additional fringe counts logged during one cycle of target motion.

The number of intercept value that are available is insufficient to allow any reasonable comment to be made. However, the mean count rate from the error measurements is 174.4 counts/s giving 872 counts during a half cycle at 0.1 Hz, this corresponds to a displacement of 0.276 mm., which is of the same magnitude as the intercepts.

It is important to note that the sense of motion signal depends upon the two fringe signals to operate, and if either of these does fail, then the sense of motion signal will also fail. In this situation the total background count will become considerably larger. This effect makes assessment of background motion more difficult, but could be used to provide an additional warning of sense of motion signal loss.

5.5 Signal Processing

This section is intended to give a brief comment on the performance of the signal processing equipment that was used to log the detected signals. Much of this may have been mentioned in earlier sections of the results. Here it is brought together for convenience.

The frequency response of the signal processing was important as the detected signals could easily reach high frequencies. A set of bench tests for the two voltage amplifiers that were used showed a maximum response up to about 100 kHz, figure 4.8, as stated in the manufacturer's specifications. This was compounded by the fact that the same op amps were used in at least three locations along the path of the signal, resulting in an extremely sharp roll off above 100 kHz., which was demonstrated in the accelerometer correlation measurements (section 5.3.1). No evidence was found in the measurements that there was a low frequency roll off, as was postulated from figure 5.2 showing the variation in signal amplitude at different points during the drive cycle. This could be expected, as the number of counts lost because of a low frequency loss would be a very small fraction of the total and would be offset to some extent by the background count rate, which has a value of 174 Hz, which is in excess of the suggested value for the roll off, of about 100 Hz. The mechanism responsible is thought to be a d.c. blocking capacitor between the transimpedance and the voltage amplifiers.

Since the analogue frequency response lay totally inside that of the detectors and the digital circuits, it dictated the effective range of velocities that could be processed by the LDI.

It was also mentioned in section 5.4 that with no illumination at the detectors the noise levels were insufficient to give rise to spurious counting in the processing. When the laser illumination was removed, the detectors gave a sufficiently strong signal from the fluorescent strip lighting in the laboratory to cause a 100 Hz signal to be logged. This was not present when the reference laser signal was incident on the detectors.

The control of the logging process, which is not an integral part of the device in its envisaged final form, failed to operate correctly when very slow drive signals were being used. Failure was by false triggering of the reset line, which may have been due to the drive signal dwelling for too long in the vicinity of the switching levels of the device.

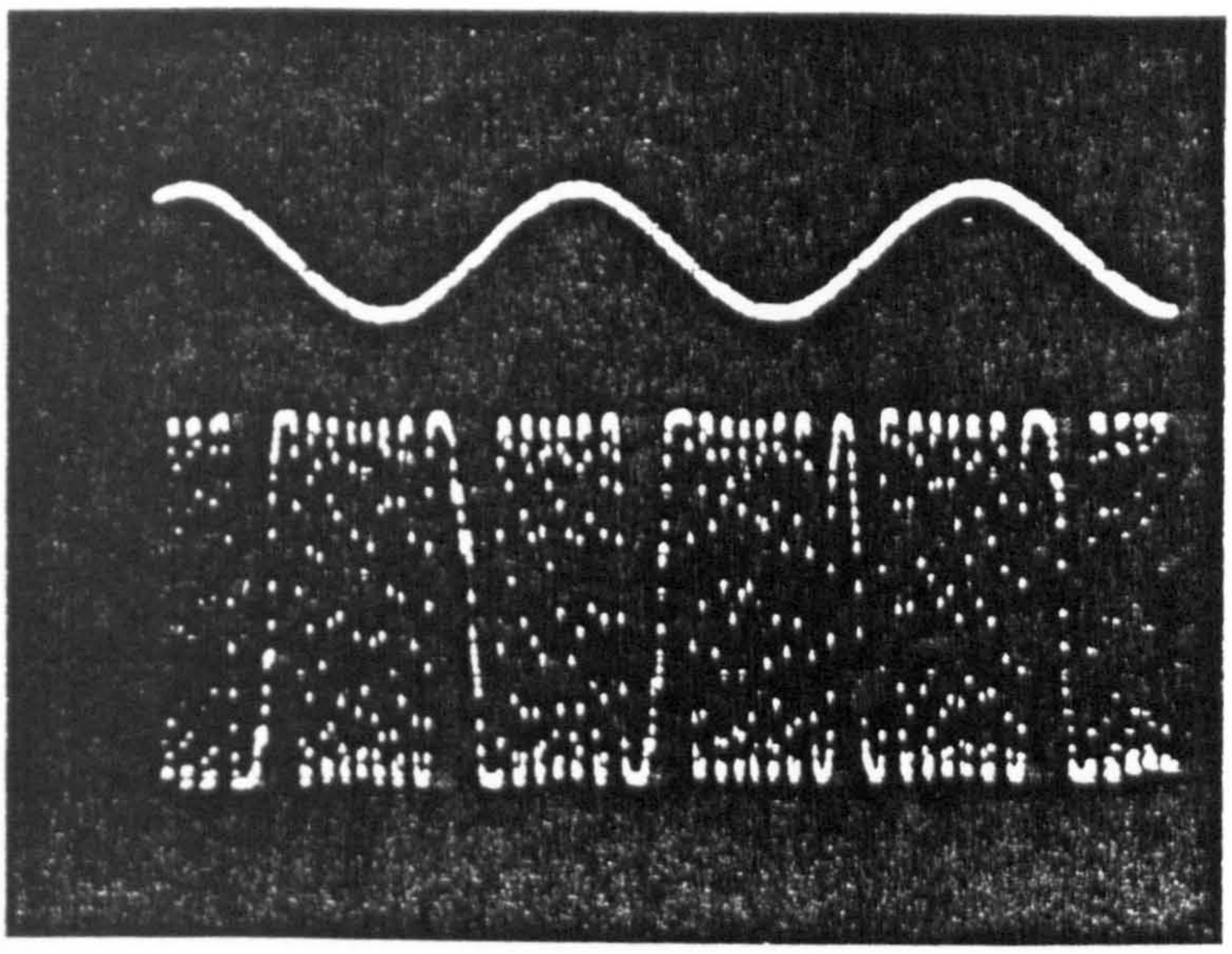

Figure 5.1 500 Hz Drive Signal and Detector Signal

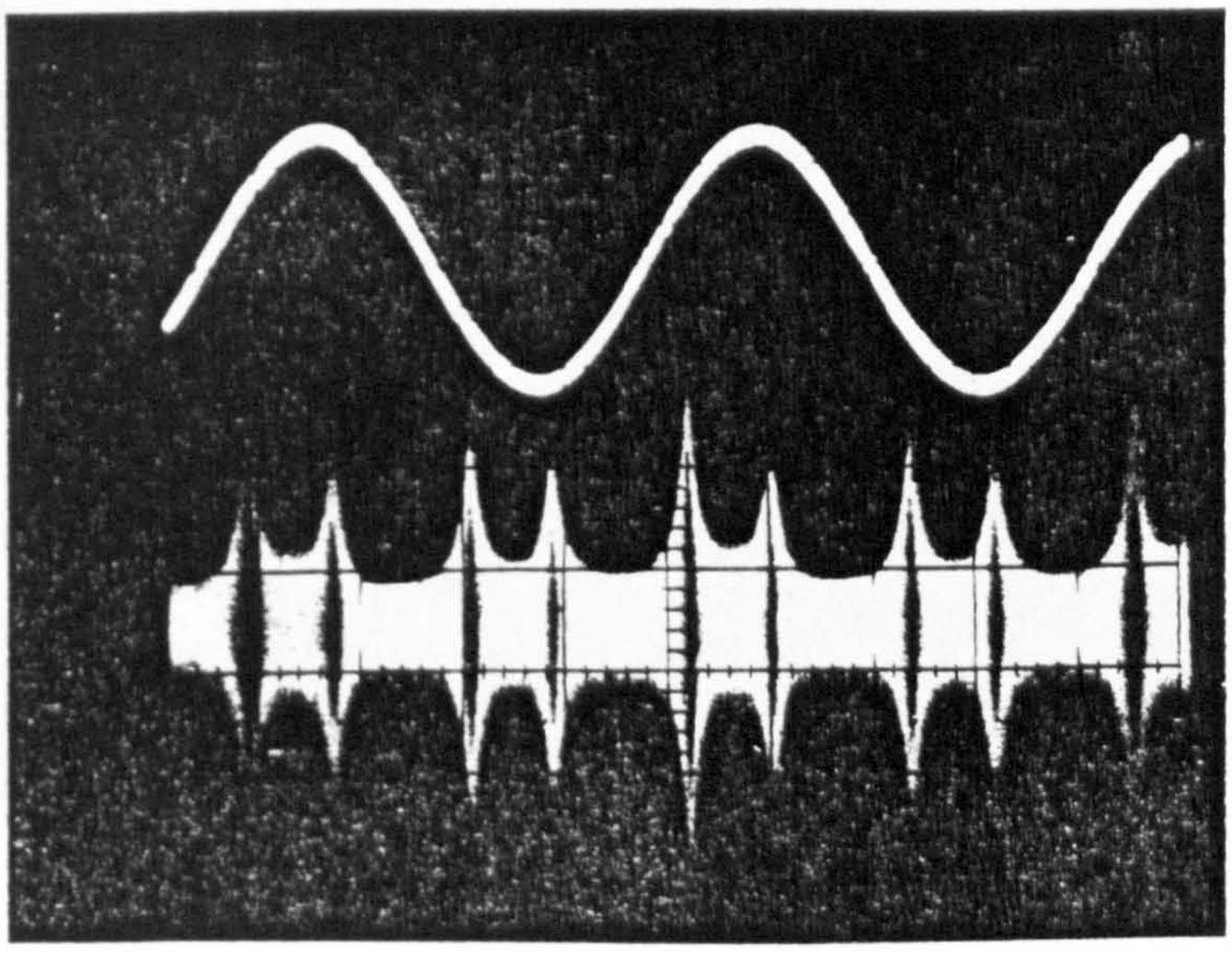

Figure 5.2 44.5 Hz. Drive Signal and Detector Signal

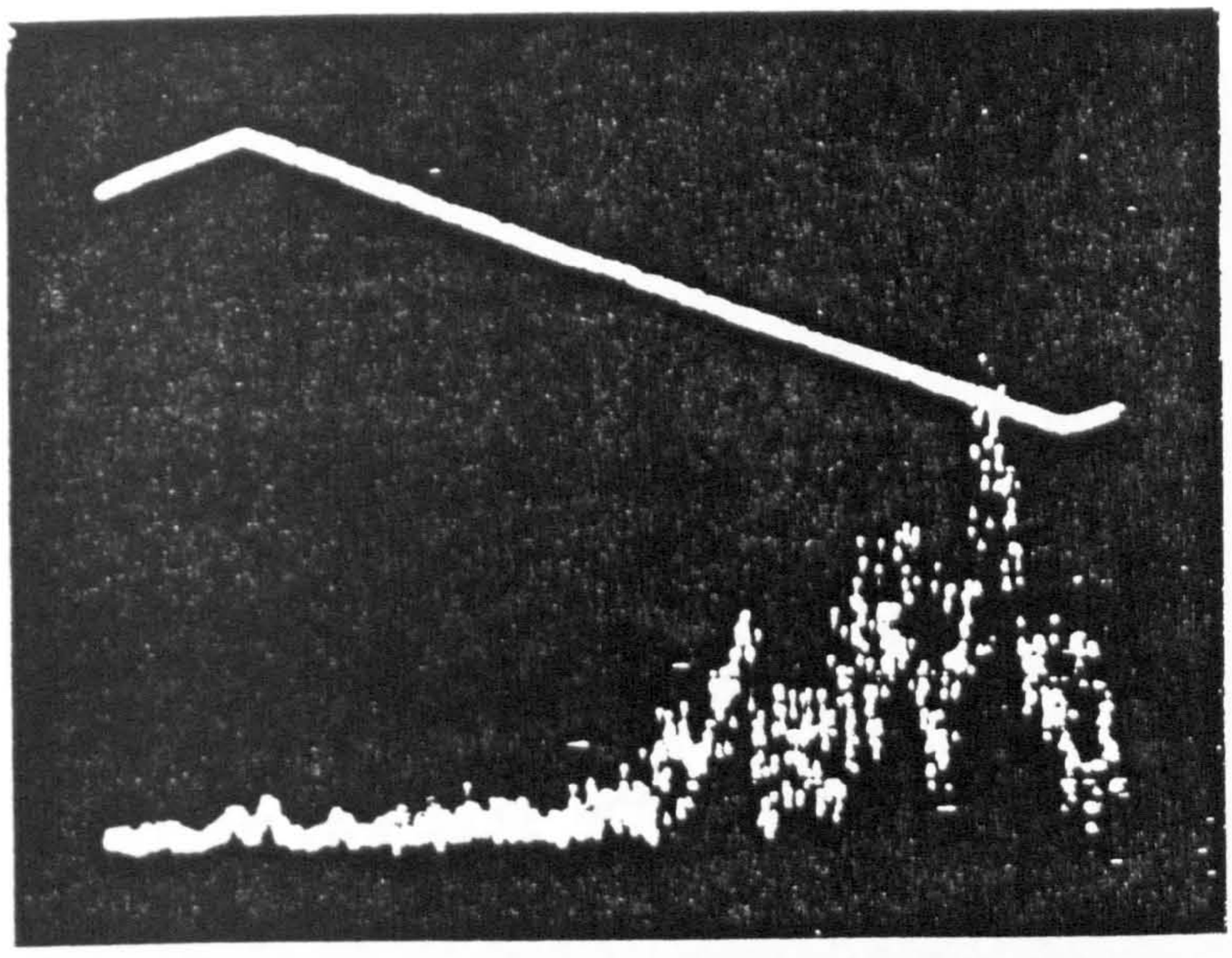

Figure 5.3 0.03 Hz. Drive Signal and Detector Signal

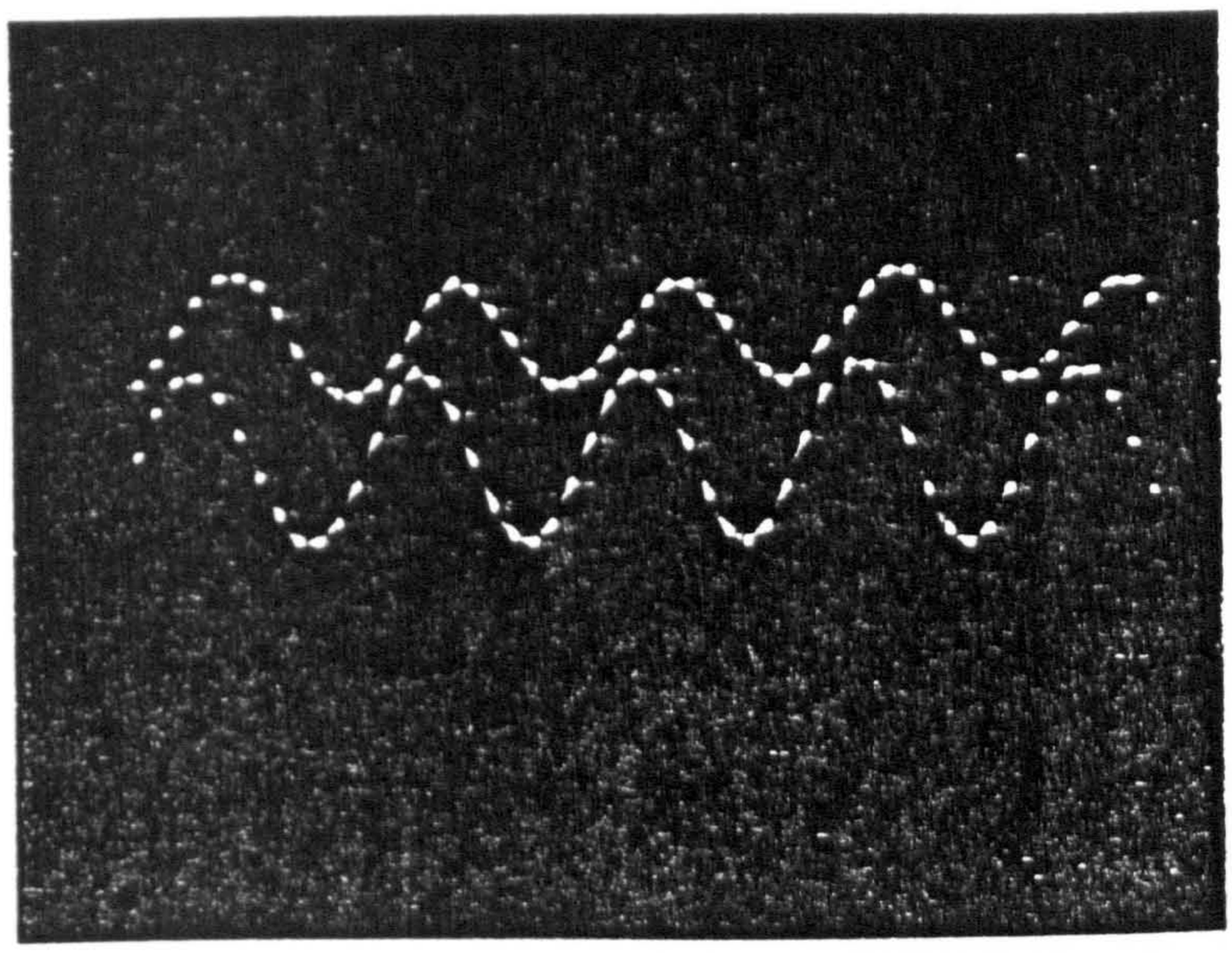

Figure 5.4 Detected Signals Showing Phase Difference

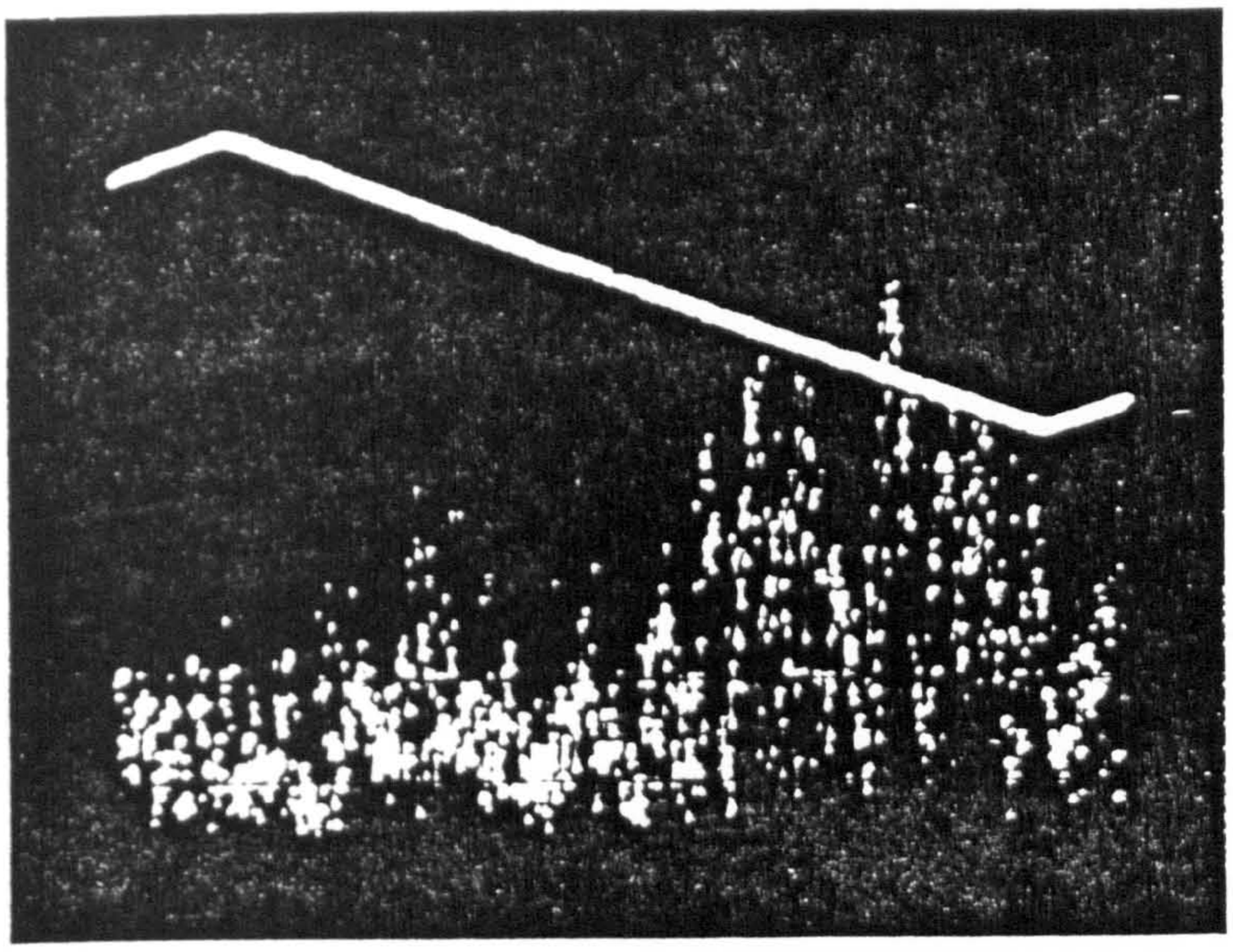

Figure 5.5 Detected Signal from an Unfocussed Illuminating Beam (c.f. figure 5.3)

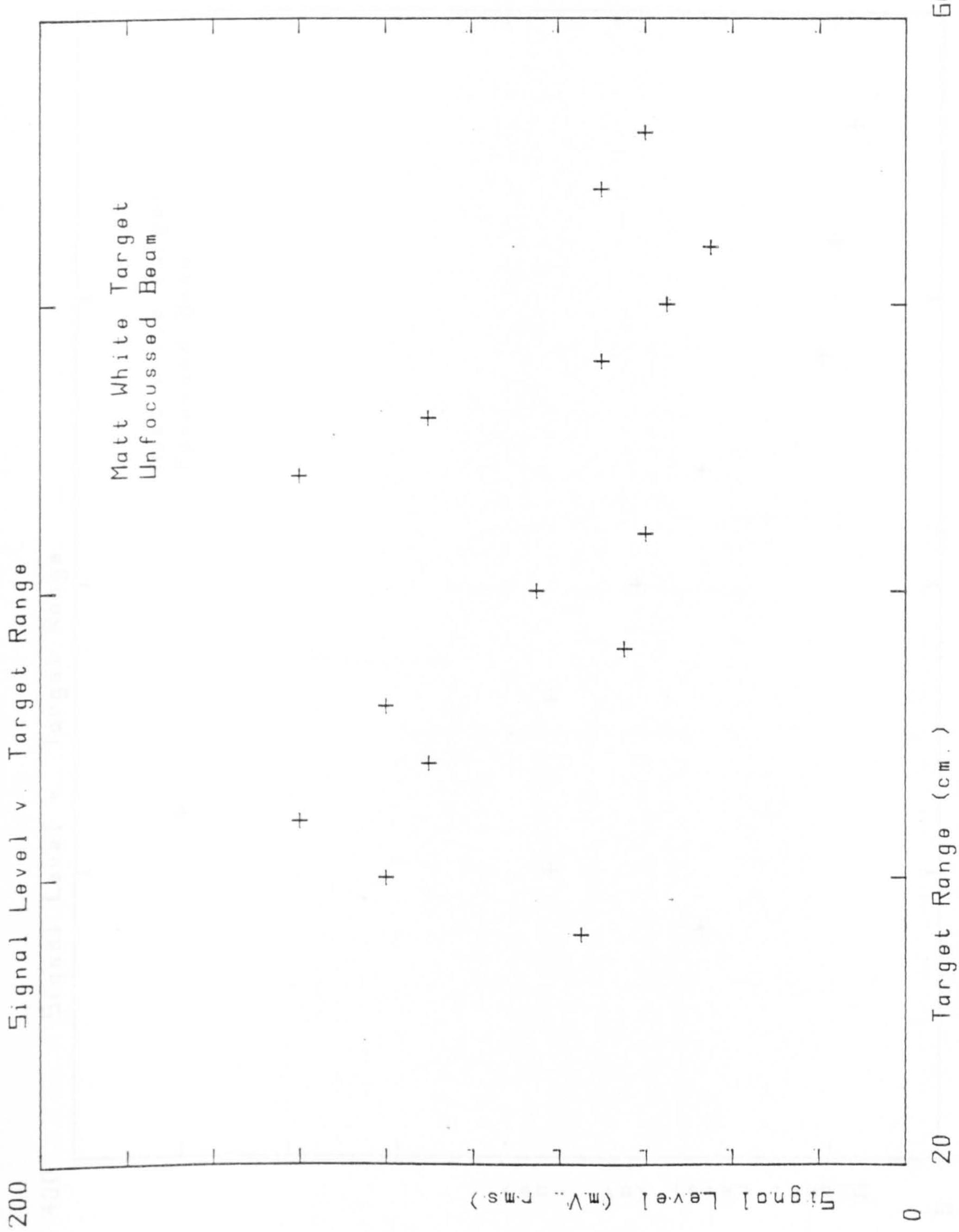

Figure 5.6 Signal Amplitude Data

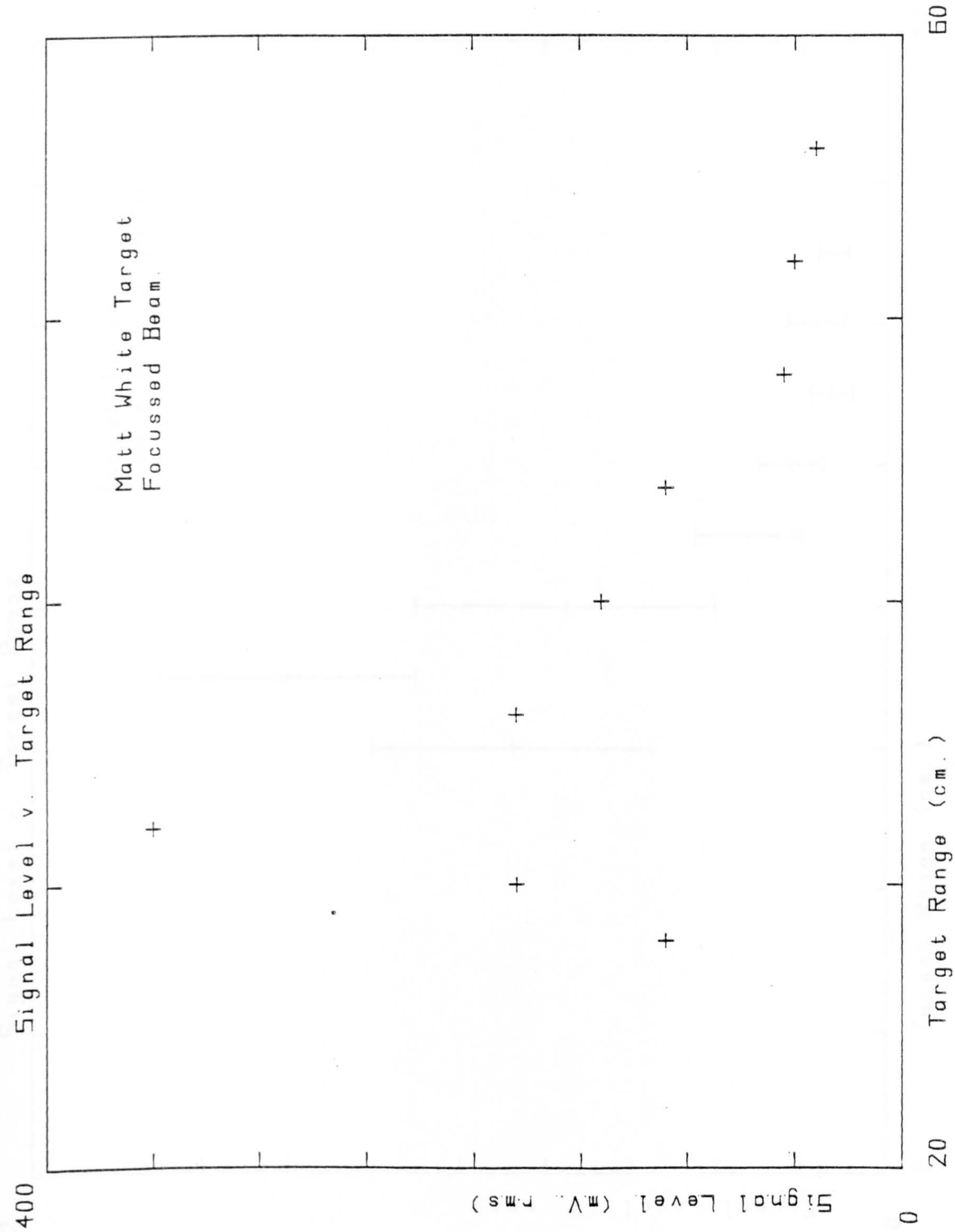

Figure 5.7 Signal Amplitude Data

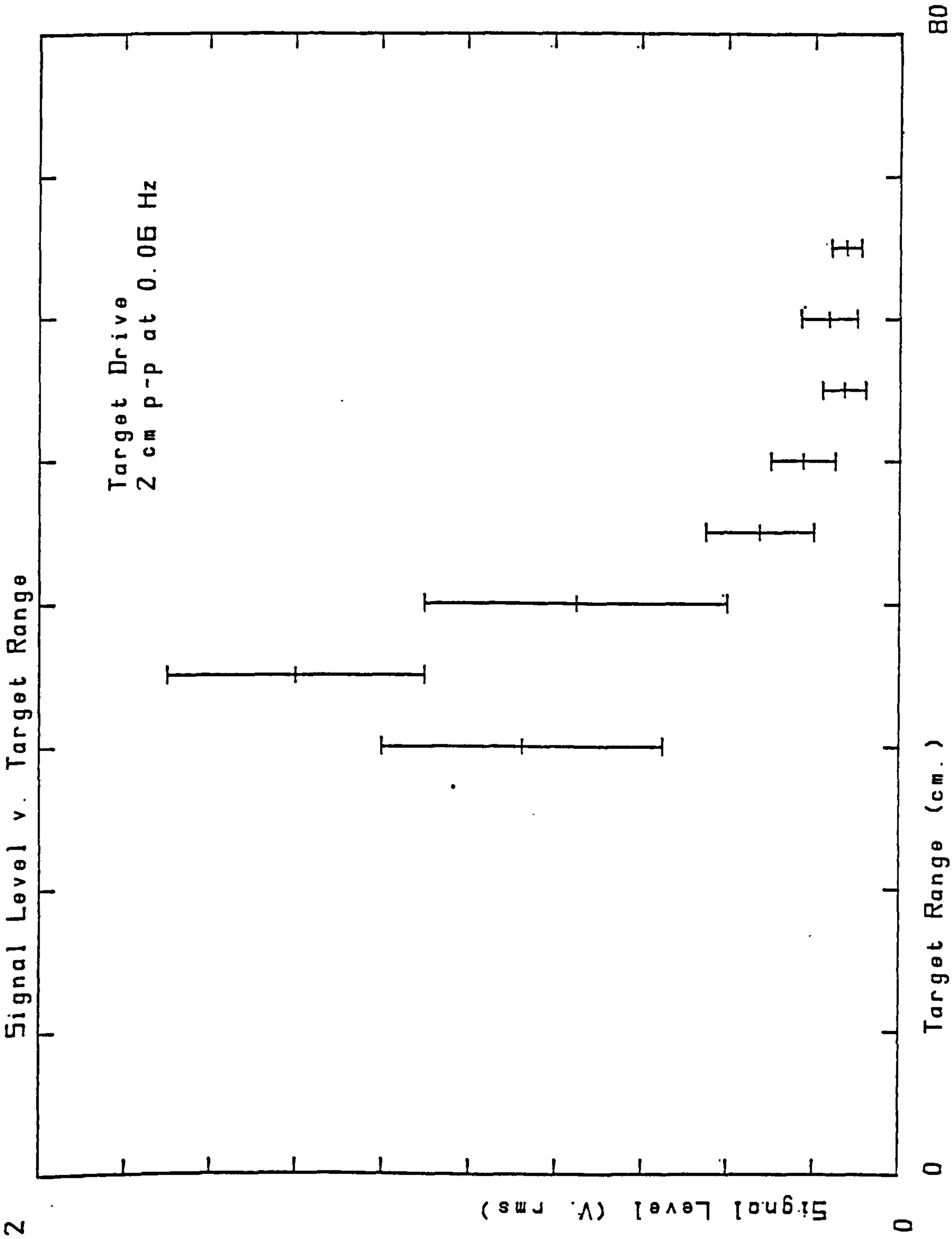

Figure 5.8 Signal Amplitude Data

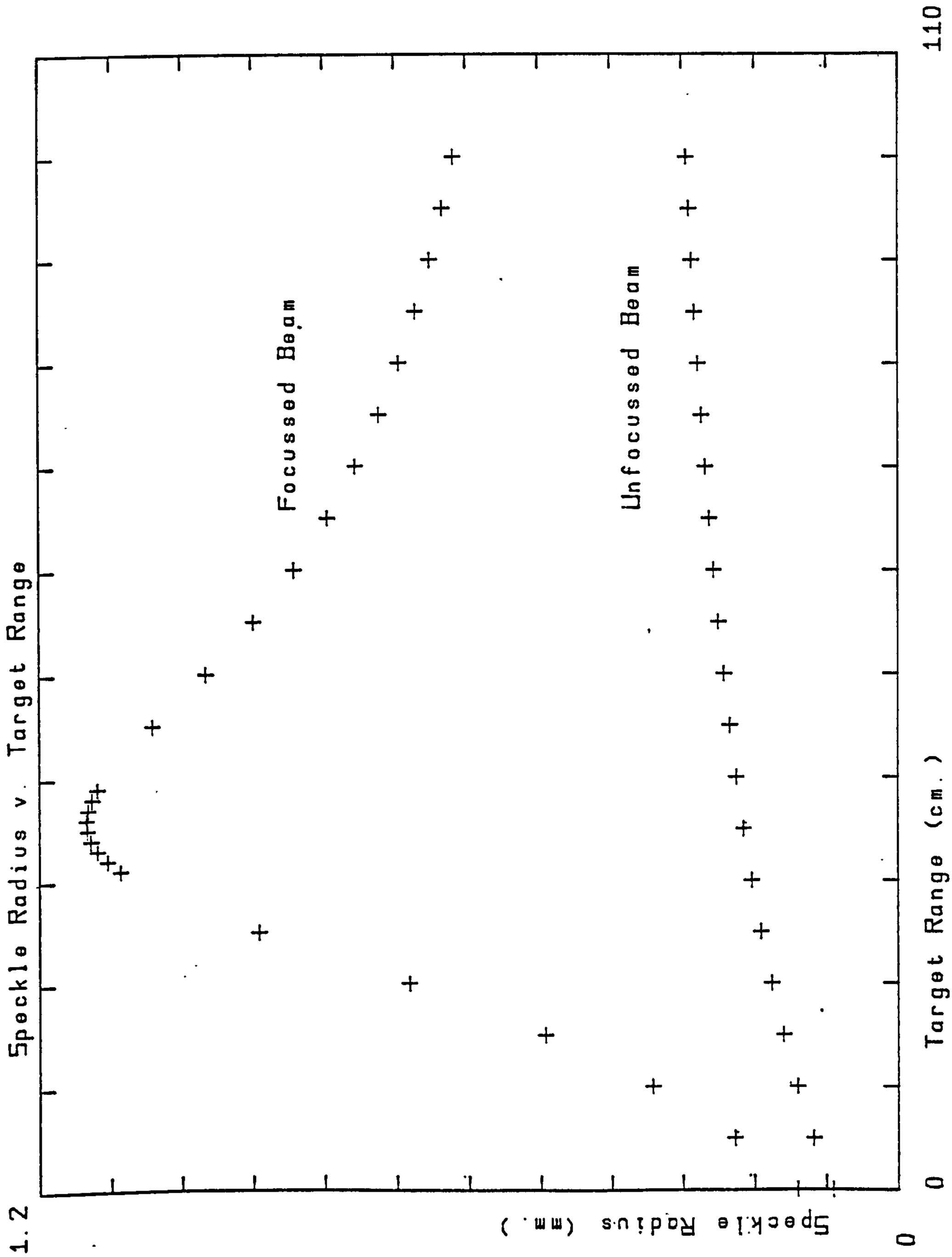

Figure 5.10 Speckle Size as a function of Target Range

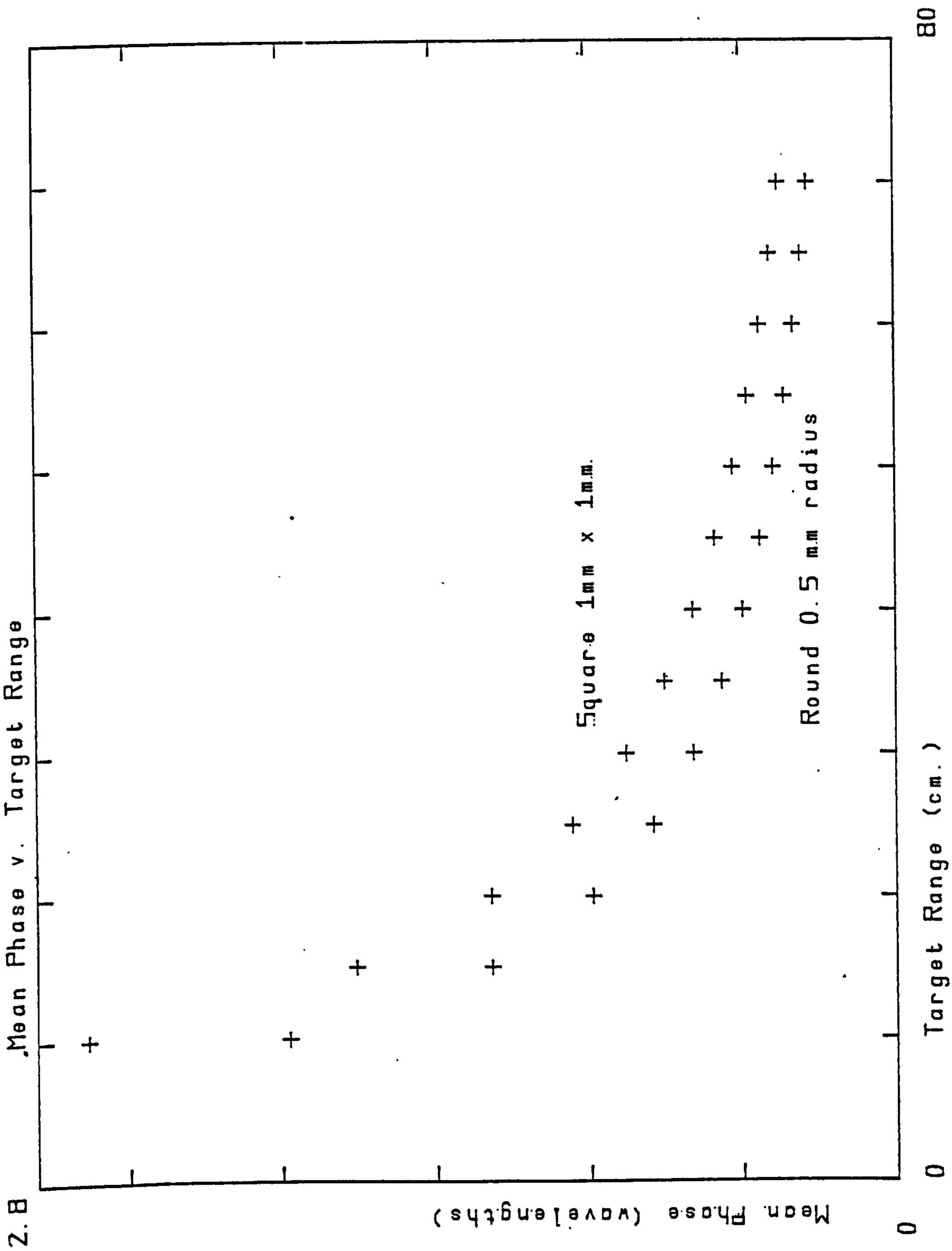

Figure 5.11 Mean Phase Difference at the Detector

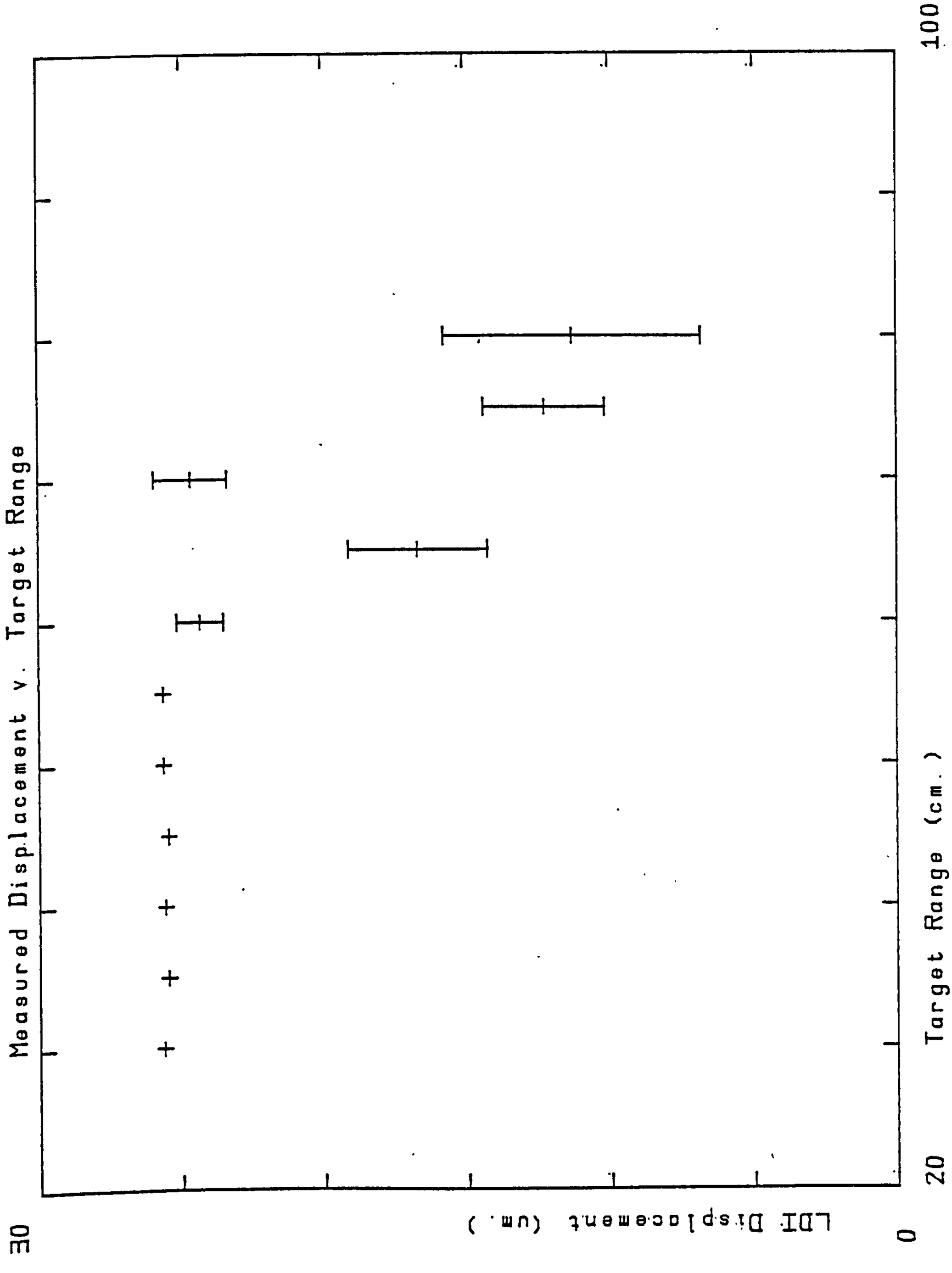

Figure 5.12 Measured Displacement as a function of Range

Focussed Illuminating Beam

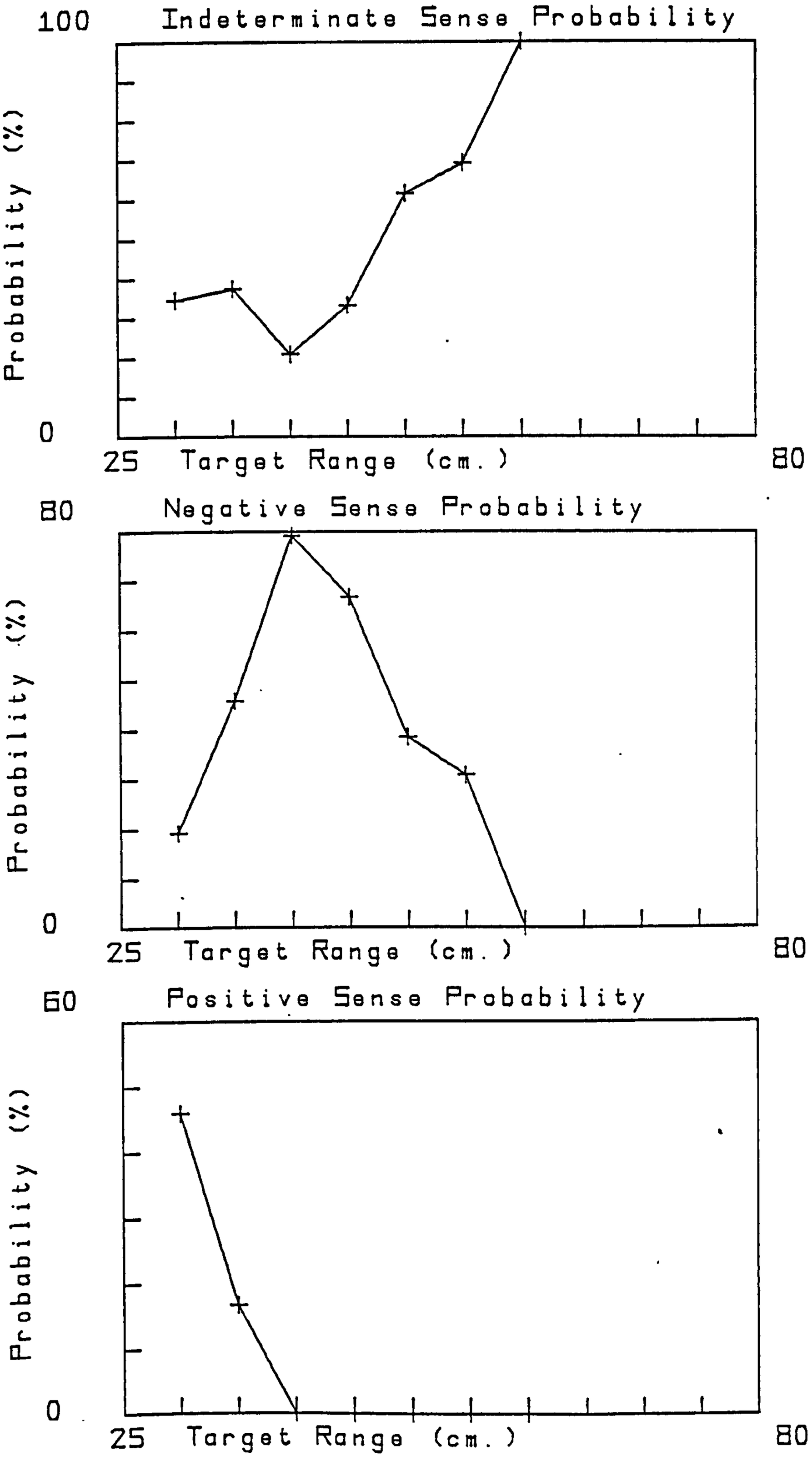

Figure 5.13

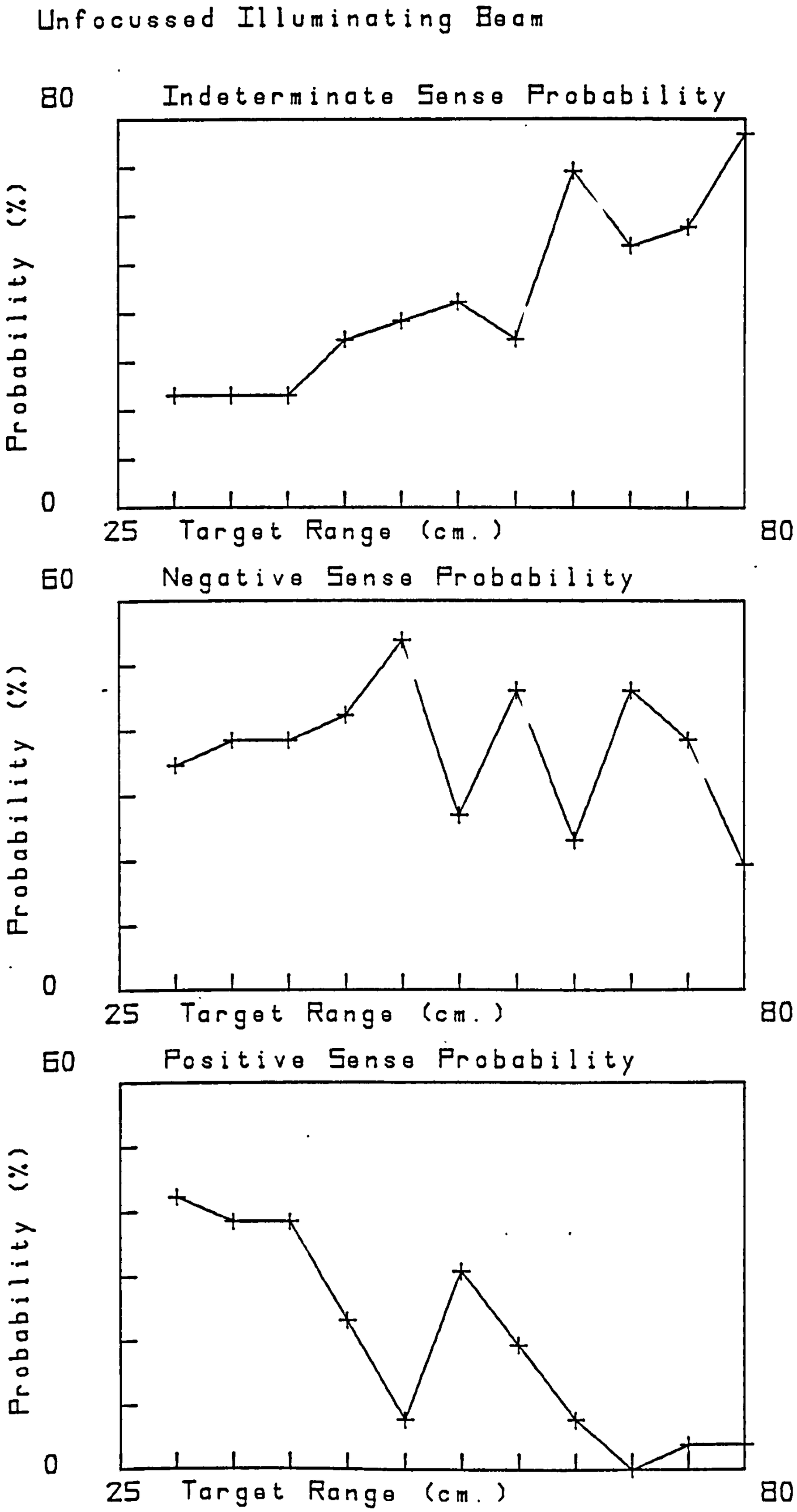
Unfocussed Illuminating Beam
80
Indeterminate Sense Probability
Probability (%)
0
25
Target Range (cm.)
80
60
Negative Sense Probability
Probability (%)
0
25
Target Range (cm.)
80
60
Positive Sense Probability
Probability (%)
0
25
Target Range (cm.)
80

Figure 5.14

Illuminating Beam Polariser and Lens Absent

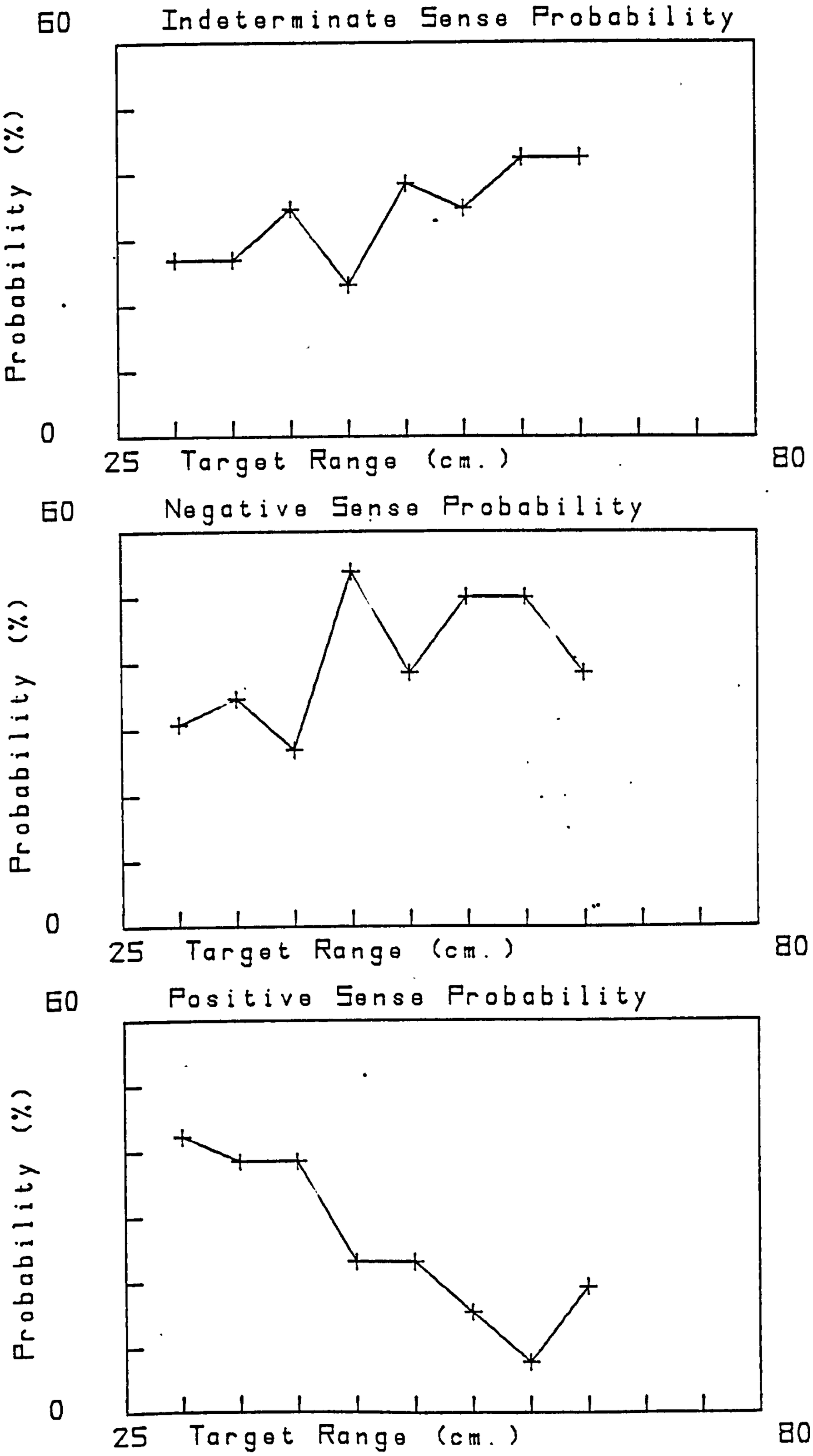

Figure 5.15

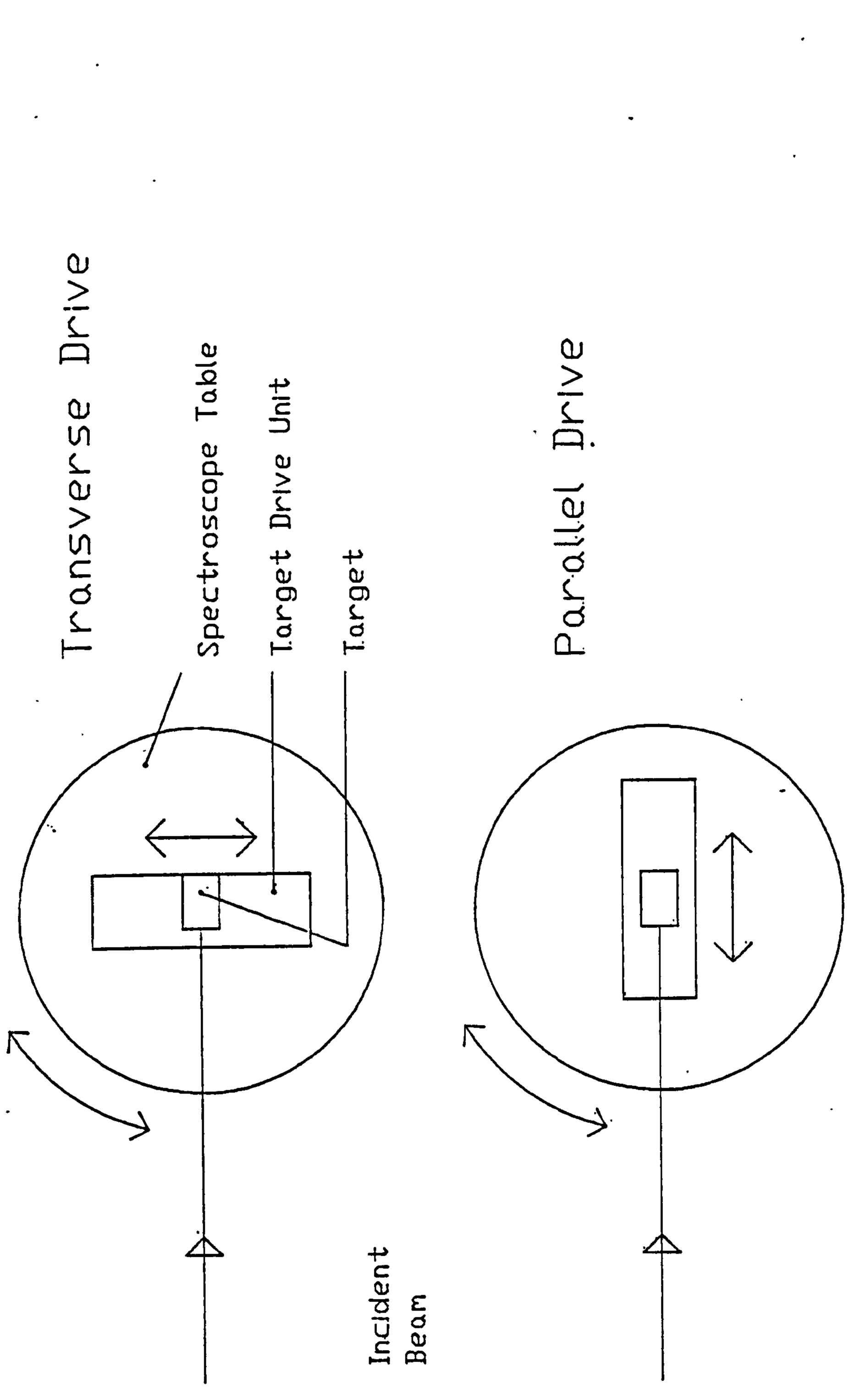

Figure 5.16 Mounting for Inclined Target Measurements

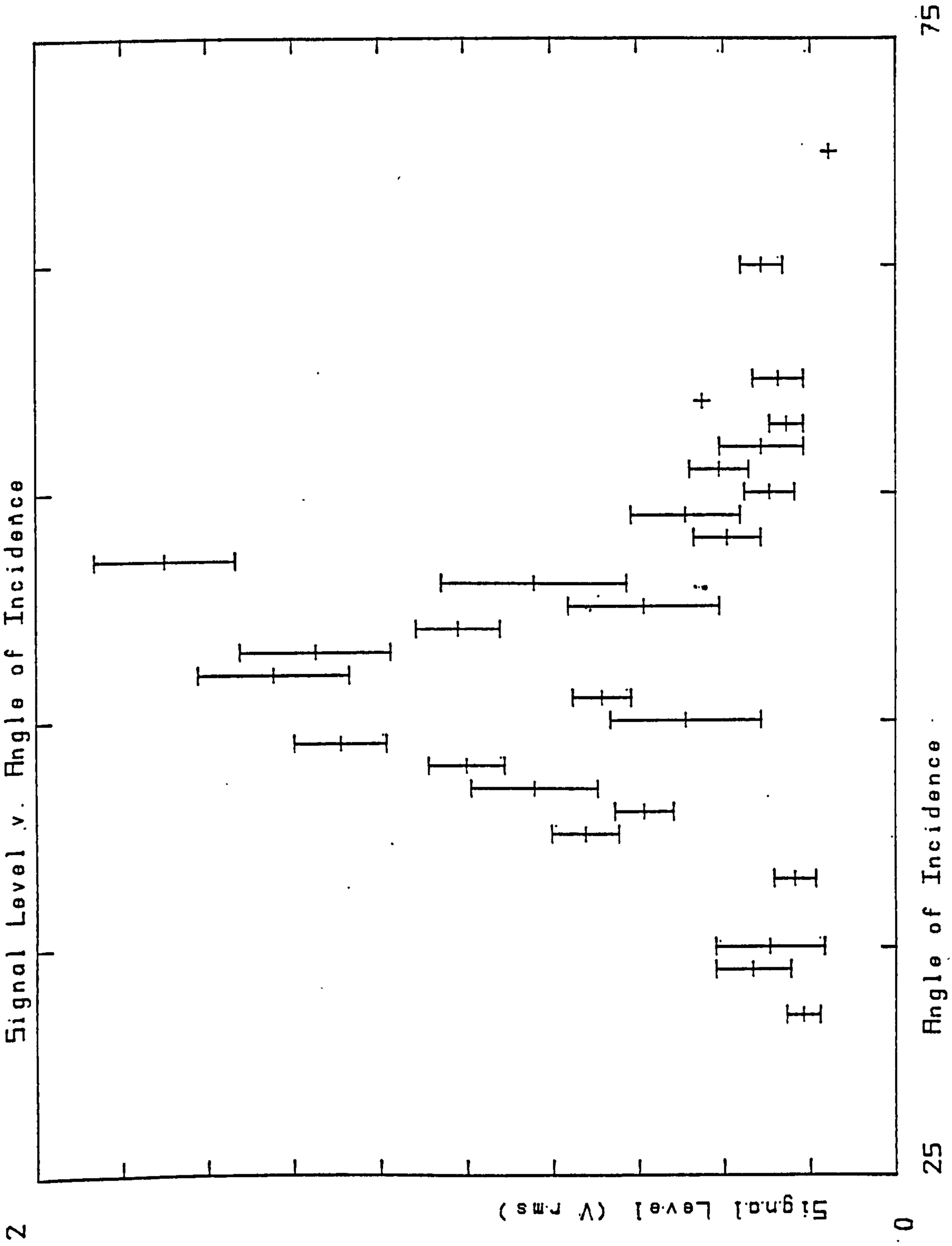

Figure 5.17 Signal Amplitude for Varying Incidence

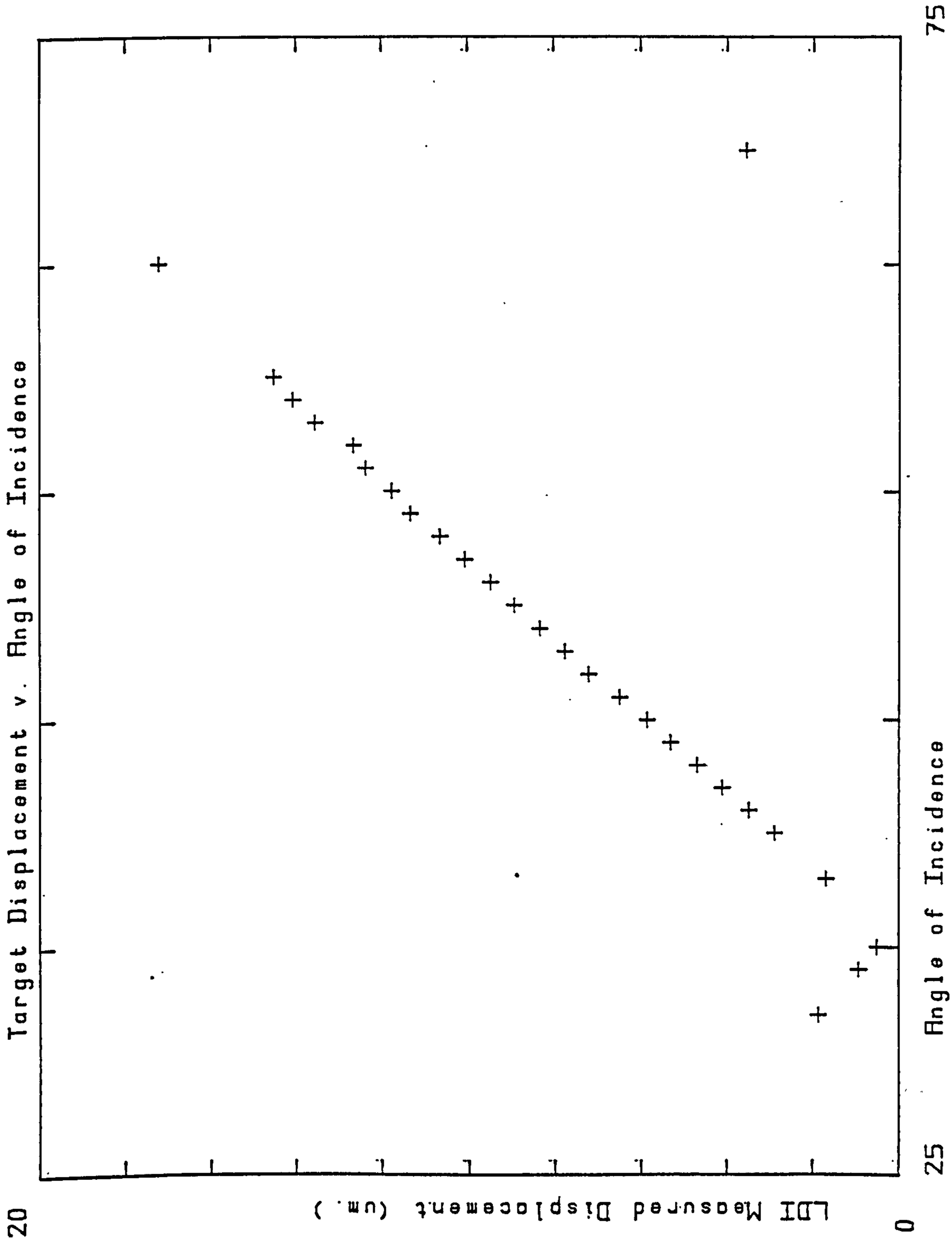

Figure 5.18 Measured Displacement for Varying Incidence

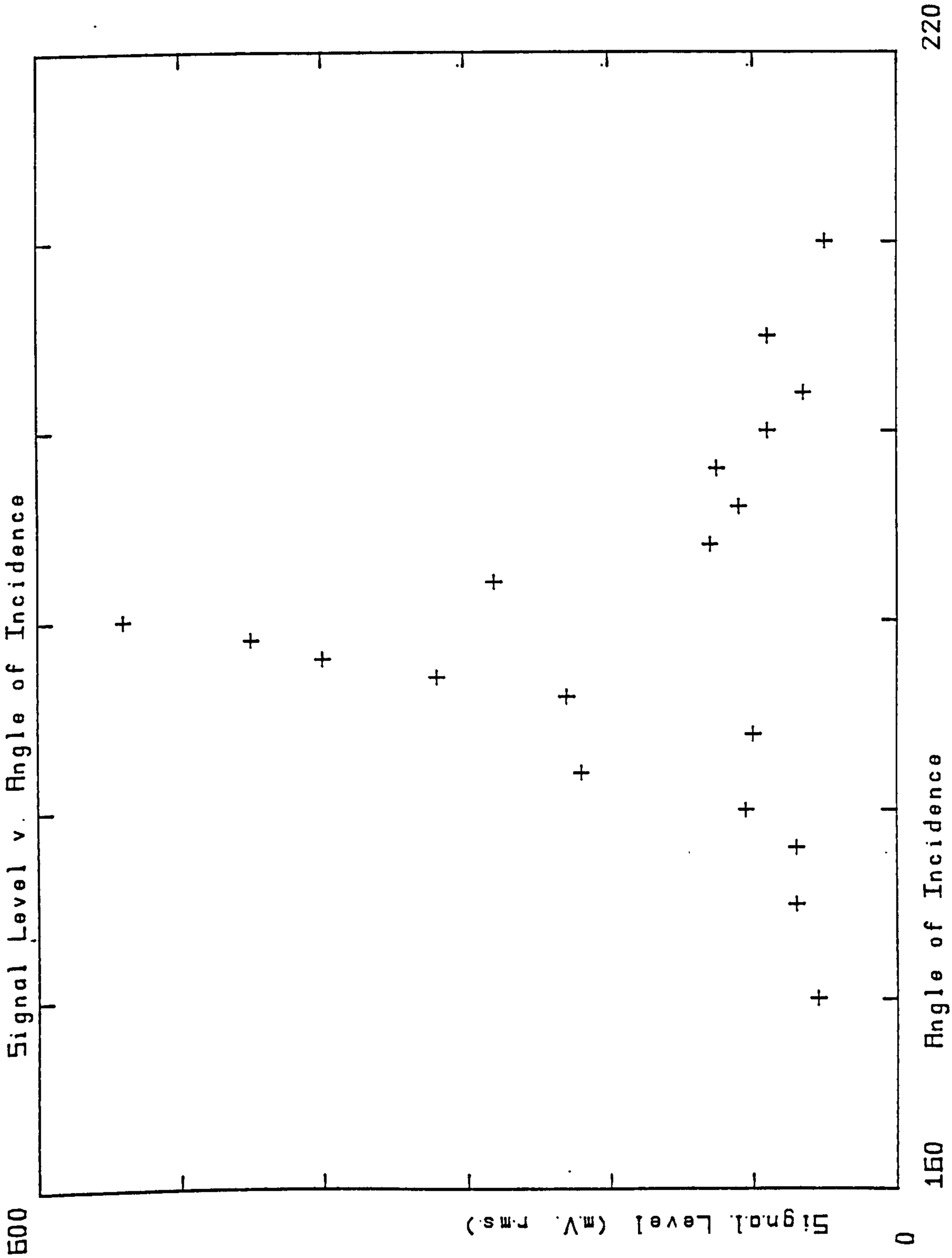

Figure 5.19 Signal Amplitude for Varying Incidence

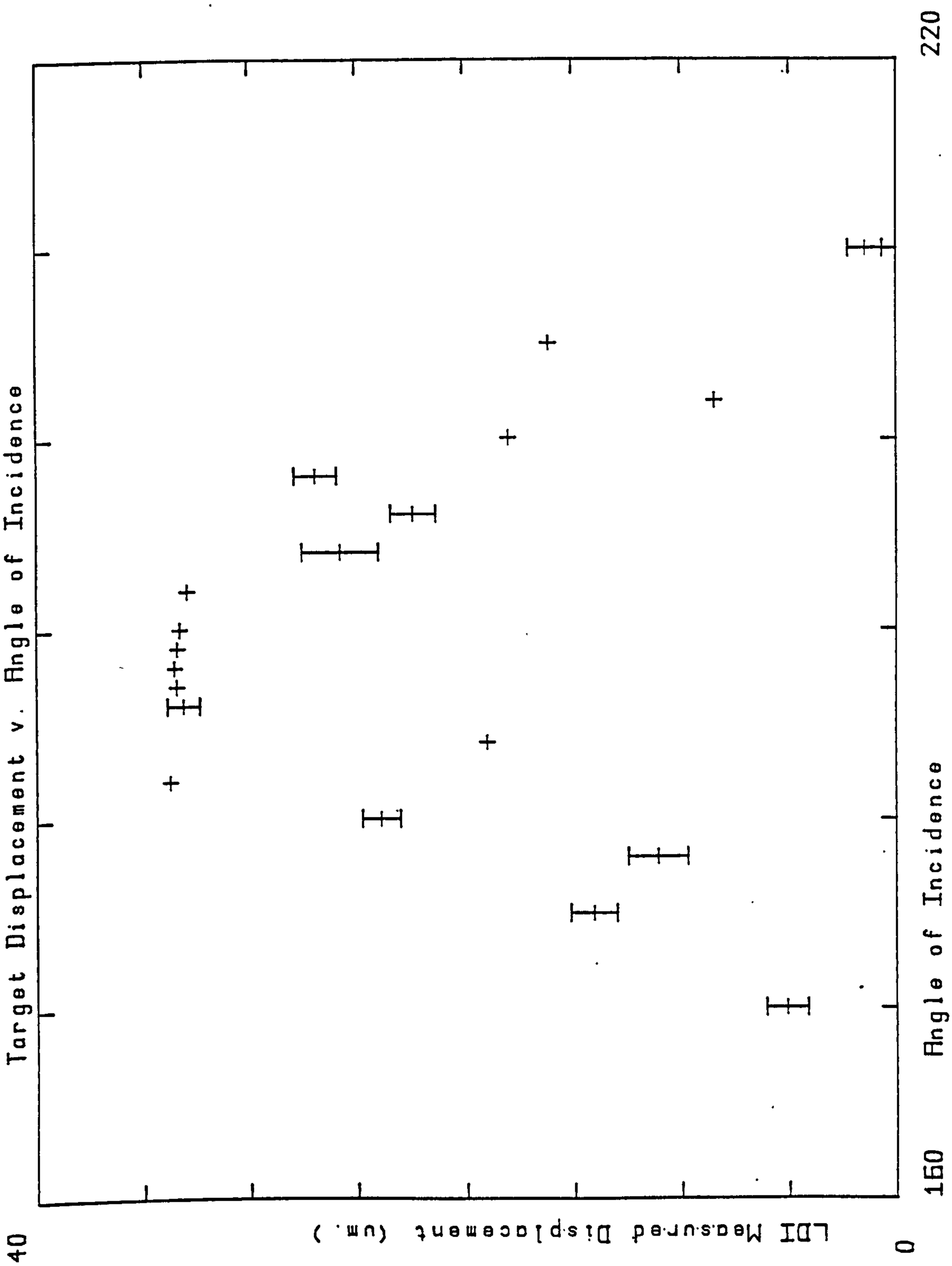

Figure 5.20 Measured Displacement for Varying Incidence

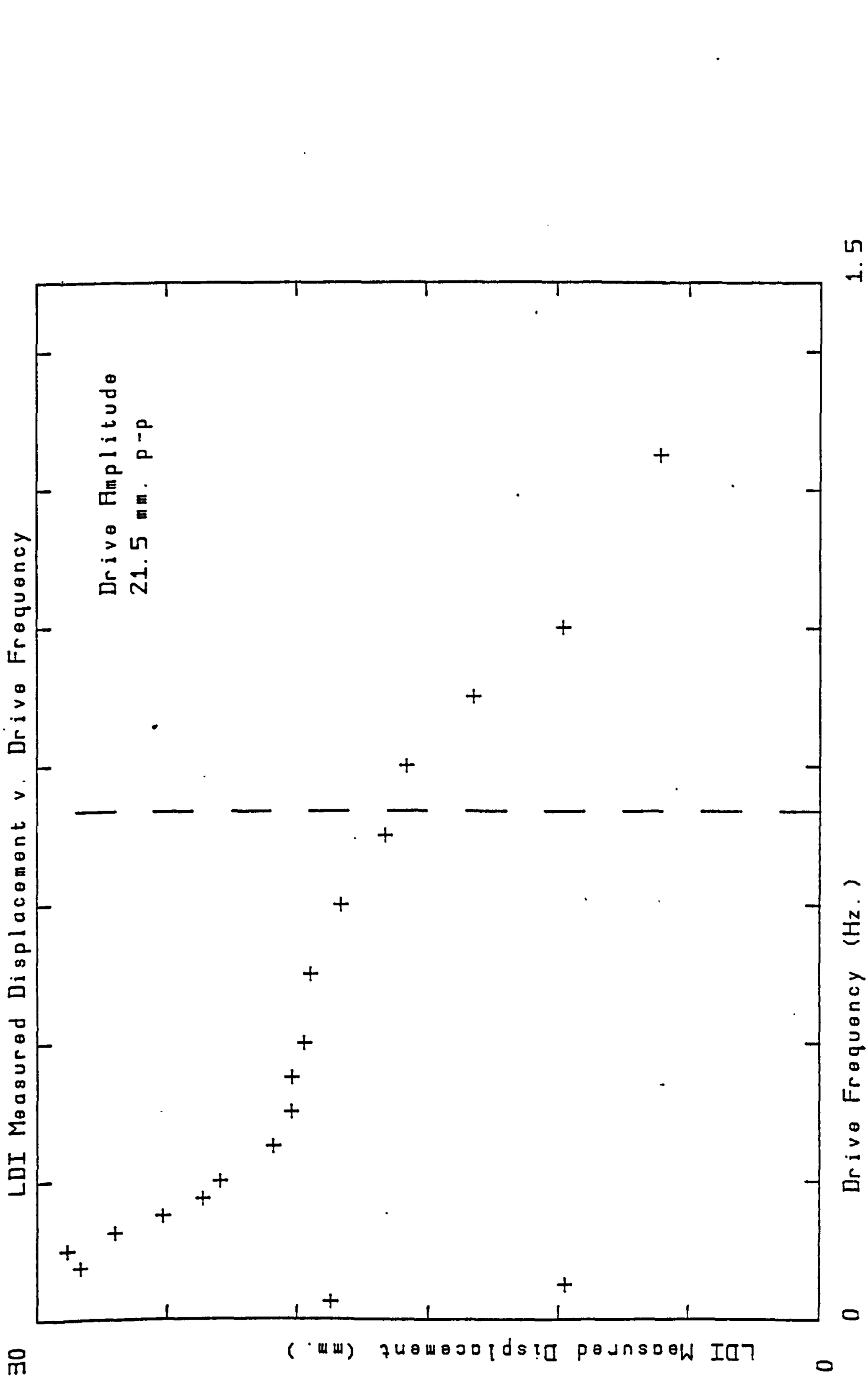

Figure 5.21 Measured Displacement v. Drive Frequency

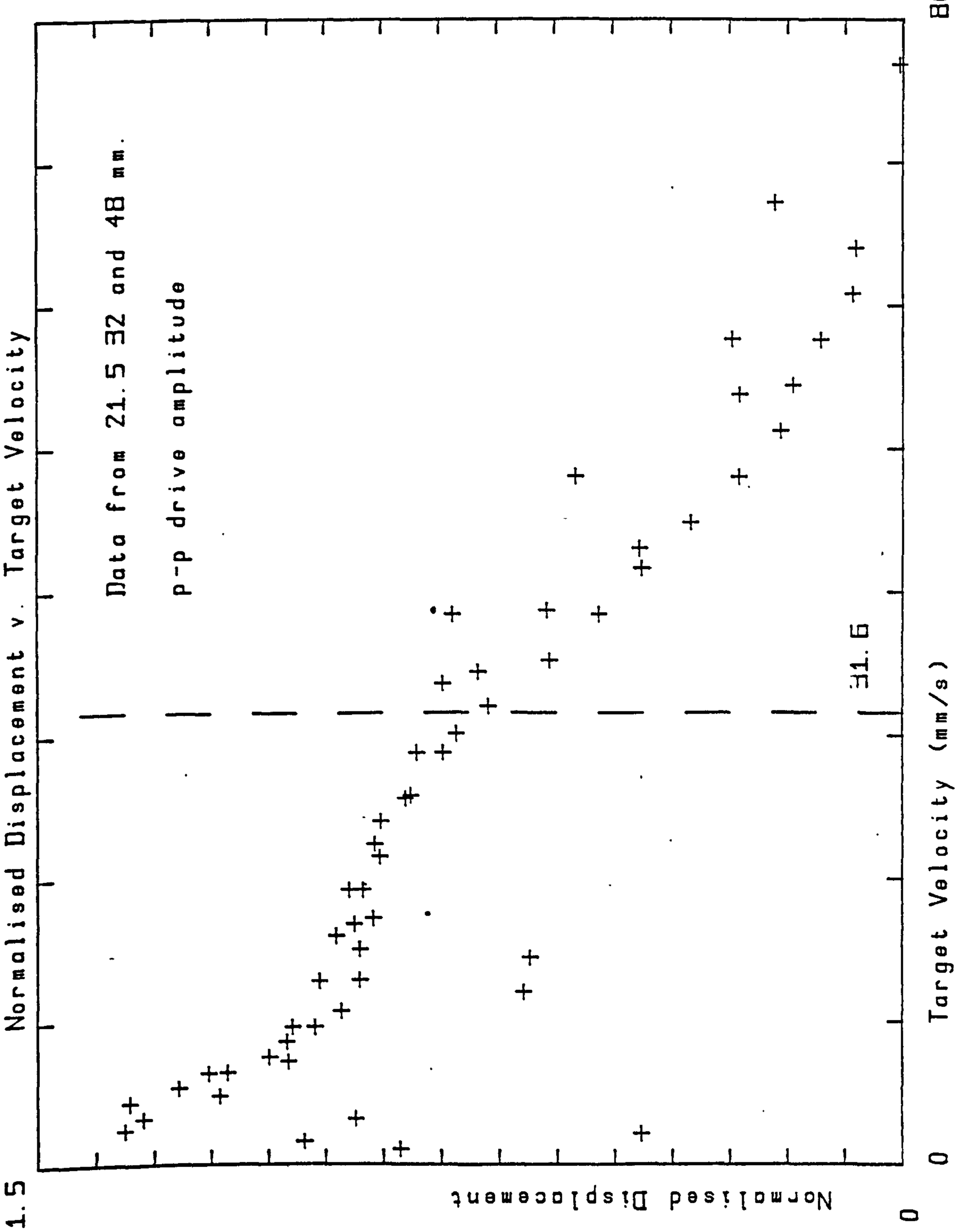

Figure 5.22 Measured Displacement v. Target Velocity

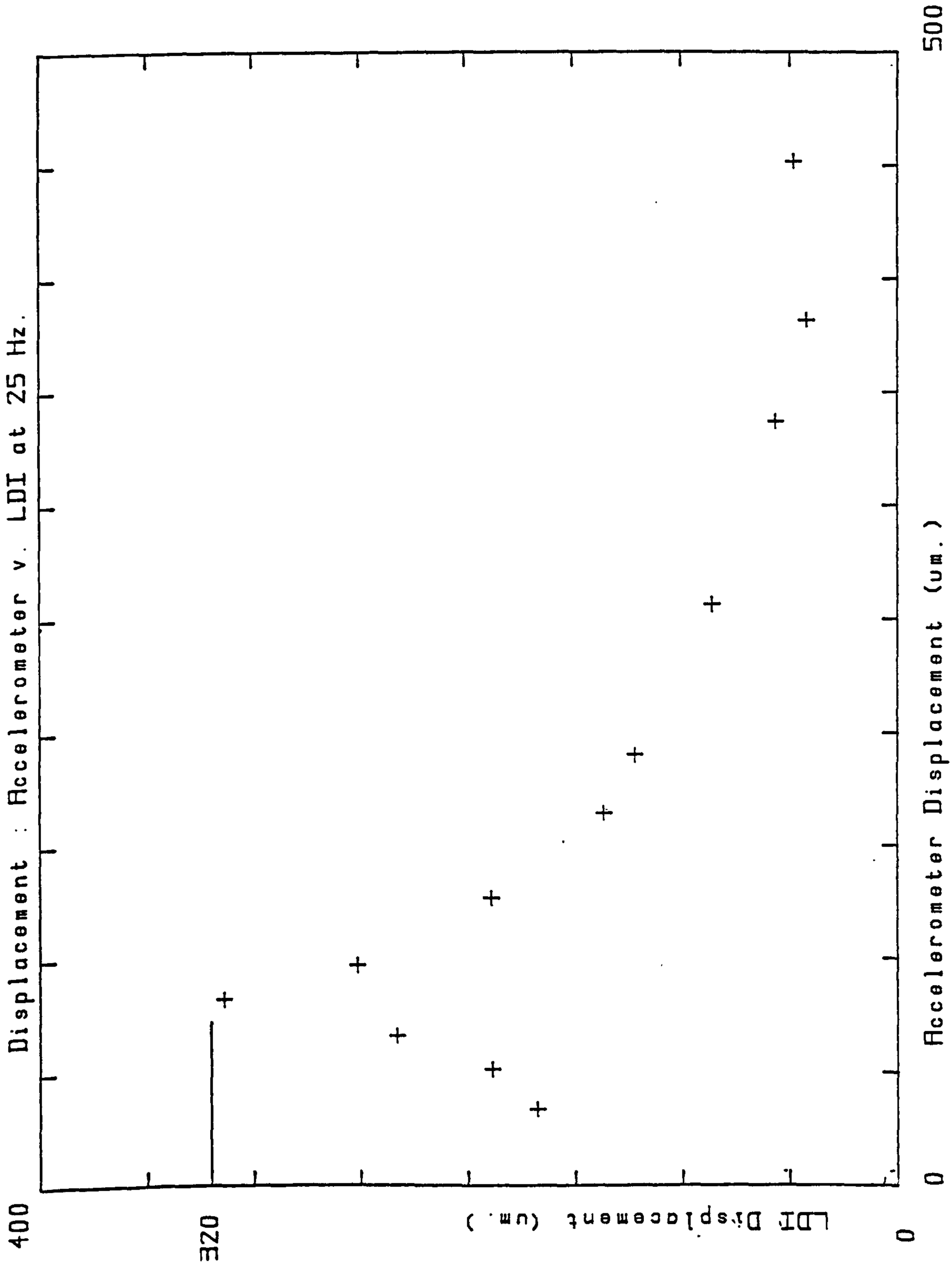

Figure 5.23 Accelerometer v. LDI at 25 Hz.

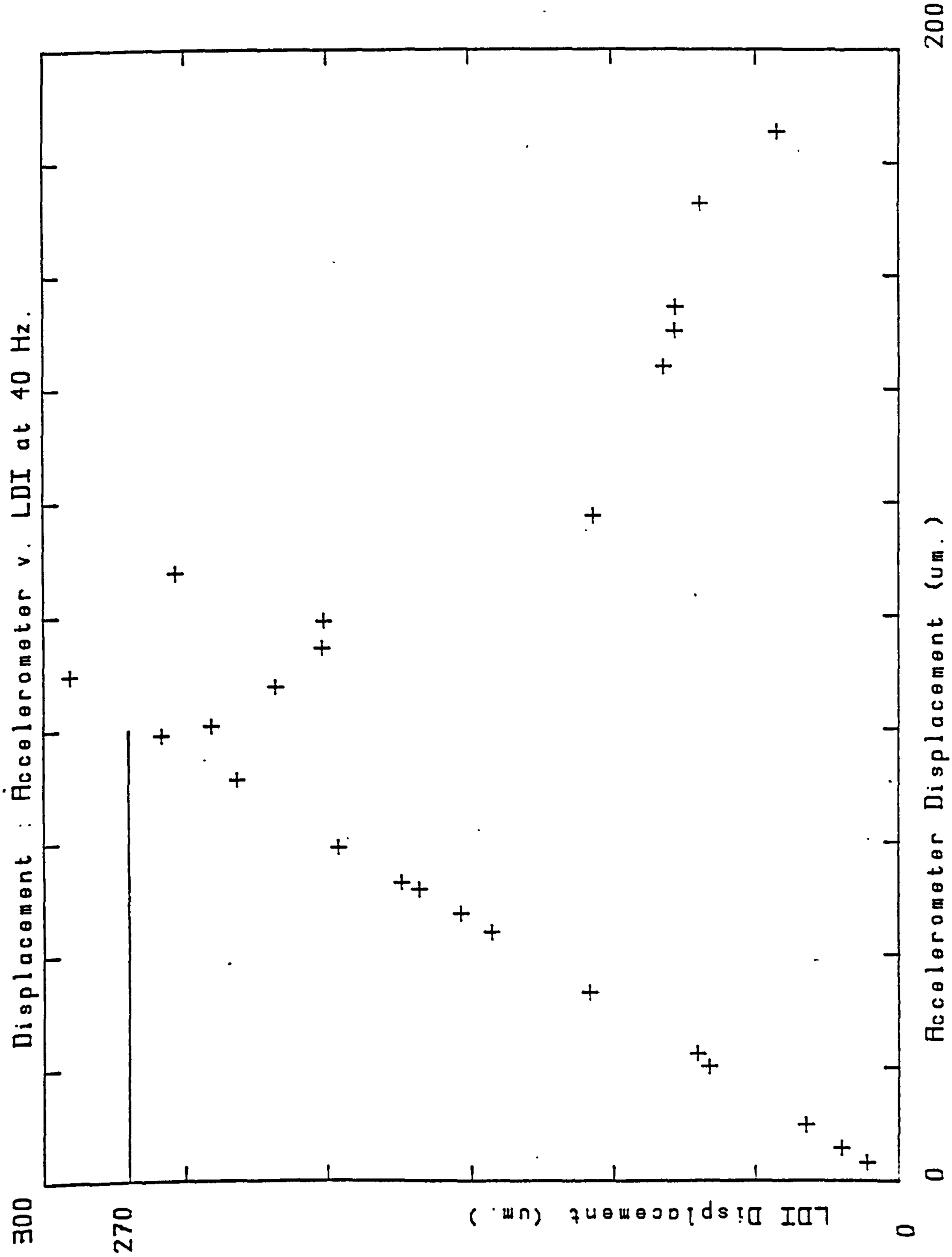

Figure 5.24 Accelerometer v. LDI at 40 Hz.

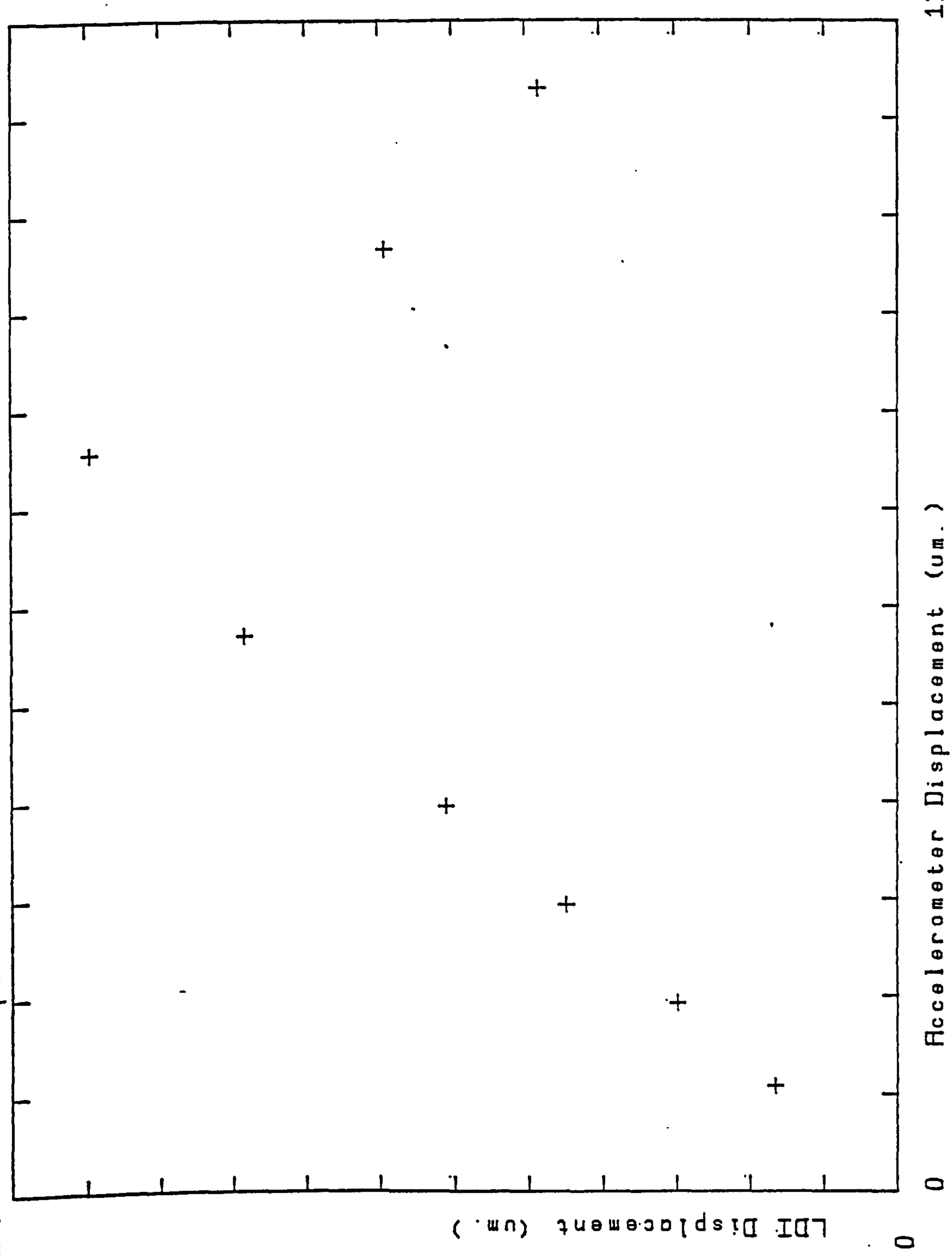

Figure 5.25 Accelerometer v. LDI at 50 Hz.

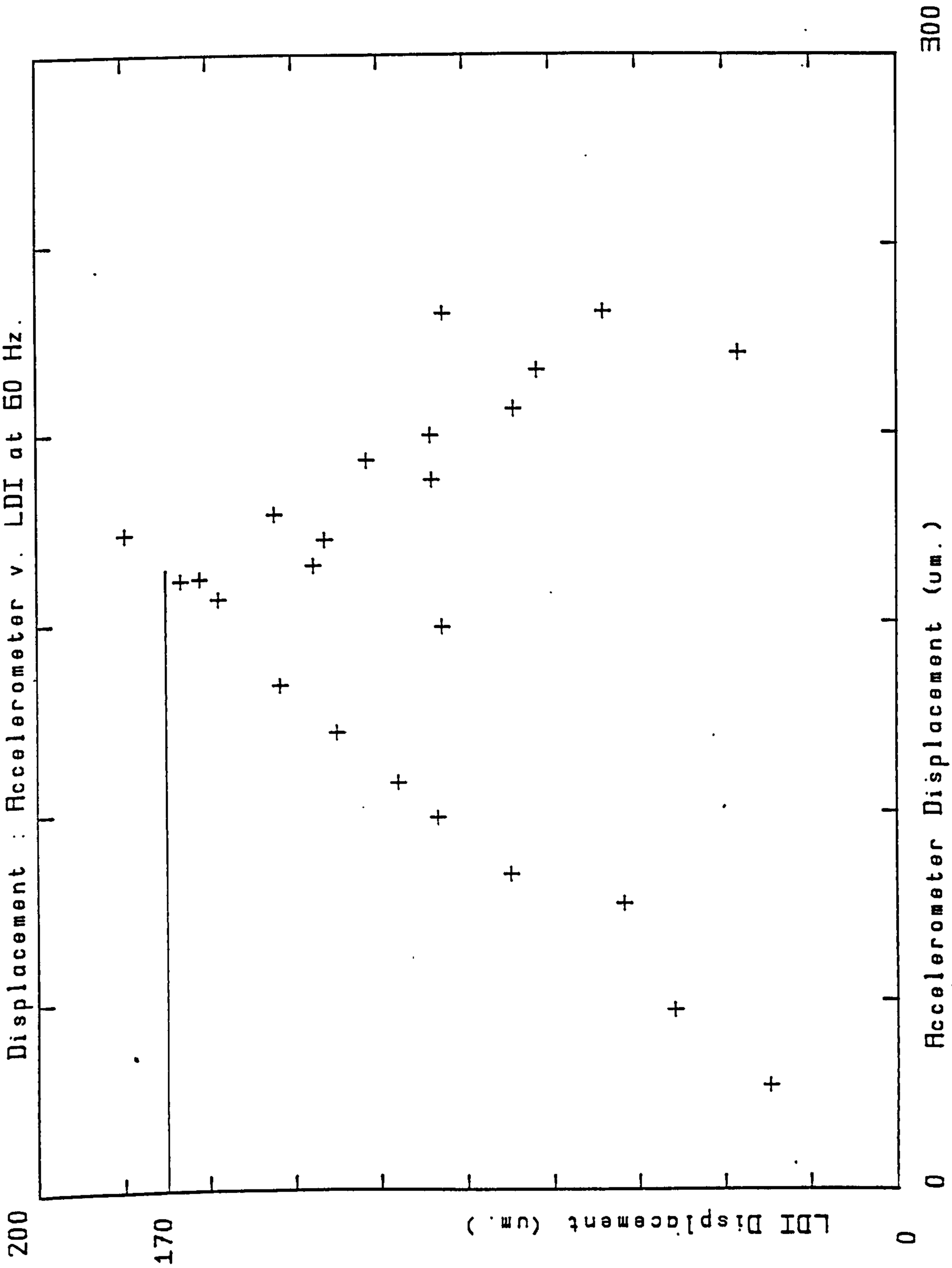

Figure 5.26 Accelerometer v. LDI at 60 Hz.

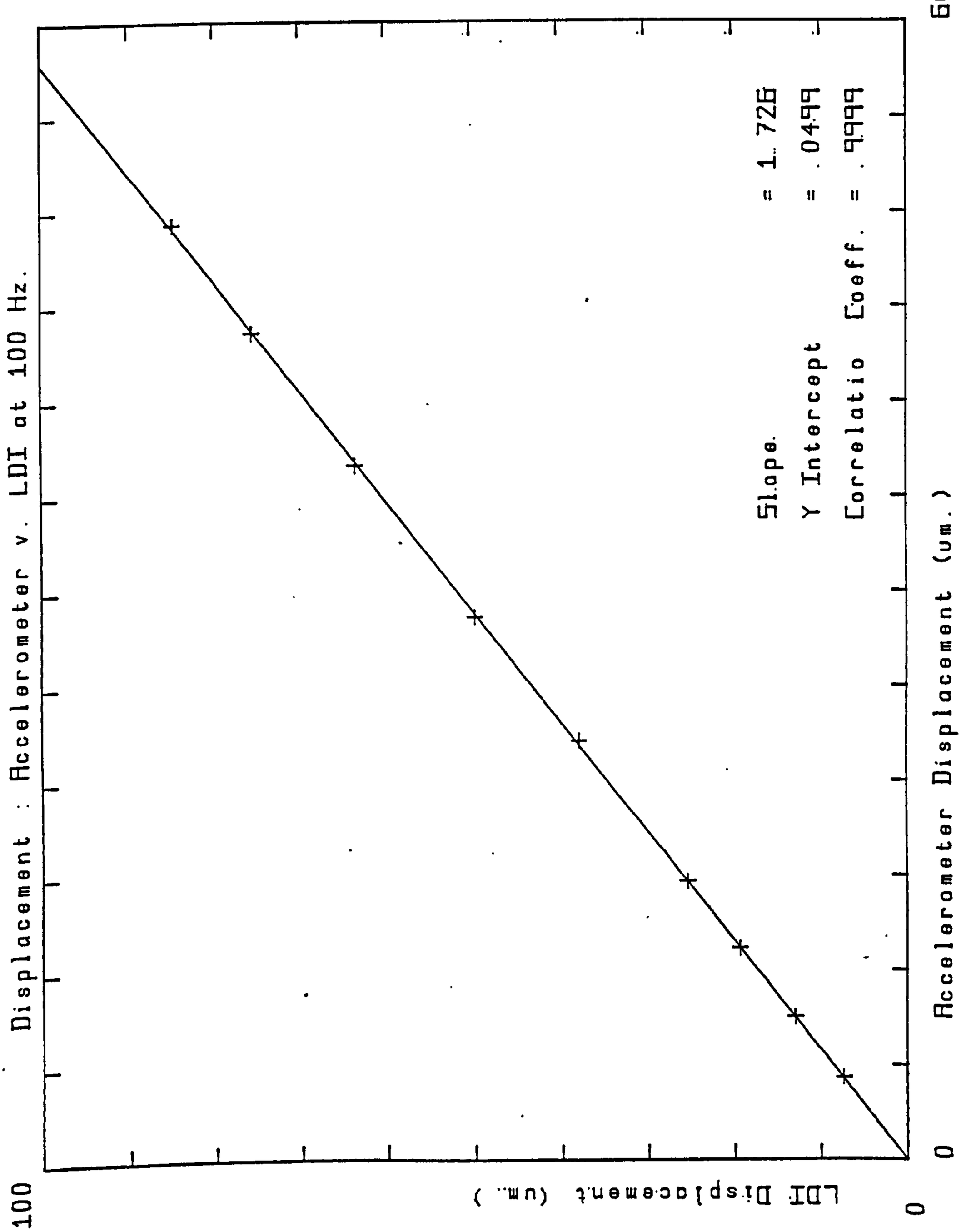

Figure 5.27 Accelerometer v. LDI at 100 Hz.

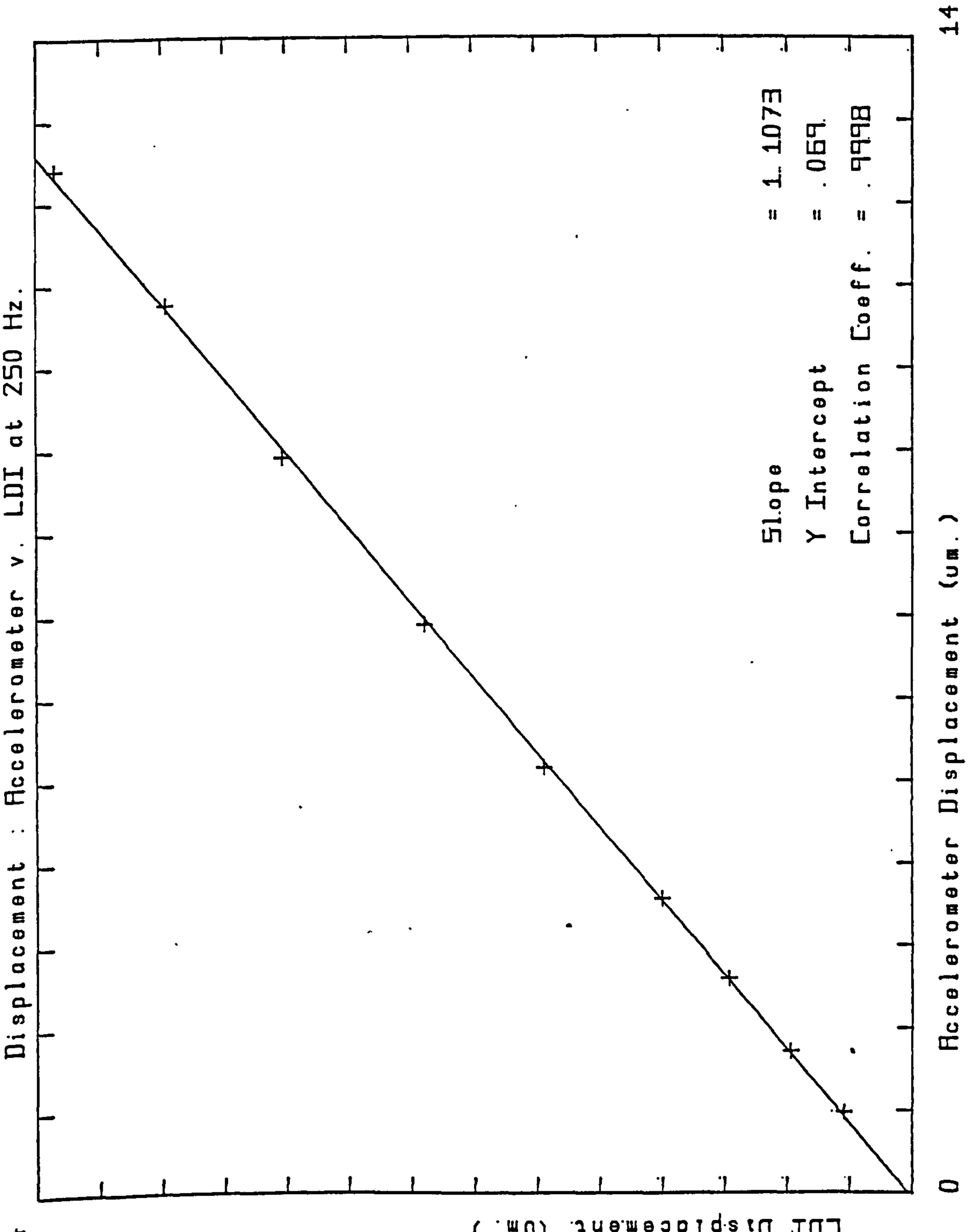

Figure 5.28 Accelerometer v. LDI at 250 Hz.

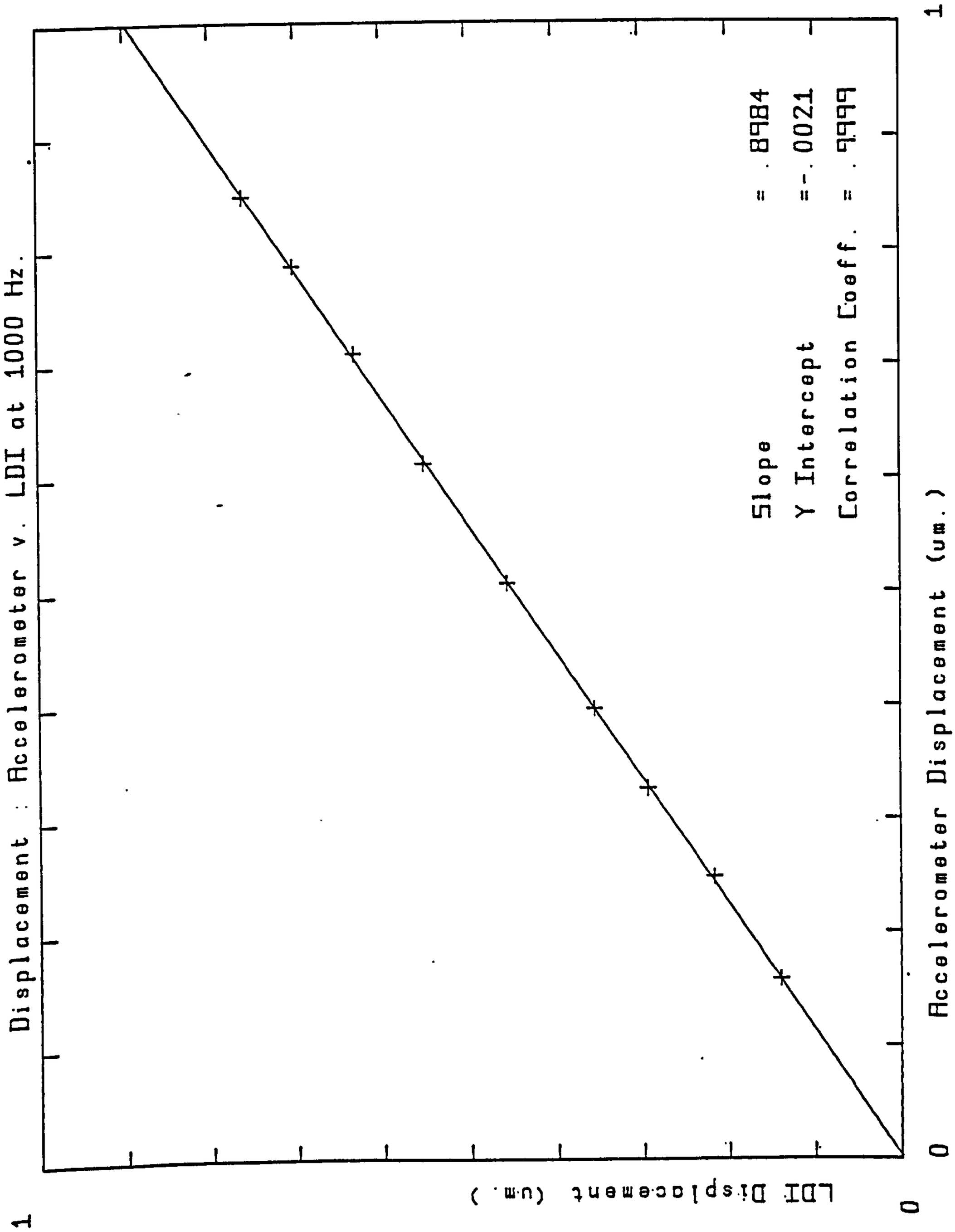

Figure 5.29 Accelerometer v. LDI at 1000 Hz.

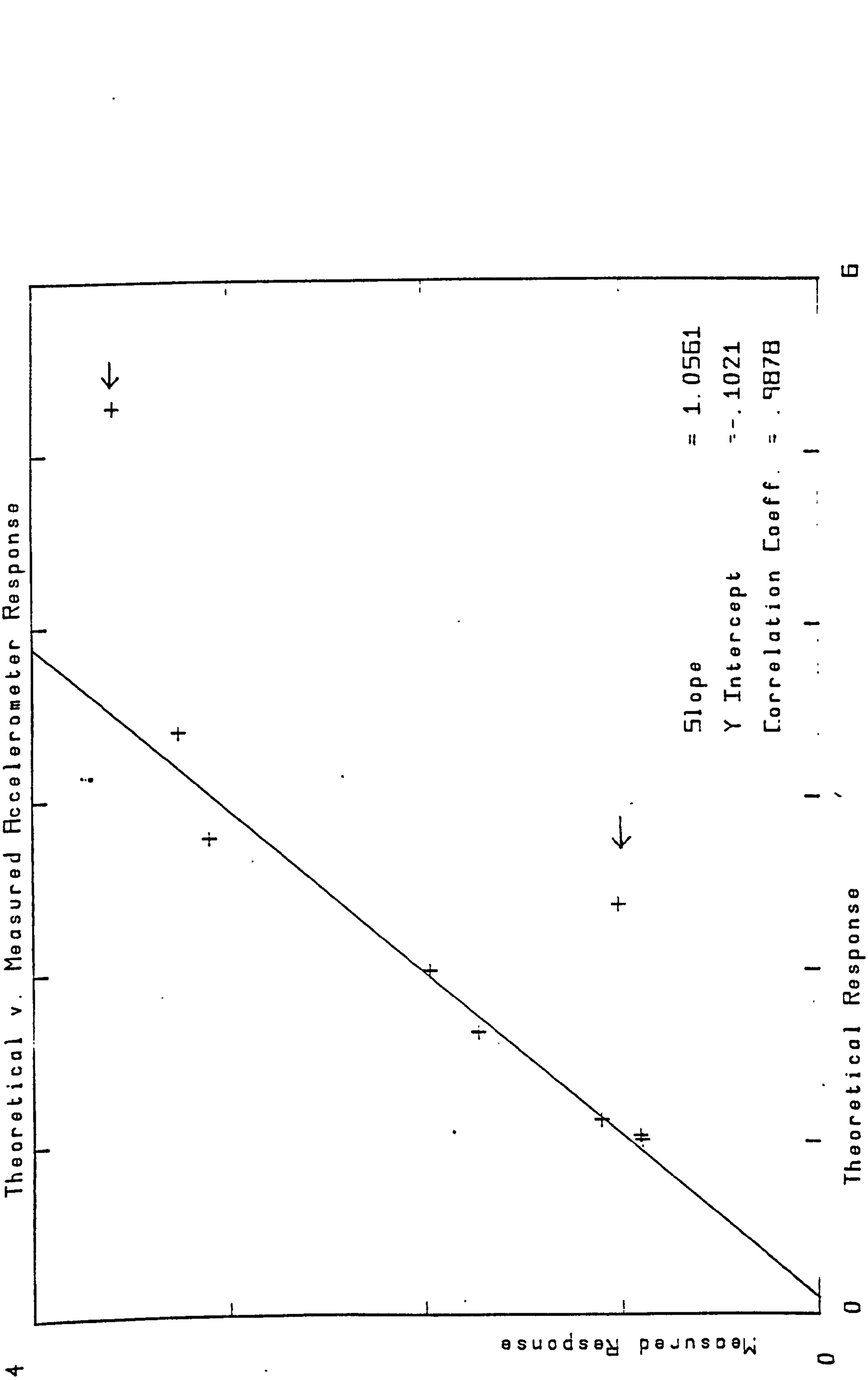

Figure 5.30 Accelerometer Response

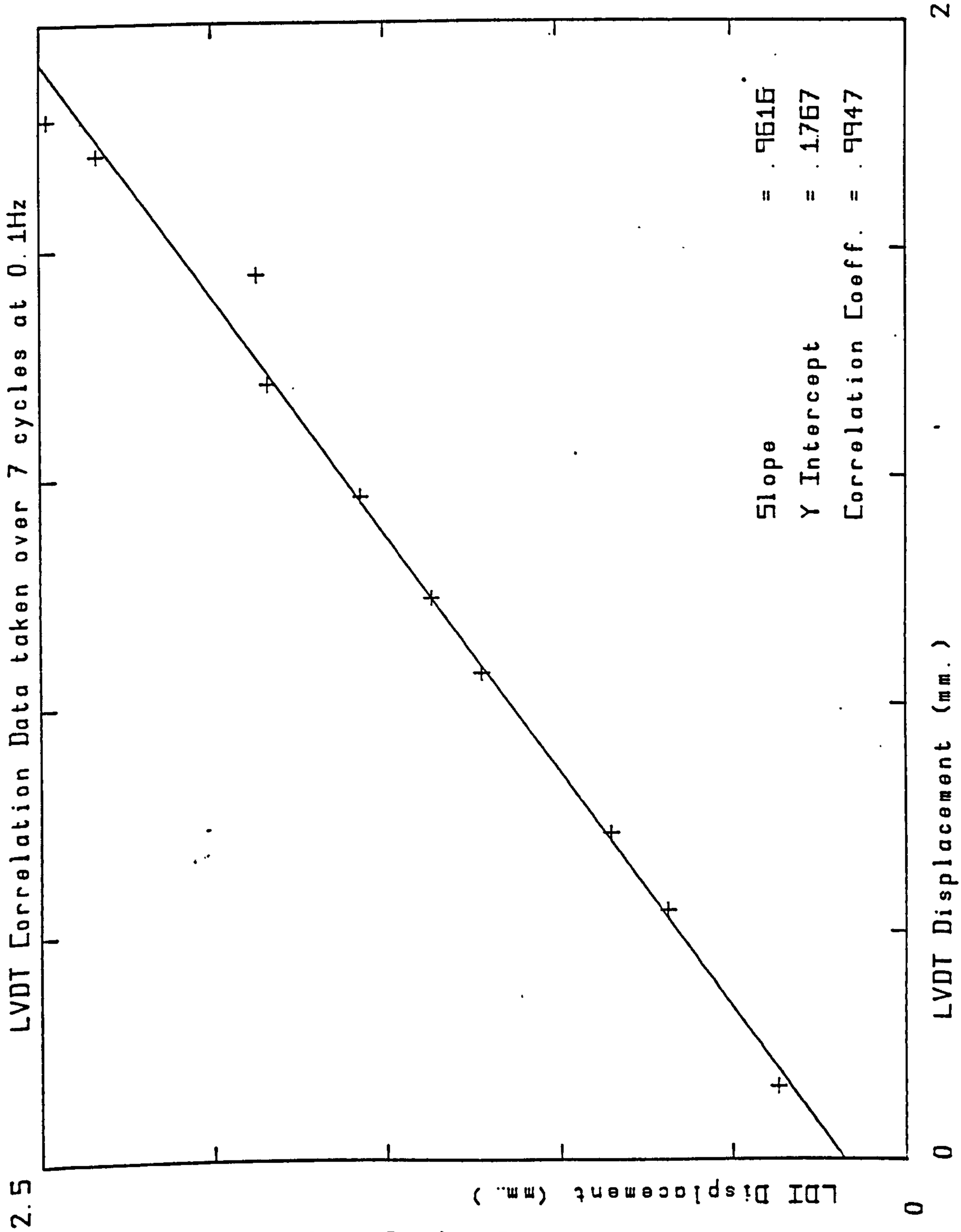

Figure 5.31 LVDT Correlation Data

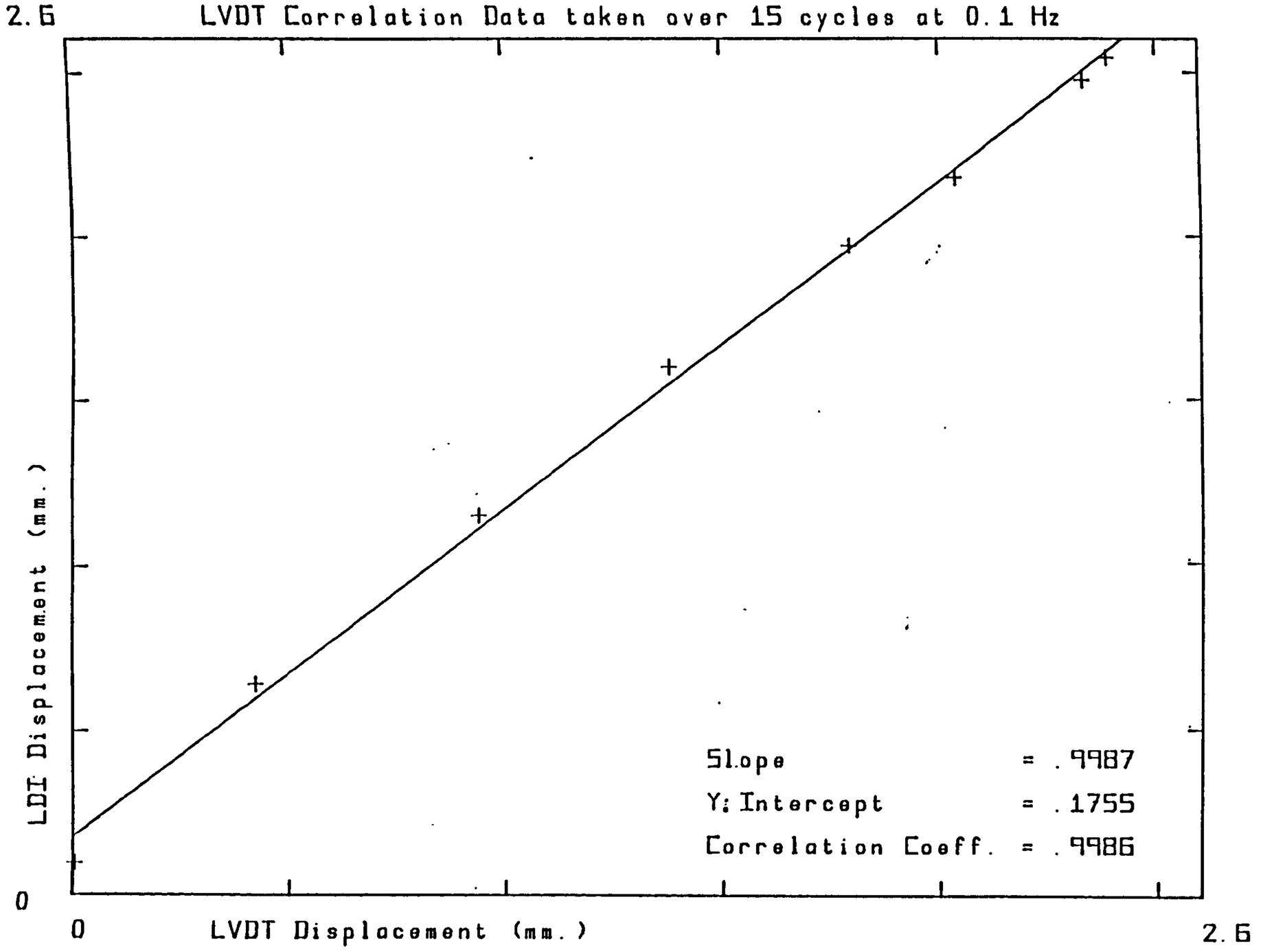

Figure 5.32 LVDT Correlation Data

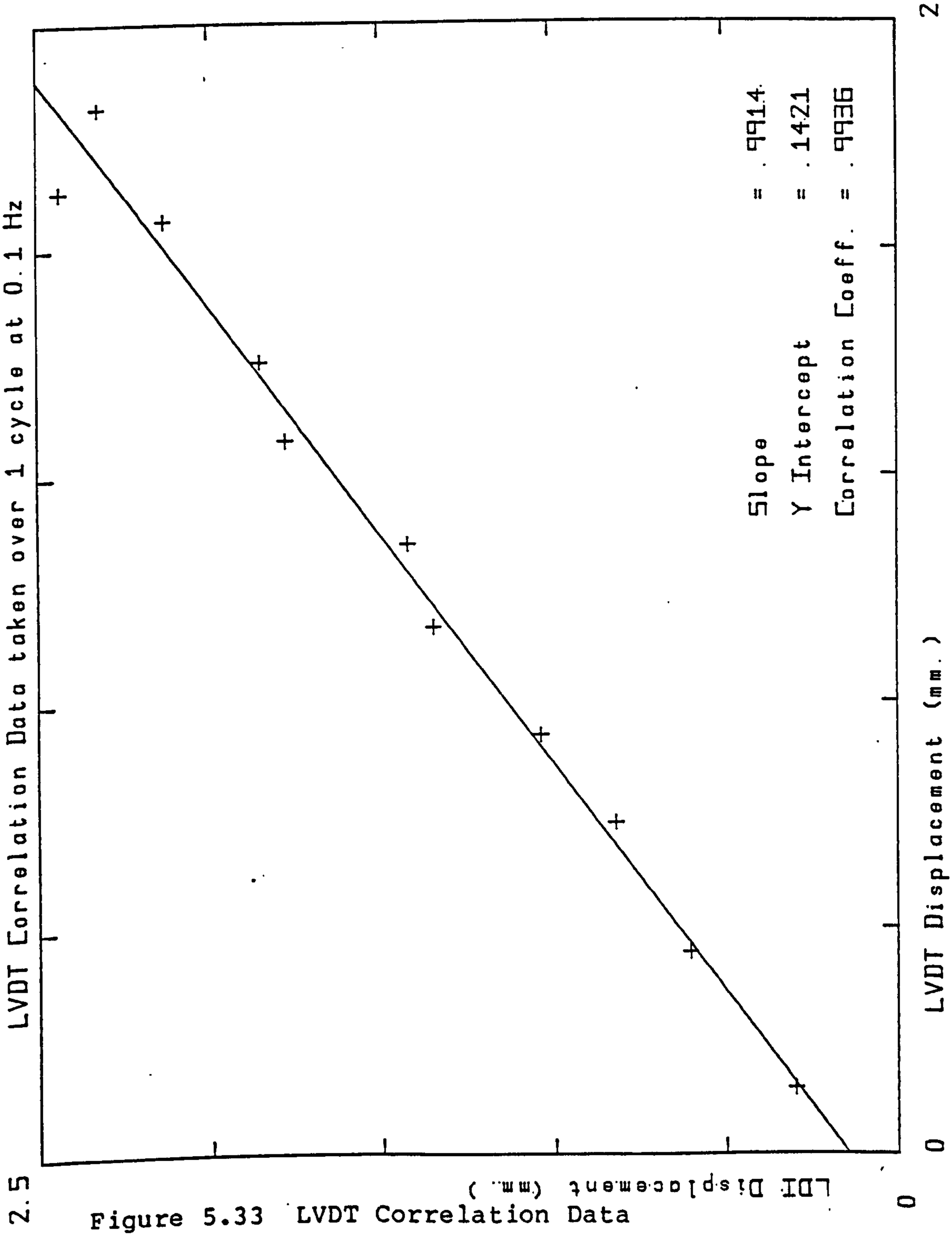

Figure 5.33 LVDT Correlation Data

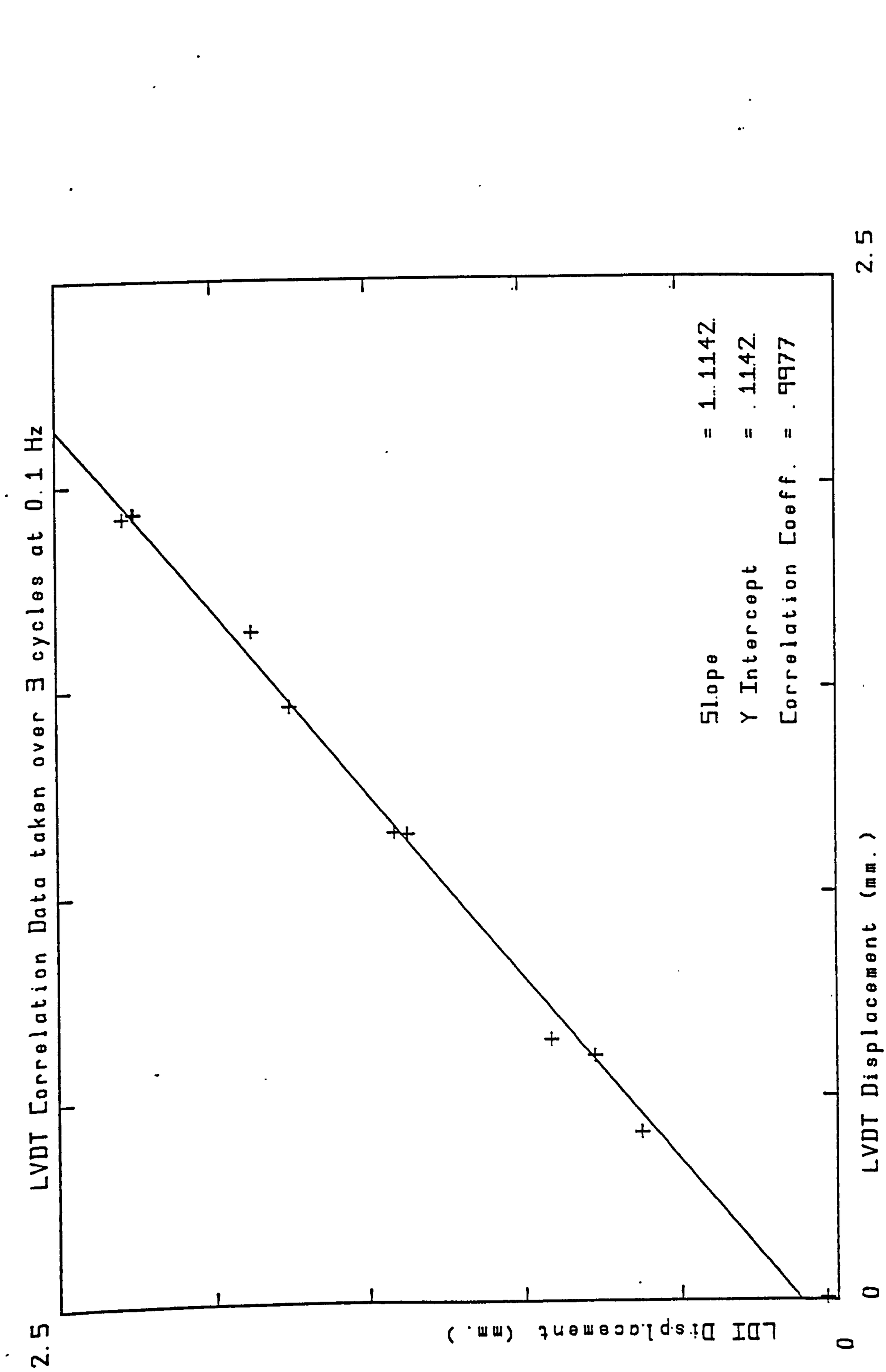

Figure 5.34 LVDT Correlation Data

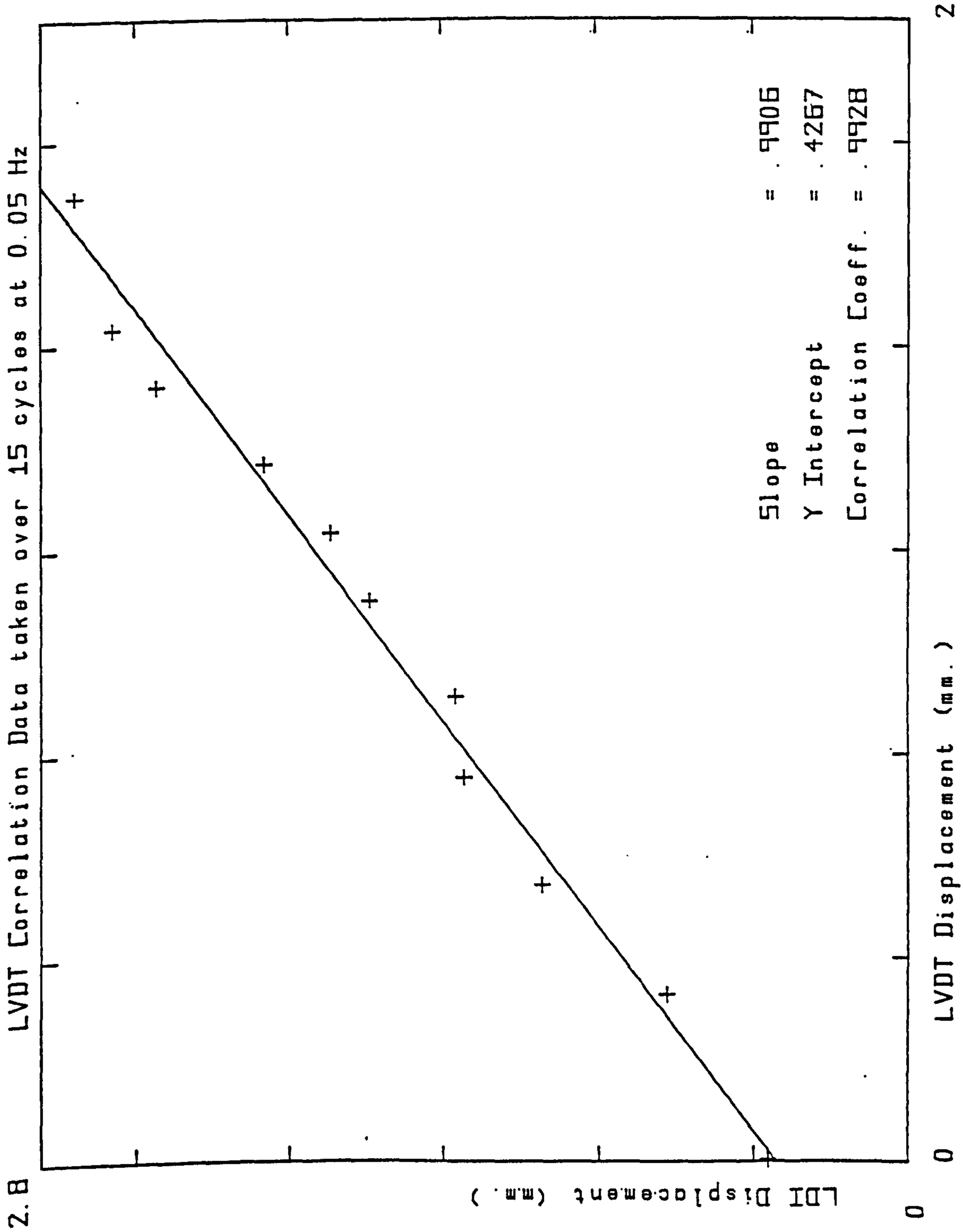

Figure 5.35 LVDT Correlation Data

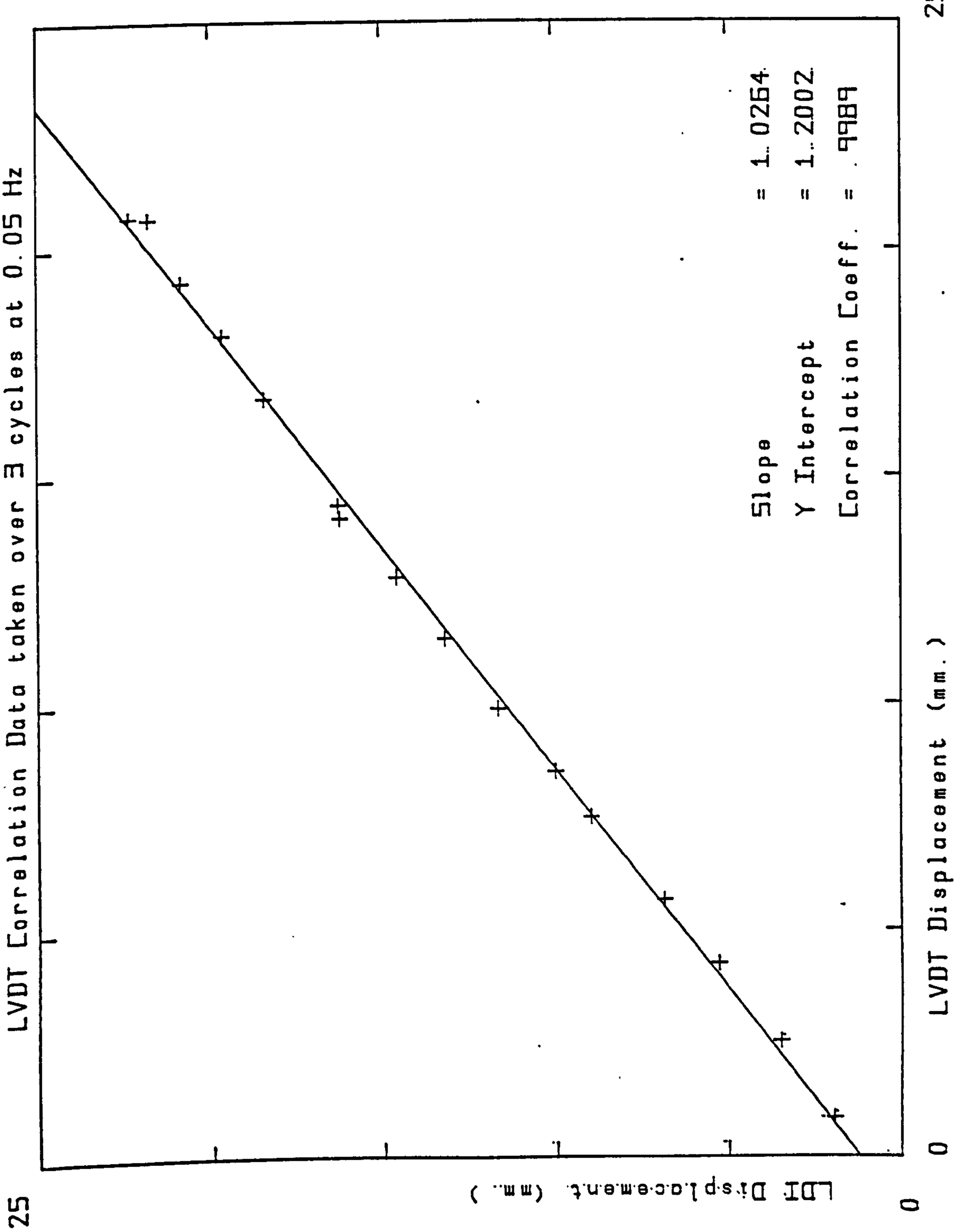

Figure 5.36 LVDT Correlation Data

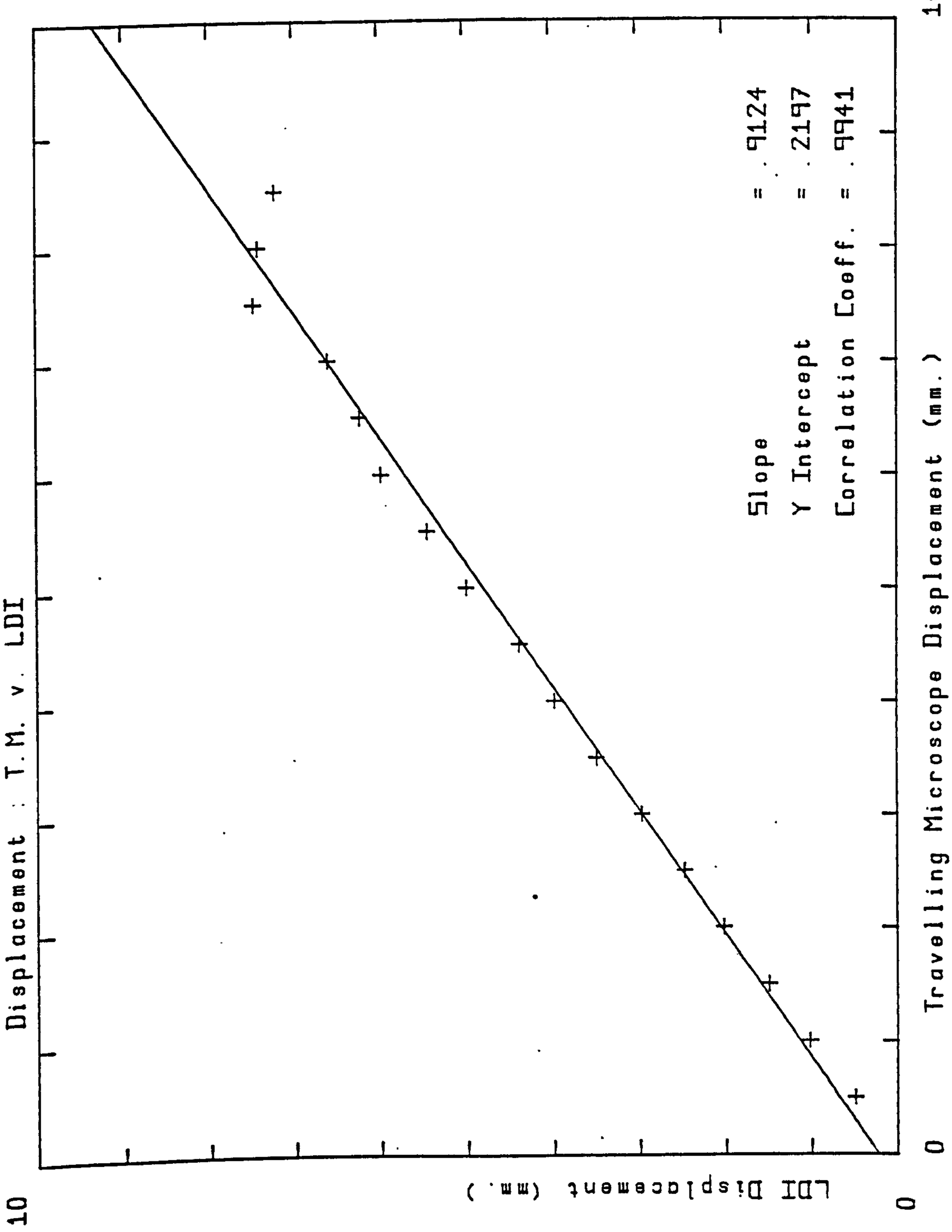

Figure 5.37 Manual Translation Correlation Data

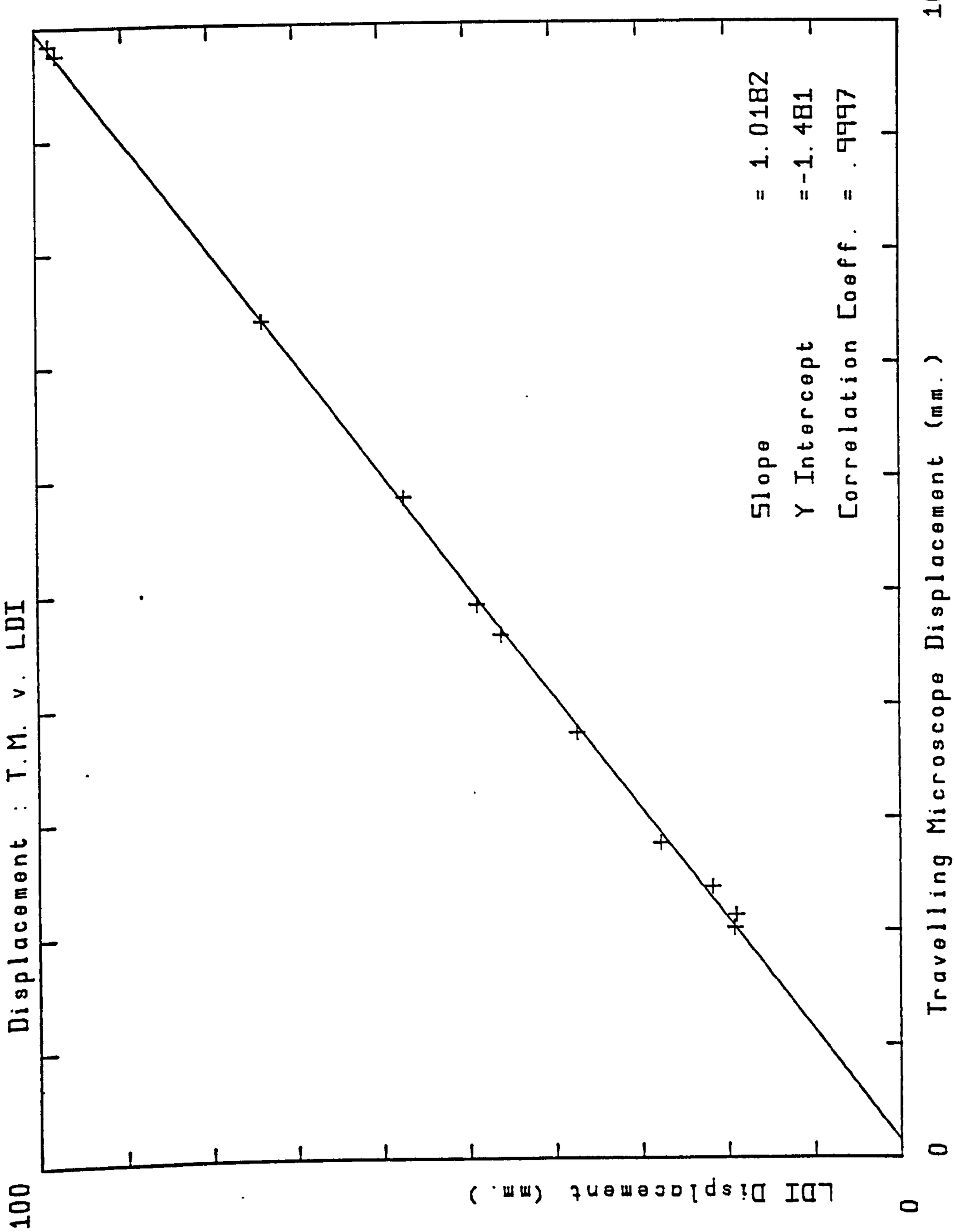

Figure 5.38 Manual Translation Correlation Data

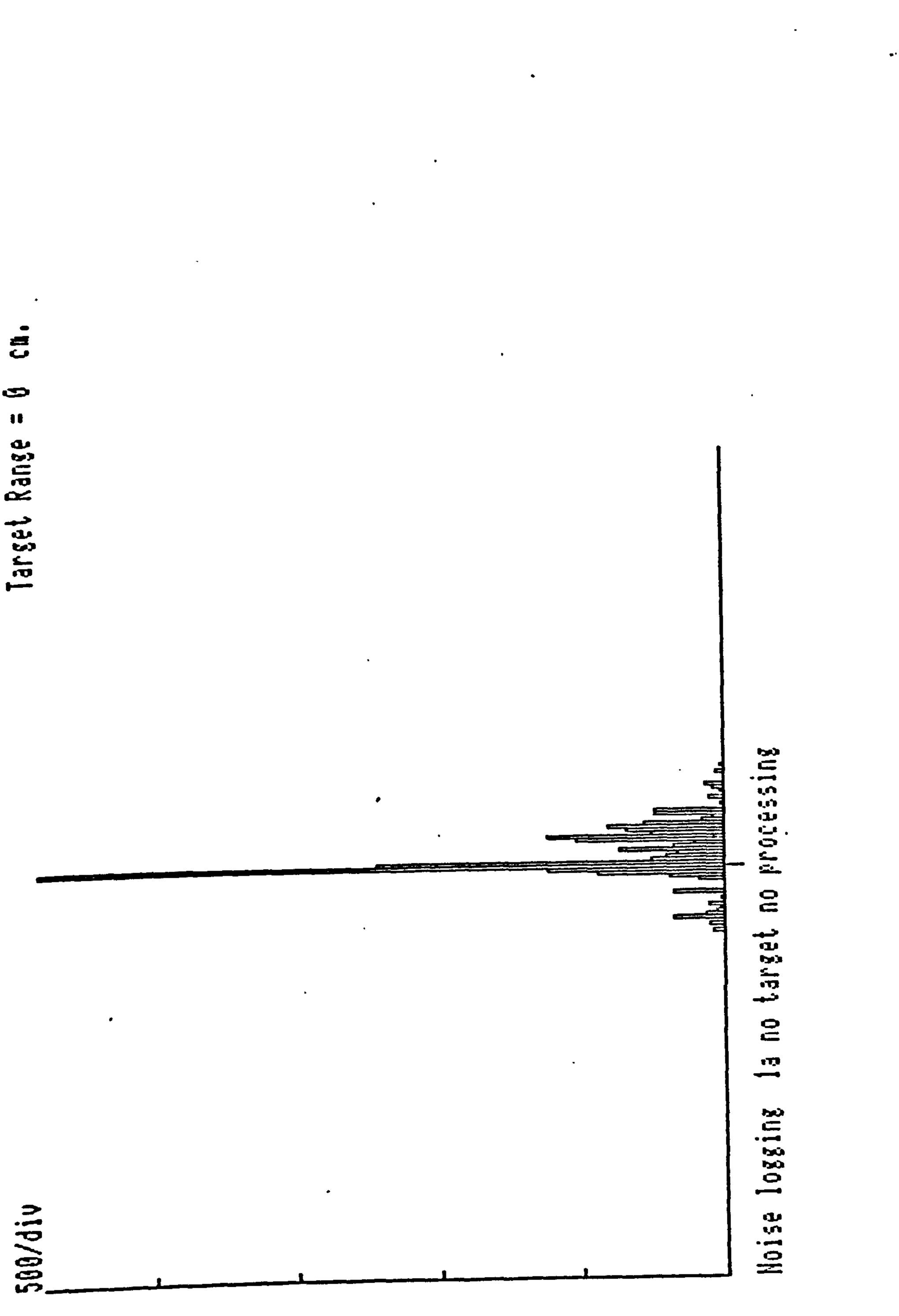

Figure 5.39 Noise Histogram from Coimputer Data Logging

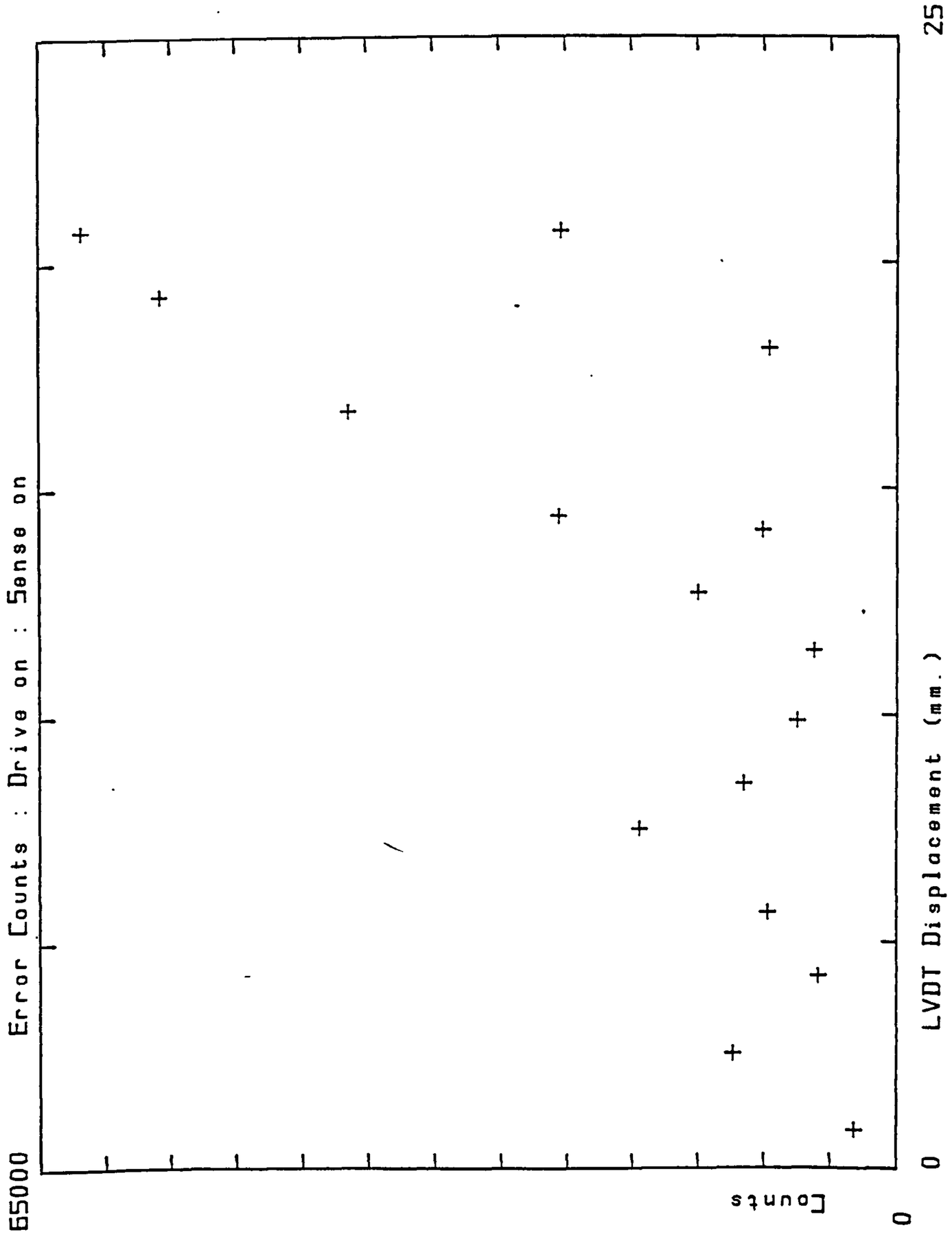

Figure 5.40 Error Data from the LDI

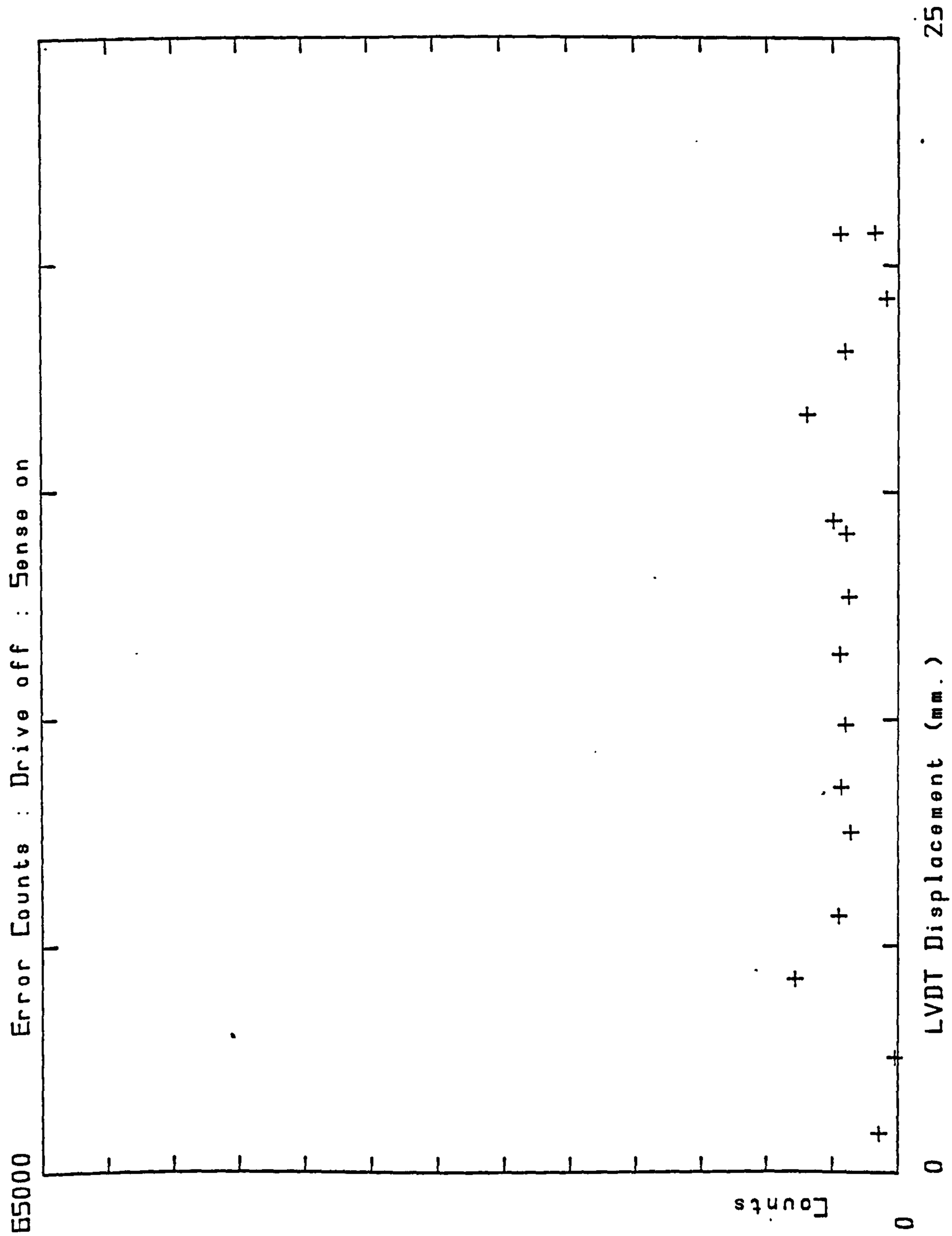

Figure 5.41 Error Data from the LDI

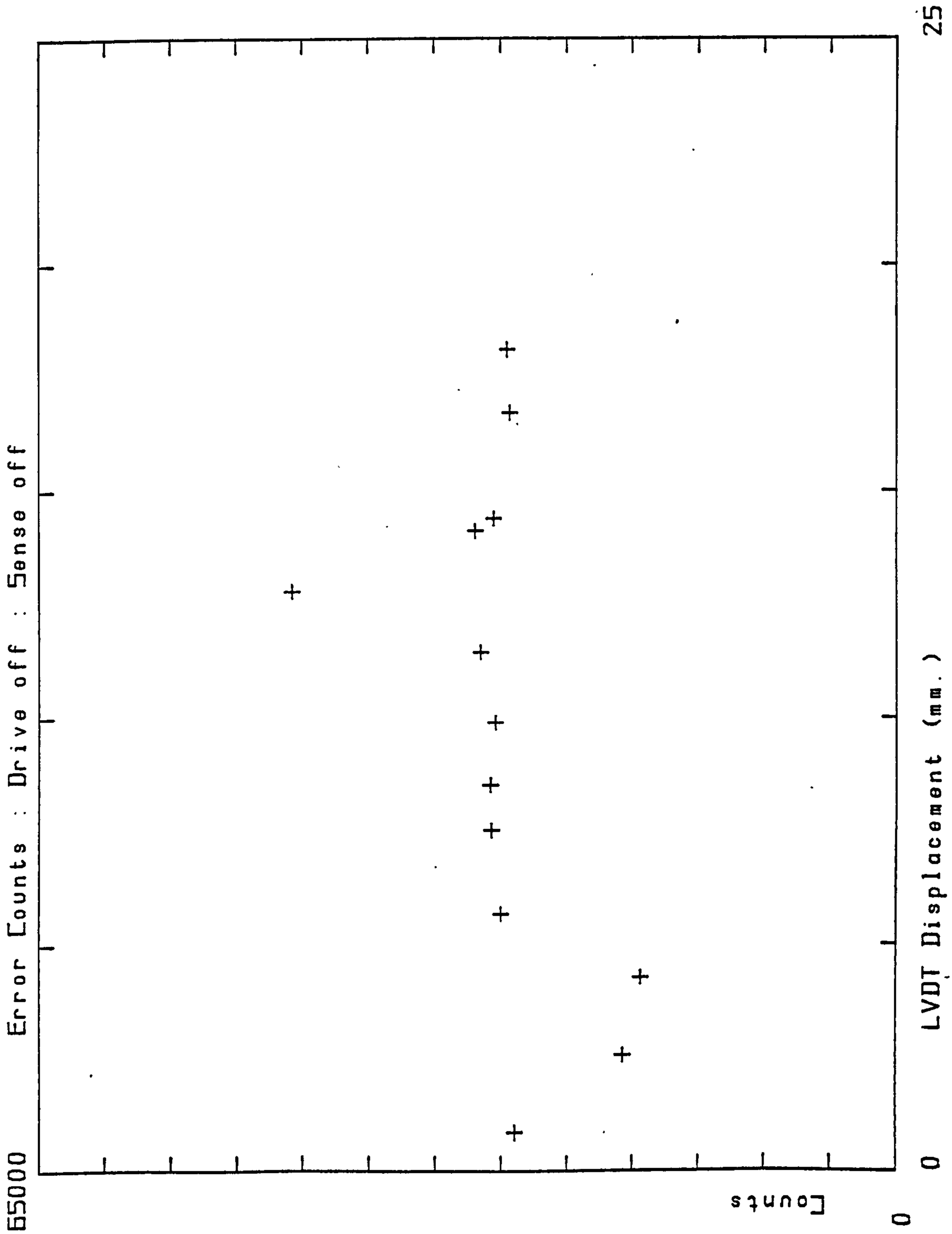

Figure 5.42 Error Data from the LDI

6. CONCLUSIONS

6.1 Capabilities and Limits of the System

6.1.1 Displacement

The maximum continuous target displacement that has been measured with the LDI is 200 mm., centred 400 mm from the datum point of the device. This is considered to be a very good operational depth of field for operation at this range. Smaller amplitude motions were measured at distances up to 800 mm from the device datum, this being the maximum accessible range in the experimental configuration. It is considered that the maximum working range of the LDI could be extended to several metres with improved detectors and signal processing. The digitising of the detected signals led to a displacement resolution of half the operating wavelength (0.316 um.). The minimum theoretical resolvable amplitude from one output of the LDI using digital fringe counting is a quarter of the operating wavelength, however if both the detected signals in a quadrature based system were used it should be possible to realise eighth wavelength resolution (0.08 um.). While it is doubtful that a measurement of this resolution could be made as a single point to point measurement, the device has measured sub micrometer displacements from a vibrating target where the duration of periods of low velocity was too short to allow the background to cause additional displacement counts to be logged. Because the exact phase relationship between the

two detected channels was uncertain, use of the maximum achievable resolution was precluded.

The LDI does not require calibration as it measures displacement in terms of the wavelength of the laser, which is a constant in a given medium.

Continuous displacement measurements in excess of those mentioned above could be realised by a direct increase in the laser power used to illuminate the target thus providing stronger signals at extended ranges. It is also possible that under a better defined set of working conditions, with a well known maximum expected range of motion the available laser power could be better employed. This may involve the collection of light from more than one speckle, with a consequent decrease in the coherence of the detected signal. This trade off between intensity and signal coherence is unavoidable.

Results were obtained comfortably from targets with reflectivities of (circa) 70%. Signals could also be obtained from lower reflectivity targets under a more restricted range of conditions. In most cases it was found that inclination of the target surface to the illuminating beam did not detract strongly from the signal strength. The study of light scattering from optically rough surfaces is a separate topic in its own right, but many of the results are of particular interest in assessing how much light is available to the LDI for a given target under any particular set of conditions, and consequently what range of operation can be expected from the LDI.

As no particular range criteria were specified in the original aims of this project the research investigated both focussed and unfocussed beams illuminating the target. Focussing of the beam gave stronger signals in the vicinity of the beam waist, but these decreased more rapidly than those for an unfocussed beam at points remote from the waist. This can be attributed to smaller speckles that result from a more rapidly diverging beam in the focussed case, leading to loss of coherence at the detector. The decrease in received intensity with increasing range is responsible for the decrease in signal strength in both cases.

Correlation measurements against an LVDT and an accelerometer were highly linear. This indicated good stability and repeatability in the LDI between successive measurements. The higher quality of the accelerometer correlations is attributed to the higher frequencies used, allowing less time for background noise to contribute to the measurement and to the relative stability of the speckle field over the amplitudes of vibration examined. Background noise is discussed further below.

Measurements of non-paraxial target motion made by the LDI indicate that it may be positioned with the illuminating beam inclined at a known angle to a moving target. This provides an alternative method of measuring the movement of an object from an off axis position rather than from an axial position. In this manner it is able to function similarly to existing dual beam LD devices without their

vulnerability to out of plane movement of the target, however it will be vulnerable to undulations in the target surface which will cause a change in the angle of incidence of the illuminating beam.

6.1.2 Velocity

The LDI has shown itself to be capable of measurement of the velocity of an unprepared target up to a maximum value of 31.6 mm/s and down to a minimum value of 55 um/s under laboratory conditions. The upper limit is due to the Doppler frequency reaching the maximum response frequency of the signal processing electronics and is shown dramatically in the results of measurements from targets vibrating at frequencies below 60 Hz. The measured displacement collapses rapidly above a particular value of the peak to peak displacement corresponding to a velocity in excess of the limit. There is scope to make significant advances in this direction with more sophisticated electronics. The maximum frequency response of the photodiode detectors is cited as 500 MHz, corresponding to a Doppler shift derived from a target velocity of over 150 m/s. The optical part of the system is not a significant factor in considering the maximum achievable Doppler signal. This indicates that there is considerable scope for improvement in the electronics before other factors need to be taken into account.

The lower limit is set by the presence of background motion both between the target and the LDI and within the LDI itself. The latter source of noise is minimal, but it can be definitively excluded by rigid construction in a working LDI design. The presence of background motion was effectively demonstrated by measurements on otherwise similar drive waves which were sinusoidal and trapezoidal. The 50 % stationary period of the trapezoidal signals allowed more background noise to intrude giving larger values for the amplitude of the target motion. Elimination of this unwanted motion between the LDI and the target is more difficult and depends upon careful selection of the location of the mounting of the LDI. Selective signal processing may also allow improvement in this direction.

Remaining background motion can be reduced if it can be measured independently of the motion of interest. Subsequent processing can predict those points during the motion where background will contribute to the measurement and compensate for it. If this background could be effectively nullified then the lower limit for velocity measurement would depend on the low frequency response of the signal processing equipment.

The electronic signal processing, although of restricted frequency response was found otherwise to make no adverse contribution to the measurement process. Further development would allow more rigourous assessment of the LDI.

6.1.3 Sense of Motion

An unusual feature of this device is the use of phase based sense detection. However, as indicated above it does not only extract the sense of motion but also allows a potential increase in the resolution of the measurements. For small amplitude measurements the technique was reliable, giving a repeatable sense signal. As the amplitude of the motion increased the effect became less reliable, requiring some care to obtain a stable signal. It is thought that the failure of the sense signal is due to a loss of signal intensity at one of the detectors. This may be due either to depolarisation leading to a lower intensity being transmitted back through the clean-up polariser into the LDI, or a decrease in the coherence condition at the detectors due to decreasing speckle size. This is supported by the results monitoring the stability of the sense of motion signal with varying target range. Where the target is illuminated by a focussed beam the sense signal shows good stability. Near the beam waist there will be a smaller illuminated region on the target leading to larger speckles at the detectors, elsewhere the sense signal is more prone to failure. As both signals are required for the sense of motion signal to be operative, loss on either channel will cause the sense signal to fail. This dependence of the sense signal on both detected signals is a potential weakness in the device.

The Michelson based design does not make full use of the available reference beam intensity as this may saturate the detectors, however the current arrangement does not necessarily represent the best case. If further reference beam intensity can be used then the signal strengths may be improved via the inherent gain of the heterodyning process to give more stable signals for sense detection while also improving the maximum working range of the device. One of the risks associated with this is that there is a greater chance of destabilising the laser.

6.2 Further Work

There are various possible directions for further work beyond the direct extensions of ideas examined here. The use of optical fibres in laser Doppler anemometers is widespread and there may be benefits from incorporating polarisation preserving fibres into a version of this solid target monitoring LDI, possibly in reducing the effects of background motion and environmental effects. It would also be worthwhile investigating the possibility of introducing a semiconductor laser source, as has recently been incorporated into a commercial anemometric device, as this could reduce both cost and size. The laser Doppler interferometer has been shown to be an effective method of measuring both the sense and magnitude of sub millimeter amplitude motions. The quality of the measurement decreases with increasing amplitude, with the sense of motion signal

falling off faster than the magnitude. Although it does not yet appear to offer a suitable solution to the problem of measurement and positional control in robotic systems, the device has reached a stage where the research could be usefully pursued both in the original direction and in the field of vibration measurement, possibly with industrial collaboration.

Appendix 1 Noise in Heterodyne Detection

There are according to Levi (1980), three main sources of noise at the output of a detector under illumination, these are thermal or Johnson noise and shot noise resulting from the illuminating beam current and from the dark current. The Johnson noise is given by :-

$$i_j^2 = 4.k_B.T.f_b/R \quad , \qquad (a.01)$$

and the shot noise by :-

$$i_{sh}^2 = 2.e.f_b.(i_{dd} + i_{ref}) \quad . \qquad (a.02)$$

Here k_B is Boltzmann's constant, T the effective temperature of charge carriers in the detector, f_b the bandwidth, R the detector resistance and e the charge on the carriers in the detector. i_j^2 and i_{sh}^2 are the mean square noise currents. The reference beam current i_{ref} is proportional to the intensity of the reference beam I_{ref}.

$$i_{ref} = k.I_{ref} \quad . \qquad (a.03)$$

Similarly the signal current is proportional to the amplitudes of the reference and signal beams, so the signal power is proportional to the intensities and is given by:-

$$i_s^2 = k^2.I_{ref}.I_s \quad , \qquad (a.04)$$

where k is the detector response. Combining these equations and introducing the reference beam intensity explicitly

into the noise equation gives a S/N ratio of:-

$$S/N = k^2.I_{ref}.I_s/(2.e.f_b(i_{dd} + k.I_{ref}) + 4.k_B.T.f_b/R) \quad . \qquad (a.05)$$

If the reference beam intensity is allowed to become very large it dominates the denominator terms, reducing equation a.05 to :-

$$S/N = k.I_s/(2.e.f_b) \quad . \qquad (a.06)$$

From this result it can be seen that when the shot noise resulting from the reference beam dominates the other noise sources the signal to noise ratio becomes constant, depending only on the signal beam intensity and physical and device constants.

Appendix 2 Frequency Shifting

The most widely used frequency shifting device is the acousto-optic, or Bragg cell. A sound wave transmitted through a transparent medium causes local variations in the density, and consequently via the Lorentz-Lorenz equation in the refractive index. In a sufficiently large medium, the index variations can be considered to be a series of parallel planes, moving through the material with the velocity of sound. These act as a moving diffraction grating. (The name Bragg cell derives from similar diffraction of X rays by crystal planes.) Since the scattered light is diffracted in a different direction from the incident beam, a Doppler shift induced in the incident beam, from scattering by particles moving in the material, is not cancelled by the Doppler shift induced into the emergent beam. The (Bragg) diffraction condition is :-

$$2.\lambda_s.(\cos(a) + \cos(b)) = n.\lambda \quad . \quad (a.07)$$

λ_s is the wavelength of sound in the material, a and b are the angles between the direction of propagation of the sound and the incident, and diffracted beams, respectively, n is an integer representing the order of diffraction, and λ the wavelength of the light beam.

The component of the sound wave velocity, and hence the particle motion responsible for the Doppler shift in the

direction of the incident beam is :-

$$v_i = v_o.\cos(a) \quad , \qquad (a.08)$$

and for the scattered beam :-

$$v_s = v_o.\cos(b) \quad , \qquad (a.09)$$

where v_o is the sound wave velocity. The resulting Doppler shift will be due to both of these velocities, and is given by :-

$$f_d = 2.f_o.v_o(\cos(a) + \cos(b))/c_o \quad ,$$
$$= 2.v_o.(\cos(a) + \cos(b))/\lambda \quad . \qquad (a.10)$$

Rearranging equation a.07 and substituting gives :-

$$f_d = n.v_o/\lambda_s \quad . \qquad (a.11)$$
$$= n.f_s \quad , \qquad (a.12)$$

where f_s is the frequency of the sound wave. This derivation does not include the effect of the refractive index of the material. If this is incorporated the velocity of light in the medium is reduced, giving a longer wavelength, and consequently a shallower diffraction angle hence a smaller Doppler shift. The efficiency of the process depends on the contrast of the diffraction grating. This is governed by the Lorenz-Lorentz equation and the Raman Nath equation. The exact derivation of this is given in Levi (1980). It should be noted that efficient operation is obtained from these devices only in a small frequency range centred on the resonant frequency of the

transducer-exciting the ultrasonic wave train.

An analogous argument gives the Doppler frequency induced by a rotating radial grating.

For a rotating scattering disk such as used by Halliwell (1979), the directions of incidence and scattering are arbitrary. That is, the Bragg constraint is lifted, but the structure of the derivation of the frequency shift is still similar.

Deliberate frequency shifts can also be introduced by discontinuous methods. These generally alter the optical path length at a constant velocity, using a sawtooth signal. For example Truax et al (1984) who used a vibrating retro-reflector. The principle is a direct introduction of the Doppler effect as described in section 3.1.1.

Appendix 3 Mean Phase Across Target Surface

The accepted approximation for the radial distance d, between a chord and an arc on a circle of radius R, with a chord length r, is :-

$$d = r^2/R \quad . \qquad (a.13)$$

The average value of this difference across a given area A, is defined as :-

$$\bar{d} = \frac{\oint d.\, dA}{\oint dA} \quad . \qquad (a.14)$$

For a circular detector surface, radius r_d, this becomes :-

$$\bar{d} = (1/A) \times \int_0^{r_d} 2.\pi.r.r^2/R \; dr \quad . \qquad (a.15)$$

On integration this gives :-

$$\bar{d} = (1/A).\pi.r_d^{\,4}/4.R \quad . \qquad (a.16)$$

As $A = \pi.r_d^{\,2}$, $\bar{d}$ becomes ,

$$\bar{d} = r_d^{\,2}/(2.R) \quad . \qquad (a.17)$$

For a rectangular detector surface with sides 2u and 2v, the basic equation becomes :-

$$\bar{d} = 1/(4.u.v) \times \int_{-v}^{v} \int_{-u}^{u} (x^2 + y^2)/R \quad dx.dy \quad . \qquad (a.18)$$

On evaluation this becomes :-

$$\bar{d} = 1/(4.u.v) \times 4/(3.R).u.v.(u^2 + v^2) \quad . \qquad (a.19)$$

Which when simplified becomes :-

$$\bar{d} = 1/(3.R) \ .(u^2 + v^2) \quad . \qquad (a.20)$$

Appendix 4 Error Count Derivation

A fuller account is given here of the derivation of a general term for the additional count logged by an LDI, when a background motion exists.

The background velocity will be characterised by an rms value v_b. If the target motion of interest is defined as v(t), and an inverse mapping exists t(v), it is possible to define the fraction of a measurement period during which the background exceeds the target velocity as :-

$$f = \frac{\int_0^{v_b} t(v).dv}{\int_0^{\infty} t(v).dv} \quad . \qquad (a.21)$$

If the motion of the target is periodic, with a maximum amplitude of v_o, this may replace the top limit of integration in the denominator, which then becomes t_m, the periodic time of the signal or the measurement time for any other type of motion.

The excess measured displacement over the target displacement during the measurement time is given by :-

$$d_{xs} = f.t_m.v_b \quad . \qquad (a.22)$$

For the particular case of a sinusoidal drive motion which may be taken as a first approximation to all other periodic motions, the measured excess displacement during one cycle

due to a given rms background motion is :-

$$d_{xs} = (t_m.v_b/v_o).\int_0^{v_b} \cos^{-1}(v/v_o).dv \qquad (a.23)$$

The solution of the integral I, is given in mathematical tables (Dwight 1961) as :-

$$I = v.\cos^{-1}(v/v_o) - (v_o^2 - v^2)^{1/2} \quad . \qquad (a.24)$$

Substituting v_b, simplifying and inserting the result into equation a.23 gives the following expression for the excess displacement measured during each cycle :-

$$d_{xs} = (\cos^{-1}(v_b/v_o) - ((v_o/v_b)^2 - 1)^{1/2}) \; x \; v_b^2/(f_t.v_o) \quad . \qquad (a.25)$$

This gives a value of the excess measure displacement that decreases to zero as the background velocity decreases as would be expected.

Appendix 5 BIBLIOGRAPHY

Adrian,R.J., Goldstein,R.J.

Analysis of a laser Doppler anemometer

J. Phys. E, Sci. Instrum., 4, 505, (1971)

Agrawal,Y.C., McCullough,J.R.

Directional pedestal-free laser Doppler velocimetry without frequency biassing pt 1.

Appl. Opt., 20.9, 1553, (1 May 1981)

Agrawal,Y.C., Riley,J.B.

Directional laser velocimetry without frequency biassing pt 2

Appl.Opt., 23.1, 57, (1 Jan. 1984).

Alphonse,G.A.

Broadband acousto-optic deflectors : New results

Appl. Opt., 14.1, 201, (Jan. 1975).

Barker,L.M., Hollenbach,R.E.

Laser interferometer for measuring high velocities of any reflecting surface

J. Appl. Phys., 43.11, 4669-, (Nov. 1972).

Beckmann, P.

Scattering of light by rough surfaces

Prog. Opt., 6, 55-69, (1967)

Belousov,P.Yu., Dubnishchev,Yu.N., Pavlov,V.A.

Velocimeter with an optical Doppler-frequency discriminator

Opt. Spectrosc. (USSR), 43.4, 457-460, (Oct. 1977).

Boiko,V.M., Papyrin,A.N., Poplavskii,S.V.

High speed laser Doppler velocimeter with direct spatial analysis

Opt. Spectrosc. (USSR), 48.2, 200-202, (Feb. 1980).

Born, M., Wolf, E.

Principles of Optics 2nd Edn.

Pergamon Press 1959

Bossel,H.H., Hiller,W.J., Meier,E.E.A.

Noise-cancelling signal difference method for optical velocity measurements

J. Phys. E. Sci. Instrum., 5, 893-, (1972).

Botcherby,S.C.L., Bartley-Denniss,G.A.

The laser in the measurement of velocity and length of materials

Proc. Inst. Mech. Eng., 183.3D, 25, (1968).

Bouricius,G.M.B., Clifford,S.F.

An optical interferometer using polarisation coding to obtain quadrature phase components

Rev. Sci. Instrum. 41.12, 1800-, (Dec. 1970).

Buchhave,P.

Laser Doppler vibration measurements using variable frequency shift

DISA Information, 18, 15-, (Sept. 1975).

Cookson R.A., Bandyopadhyay, P.

Mechanical vibration measurements using a fibre optic L.D. probe

Opt. & Laser Technol., p33, (Feb. 1978).

Cookson R.A., Bandypadhyay, P.

A fibre optic laser Doppler probe for vibration analysis of rotating machines

J. Eng. for Power, 102, 607, (1980).

Cummins, H.Z., Knable, N.

Single sideband modulation of coherent light by Bragg reflection from acoustical waves

Proc. IEEE, 51, 1246, (1963).

Cummins, H.Z., Knable,N., Yeh, Y.

Observation of diffusion broadening of Rayleigh scattered light

Phys. Rev. Lett., 12.6, 150, (1964).

Dainty, J.C.

Laser Speckle and Related Phenomena

2nd edn. publ. Springer Verlag 1984

ISBN 0-387-13169-8

Davis, D.T.

Analysis of laser Doppler velocimeter

I.S.A. Trans., 7.1, 43-51, (1968).

Davis, Q.V., Kulczyk, W.K.

Vibration of turbine blades measured by means of a laser

Nature, 222, 475, (1969).

Downs, M.J., Raine, K.W.

An unmodulated bi-directional fringe-counting interferometer system for measuring displacement

Precision Engineering, 1.2, 85-88, (1979).

Dragsten, P.R., Webb, W.W., Paton, J.A., Capranica, R.B.

Light-scatterging heterodyne interferometer for vibration measurements in auditory organs

J. Acoust. Soc. Am., 60.3, 665-71, (Sept. 1976).

Drain, L.E.

The laser Doppler Technique

Wiley 1980 ISBN 0-471-27627-8

Drain, L.E., Moss, B.C.

Applications of laser interferometry to process control

Int. Conf. Optical Techniques in Process Control, The Hague, June 14-16, 1983 p 279-88.

Dubnistchev, Y.N., Belousov, P.Y.,, Stolpovski, A.A.
The application of an electro-optical frequency modulator with a rotating electric field in optical Doppler velocimeters
Opt. & Laser Technol., 31, (Feb. 1977).

Durao, D.F.G., Whitelaw, J.H.
Some performance characteristics of the prototype DISA frequency-tracking demodulator
Imperial Coll. Dept. Mech. Eng. Rpt. HTS/74/11 (1974)

Durst, F., Melling, A., Whitelaw, J.H.
Principles and Practice of Laser-Doppler Anemometry
2nd Edition 1981, Academic Press, ISBN 0-12-225260-8

Dwight, H.B.
Tables of Integrals and Other Mathematical Data
Macmillan 1961.

Dyott, R.D.
The fibre optic anemometer
Microwaves, Optics & Acoustics, 2.1, 13, (Jan. 1978).

Ebeling, K.J.
Experimental investigation of some statistical properties of monochromatic speckle patterns.
Optica Acta, 26.11, 1345-49, (1979).

Eberhardt, F.J. Andrews, F.A.
Laser heterodyne system for measurement and analysis of vibration
J. Acoust. Soc. Am., 48(3.1), 603, (1970).

Feke, G.T., Riva, C.E.
Laser Doppler measurements of blood velocity in human retinal vessels
J. Opt. Soc. Am., 68.4, 526-531, (April 1978).

Foord, R., Harvey, A.F., Jones, R., Pike, E.R.,
Vaughan, J.M.
A solid state electro-optic phase modulator for laser Doppler anemometry
J. Phys. D :Appl. Phys., 7, L36-L39, (1974).

Ford, P.J.
Private communication

Foreman, J.W. George, E.W., Lewis, R.D.
Measurement of localised flow velocities in gases with a laser Doppler flowmeter
Appl. Phys. Lett., 7.4, 77, (1965).

Foreman, J.W., George, E.W., Jetton, J.L., Lewis, R.D.,
Thornton, J.R., Watson, H.J.
Fluid flow measurements with a laser Doppler velocimeter
IEEE J. Quant. Electr., QE2.8, 260, (1966).

Foreman, J.W.
Optical path-length difference effects in photo-mixing with multimode gas laser radiation
Appl. Opt., 6.5, 821, (1967).

Foster, J.V.
A laser device for remote vibration measurement
IEEE Trans. on Aerospace & Electronic Systems, AES-3.2, 154, (March 1967).

Francon, M.
Laser speckle and applications in optics
Academic Press 1979, ISBN 0-12-265760-8

Gasvik, K.
A theory of polarisation dependent off specular peaks of scattered light from rough surfaces.
Optica Acta, 27.7, 965-80, (1980).

Gasvik, K.
Measurement of polarisation dependent off-specular peaks of laser light scattered from rough metal surfaces and dielectrics.
Optica Acta, 28.1, 131-38, (1981).

Goldstein, R.J., Kreid, D.K.
Measurement of laminar flow development in a square duct using a laser-Doppler flow-meter
J. Appl. Mechanics, 34, 813-818, (1967).

Gould, G., Jacobs, S.F., LaTourette, J.T., Newstein, M., Rabinowitz, P.
Coherent detection of light scattered from a diffusely reflecting surface
Appl. Opt., 3.5, 648, (May 1964).

Halliwell, N.A.
Laser Doppler Measurement of Vibrating Surfaces: A Portable Instrument.
J. Sound & Vibration, 62.2, 312-315, (1979)

Halliwell, N.A., Pickering, C.J.D., Eastwood, P.G.
The Laser Torsional Vibrometer: A New Instrument.
J. Sound & Vibration., 94.4, 588-592, (1984)

Haus, H.A., Townes, C.H.
Comments on "Noise in photoelectric mixing"
Proc. Inst. Radio Eng., 50, 1544-45, (1962).

Jones, J.D.C., Jackson, D.A., Corke, M., Kersey, A.D.
Solid state and fibre optic laser Doppler velocimeters
Internat. Conf. Optical Techniques in Process Control
June 14-16 1983, p1-10. The Hague.

Kaplan, Z., Maron, Y., Katzir, Y.
Differential laser Doppler interferometry for high surface velocity measurement
J Appl. Phys., 54.11, 6086, (Nov. 1983).

Kersey, A.D., Jones, J.D.C., Corke, M., Jackson, D.A.
Fibre optic sensor using heterodyne signal processing without recourse to a specific frequency shifting element
Intl. Conf. Optical Techniques in Process Control, The Hague, June 14-16, 1983, p111-119.

Knuhtsen, J., Olldag, E., Buchhave, P.
Fibre optic LDA with Bragg frequency shifting utilising polarisation preserving single mode fibre
J Phys. E: Sci. Instrum., 15.11, 1188, (Nov. 1982).

Kroeger, R.D.
Motion sensing by optical heterodyne Doppler detection from diffuse surfaces.
Proc. IEEE, Feb. 1965, p211.

Kyuma, K., Tai, S., Hamanaka, K., Nunoshita, M.
Laser Doppler velocimeter with a novel optical fibre probe
Appl. Opt., 20.14, 2424, (1981).

Levi, L.
Applied Optics
Wiley Interscience
Vol. 1, 1968, ISBN 0-471-53110-3
Vol. 2, 1980, ISBN 0-471-05054-7

Lewin, A.C., Kersey, A.D., Jackson, D.A.
Noncontact surface vibration analysis using a monomode fibre optic interferometer incorporating an open air path
J. Phys. E: Sci. Instrum., 18.6, 604-608, (June 1985).

Markho, P.H., Smith, B.V., Lalor, M.J.
An advanced apparatus for the study of roller and cage slip in high speedroller bearings
J. Lubrication Technol., 80-C2/Lub2, p1-, (1980).

Massey, G.A.
Photomixing with diffusely reflected light
Appl. Opt., 4.7, 781, (July 1965).

Nishihara, H., Matsumoto, K., Kuyama, J.
Use of a laser diode and an optical fibre for a compact laser Doppler Velocimeter
Opt. Lett., 9.2, 62-64, Feb. (1984).

Nokes, M., Hill, B.C., Barelli,A.E.
Fibre optic heterodyne interferometer for vibration measurements in biological systems
Rev. Sci. Instrum., 49.6, 766, (1978).

Oldengarm, J.
Development of rotating diffraction gratings and their use in laser anemometry
Opt. & Laser Technol., 9, 69-71, (April 1977).

Oldengarm, J., vanKrieken, A.H., Raterink, H.J.
Laser Doppler velocimeter with optical frequency shifting
Opt & Laser Technol., Dec. 1973, p249.

Oliver, B.M.
Signal-to-noise ratios in photoelectric mixing
Proc. IRE, 49, 1900-1961, (1961).

Open University

Understanding Space and Time

S 354, Units 13 & 14, Block 5, p34-

Open University Press

Pleydell, M.E., Birchenough, A.

Laser Doppler measurements for vibration and the motion of solid targets

Transducer Technol., 8.3, 13-17, (June 1985).

Read, W.S., Fried, D.L.

Optical heterodyning with noncritical angular alignment

Proc. IEEE Correspondence, 51, 1787, (Dec. 1963).

Rizzo, J.E., Halliwell, N.A.

Multicomponent Frequency Shifting Self-Aligning Laser Velocimeters.

Rev. Sci. Instrum., 48.8, 1180-1185, (Aug. 1978).

Rudd, M.J.

A new theoretical model for the laser Dopplermeter

J. Phys. E: Sci. Instrum., 2, 55, (1969).

Schwar, M.J.R.

Doppler velocity measurements using white light

Nature, 229, 621, (26th Feb. 1971).

Siegman, A.E.

The antenna properties of optical heterodyne recievers

Proc. IEEE, 54.10, 1350, (Oct. 1966).

Smeets, G. George, A.
Instantaneous laser Doppler velocimeter using a fast wavelength tracking Michelson interferometer
Rev. Sci. Instrum., 49.11, 1589-96, (Nov. 1978).

Steeger, P.F.
Probability density function of the intensity in partially polarised speckle fields.
Opt. Lett., 8.10, 528-30, (Oct. 1983).

Steele, R.
Heterodyne systems for optical fibre communications and a proposed electro-optic frequency shifter
Proc. NATO Adv. Study Inst. on Integrated Optics, Physics & Applications Aug. 17-30, Erice, Italy.

Stone, N.W.B.
Submillimeter waves in measurement techniques
Optics Technol., Feb. 1970, p8-.

Suzuki, T., Hioki, R.
Translation of light frequency by a moving grating
J. Opt. Soc. Am., 57.12, 1551, (Dec. 1967).

Tanaka, T., Benedek, G.B.
Measurement of the velocity of blood flow (in vivo) using a fibre optic catheter and optical mixing spectroscopy.
Appl. Opt., 14.1, 189, (Jan. 1975).

Temes, C.L.

Relativistic consideration of Doppler shift

IRE Trans. Aero. & Nav. Electronics, p37, (1957).

Truax, B.E., Demarest, F.C., Sommargren, G.E.

Laser Doppler velocimeter for velocity & length measurements of moving surfaces

Appl. Opt., 23.1, 67, (1 Jan. 1984).

Ueha, S., Shibata, N., Tsujuichi, J.

Flexible coherent optical probe for vibration measurements

Opt. Comm. 23.3, 407, (Dec. 1977).

Velzel, C.H.F.

Laser Doppler displacement meter with controlled grating speed

Int. Conf. Optical Techniques in Process Control, The Hague, June 14th-16th 1983, p289-294.

Vlachos, N.S., Whitelaw, J.H.

The measurement of blood velocity with laser anemometry

Imperial Coll. Rpt. HTS/74/13, Dept Mech. Eng. (March 1974).

Wang C.P.

Doppler velocimeter using diffraction grating and white light

Appl. Opt., 13.5, 1193, (May 1974).

Watson, R.C., Lewis, R.D., Watson, H.J.
Instruments for motion measurements using LD heterodyne techniques
ISA Trans., 8.1, 20-28, (1969).

Welford, W.T.
Review: Optical estimation of statistics of surface roughness from light scattering measurements
Optical & Quantum Electronics, 9, 269-87, (1977).

White, D.N.
Johann Christian Doppler and his effect, a brief history
Ultrasound in Med. & Biol., 8.6, 583, (1982).

Yariv, A.
Quantum Electronics 2nd Edn.
John Wiley & Sons Inc. 1975, ISBN 0-471-97176-6

Yariv, A.
Optical Electronics 3rd edn.
Holt, Rinehart and Winston 1985, ISBN 0-03-070289-5

Yeh, Y., Cummins, H.Z.
Localised fluid flow measurements with an He Ne laser spectrometer
Appl. Phys. Lett., 4.10, 176, (May 1964).

Younes, M.A., Croft, J.R., Hill, W.J.

Surface Roughness Assessment using the Angular Distribution of the Backscattered Field from a Small Laser Spot. Proc. SPIE, Int. Soc. Opt. Eng. (USA)., 473, 122-125, (1984). (Symposium OPTIKA 1984)